2021

Pathogenic Characterization and Therapeutic Development for Fiblrolamellar Hepatocellular Carcinoma

Solomon N. Levin

PATHOGENIC CHARACTERIZATION AND THERAPEUTIC DEVELOPMENT FOR FIBLROLAMELLAR HEPATOCELLULAR CARCINOMA

A Thesis Presented to the Faculty of
The Rockefeller University
in Partial Fulfillment of the Requirements for
the degree of Doctor of Philosophy

by
Solomon N Levin
June 2021

PATHOGENIC CHARACTERIZATION AND THERAPEUTIC DEVELOPMENT FOR FIBROLAMELLAR HEPATOCELLULAR CARCINOMA

Solomon N Levin, Ph.D.
The Rockefeller University 2021

Fibrolamellar hepatocellular carcinoma (FLC) is a rare liver cancer that primarily affects adolescents and young adults. There are no known successful systemic chemotherapies for this disease, and thus, surgery is the only potential path to a cure in patients with FLC. Once the disease has grown or metastasized to a point where surgery is no longer an option, a patient's chance for survival approaches zero. There is a recurrent genetic deletion in FLC cells, which has been found in almost all FLC tumor samples sequenced to date, but not in normal liver tissue from the same patients. The deletion encompasses ~400kb on chromosome 19 beginning after the first exon of *DNAJB1*, which codes for a member of the heat shock protein 40 (HSP40/DNAj) family, and ends before the second exon of *PRKACA*, which codes for the catalytic subunit of protein kinase A (PKAc). The deletion results in a functioning chimeric kinase with exon 1 of DNAJB1 and exons two through ten of PRKACA.

In this thesis, I will present my work in two areas with regards to this disease. First, I will present my research working on understanding the pathogenesis of FLC. While we know the oncogene that is responsible for transformation, we do not have a good understanding of how this mutation leads to cancer. I will present proteomic data that shows a unique proteomic and phosphoproteomic signature in FLC and will show that quantification of the PKA system can provide insight into the pathogenesis.

In the following chapter, I will present my research on developing the first systemic therapeutic for FLC, by targeting this mutation. I will show how I began by targeting the protein, which proved difficult given the similarities of the mutated protein to the wild-type protein. Then, I will discuss my work on developing an RNA-targeting therapy with antisense oligonucleotides and small interfering RNAs.

I will close with a discussion on my thesis work and how I envision future research to continue from what I present here.

To my father, who taught me the importance of using my talents to help others.

To my mother, who taught me to always persevere.

Acknowledgments

There is no notable success that develops by just one individual. I am humbled by the magnitude of support from numerous people in my professional and personal life that have helped me arrive at this threshold. Because evolving into a Ph.D. is such an immersive venture, I want to take a moment–or a page, really–to thank those who have understood, advised, guided, and encouraged me along the way.

It was not my original intention to attain a Ph.D. Back in 2014, I started out as a typical medical student. Unlike an MD-PhD student, I did not transition to research after my second year of med school. It was only after my third year of medical school that I decided to take a year off to focus on research through an HHMI fellowship. I didn't know it at the time, of course, but meeting Dr. Sandy Simon during that research year would change what I had planned for my professional life–a new dream of becoming a surgeon-scientist evolved. It was Sandy's care and concern for everyone on his team, his belief in my potential as he took me on, as a student with little research experience, that got me hooked. It was his commitment and empathy for those suffering from Fibrolamellar that reverberated as the pulse of his lab. It was his passion that ignited my own. Sandy didn't merely mentor me, he prompted skills I didn't know I had. As I neared the close of that fellowship year, Sandy took me aside and simply stated, "You know, if you stay, you can likely get a Ph.D. in a year or two from now". Next thing I knew, I was transitioning into the MD-Ph.D. program. No amount of written text can describe my gratitude for Sandy, who enabled me to envision and discover a different, rewarding direction through my research.

One gets to know a lot about people they work with closely, especially in a team-driven environment like a research lab. The dedicated professionals at the Simon lab became like family to me, and I am so appreciative of the strengths and contributions each of them brought to our cumulative successes. I have learned so much from you all.

Gadi, Denise, David, Rose, Mike, and Nikki, you have all been an amazing team to work with as we try to tackle this terrible disease. I am positive that our team’s strides towards a cure have made an impressive impact because of you.

Harriet, you became a great friend and an attentive sounding board. Your talent as a precise troubleshooter is certain to secure your position as an outstanding physician.

Bassem, thank you for your gift of active listening and compassionate understanding. Also, your constant encouragement and empathy for my cold room exploits were especially valuable.

Tova, thank you for joining the team and scrambling with me during these last few months. Your hard work is both recognized and so much appreciated.

One of the great things about working at Rockefeller are the fantastic resource centers and the experts within them. Deena Oren at the Structural Biology Resource Center took me under her wings in my first few months in the lab and showed me tremendous patience as I learned the skills of protein purification. Soren Heissel and Henrik Molina at the Proteomics Resource Center are always available at a moment's notice for new questions and experiments. Their expertise in this field has been so helpful. Lavo Ramos-Espiritu and Fraser Glickman at the High-throughput screening center were a pleasure to work with as I learned about the world of high-throughput screening. Finally, the Genomics Resource Center, with Connie Zhao at the helm, were extremely helpful in sequencing my RNA with speed.

To my incredible family, my mother, Esther Levin and my in-laws, Jan and Blumie Loeb who have been such great cheerleaders, you have taught me everything there is to know about parenthood, and then some. Your interest and inquisitive discussions proved your desire to share in this journey, and your continual efforts at understanding the complicated concepts of my experiments showed me how much you care.

For my daughters, Annie, Ahuva and Leah, the boisterous leaders of my fan club, and exuberant sharer of all things "Daddy", you are the reason for everything. Your pride in my pursuit of becoming a "medical scientist", as you tell everyone within earshot, is the energy that invigorates my day. Additional thanks for being the adorable models that I could share at the end of my lab meetings presentations. You unknowingly became part of the team, too!

Most of all, I thank my partner in life, my co-conspirator and best friend. Michelle, your support continues to reach far beyond your contract, and there is no accomplishment that exists in my life without you. You ignored your own needs and were not just "ok" with a new pursuit that meant extra years of schooling, but you insisted on it. I could never have gotten through these years without your encouragement and selflessness. Thanks for holding down more than your fair share of the home front as we traveled through this crazy ride. I hope to always make you as proud of my victories as I am of yours.

Table of Contents

List of Figures

List of Tables

List of Abbreviations

ASO	Antisense oligonucleotide
DsiRNA	Dicer substrate siRNA
FLC	Fibrolamellar hepatocellular carcinoma
HCC	Hepatocellular carcinoma
LC/MS	liquid chromatography mass spectrometry
LC/MS/MS	tandem mass spectrometry
LFQ	Label Free Quantification
LNA	Locked nucleic acid
PDX	Patient-derived xenograft
PS	Phosphorothioate
PSM	peptide spectrum match
siRNA	Small interfering RNA
SPS	Synchronized precursor selection
Tm	Melting temperature
TMT	Tandem mass tag

Chapter 1
Introduction

1.1 Overview of Fibrolamellar Hepatocellular Carcinoma

1.1.1 History

Hepatocellular Carcinoma (HCC) is the fourth leading cause of cancer-related deaths worldwide and is the most common form of primary liver cancer (Kim & Viatour, 2020). In the early 20th century, it was recognized that liver cancer is not one uniform disease, but one that presents in different forms pathologically (Okuda, 2002). The important distinction of cell of origin was made during this time, with those cancers that arose from the bile duct cell, now called cholangiocarcinoma, recognized to be distinct from those that arose from the liver cell. In the second half of the century, large geographical differences in the pathologies of HCC were reported.

Today, our understanding of carcinogenesis in general, and in HCC in particular, gives us insight into the vast differences of HCC types in different geographical regions and in different ethnic groups. As in all cancers, HCC can result from several types of insults in the cell of origin, such as from mutagens, which are chemicals that can lead to genetic mutation in some cells. If these mutations are in genes involved in cell growth control, a silencing mutation can result in uncontrolled cell growth. Thus, these mutagens are called carcinogens. Similarly, some viruses can also cause mutations that lead to uncontrolled cells growth.

Hepatitis B Virus (HBV) is one such oncogenic virus. Aflatoxin, a chemical produced by the *Aspergillus* mold, is a carcinogen that has also been implicated in the pathogenesis of HCC, particularly in the South African region. Hepatitis C Virus (HCV), while not inherently oncogenic, can cause chronic liver inflammation in some patients, which may ultimately lead to cirrhosis, a condition of scarring throughout the liver that predisposes it to cancer.

Back in the mid-20th century, progress continued to be made in the classification of the many different subtypes of HCC, and in 1956, in a review of the different types of liver tumors (benign and malignant) that occur in childhood and infancy, Edmonson reported a case of a primary liver cancer in a 14-year-old female. Edmonson did not give this case a distinct name but described it as a “liver cell carcinoma of an adult type, in which the stroma is rather profuse and the similarity of the cancer cells to normal cells is striking” (Edmonson, 1956). In a paper published in 1980 by Craig on which Edmondson is listed as a co-author, they describe a series of 23 patients with this distinctive histology (the case from the 1956 paper is included), and they give this cancer its name, Fibrolamellar Carcinoma of the Liver, due to its hallmark histologic feature: “fibrosis arranged in a lamellar fashion around the neoplastic hepatocytes” (Craig et al., 1980).

Besides the distinct histology seen in FLC (more on that discussed below), there were several other differences between FLC and HCC that were reported in this paper and in others since then. For one, FLC is found in younger patients, typically in their adolescence or young adulthood. In contrast, the median age for the other variants of HCC is 62 (Yang et al., 2016). Patients who are diagnosed with FLC also do not have any underlying liver pathology, a stark difference from the underlying cirrhosis or inflammation seen in patients with HBV, HCV, or aflatoxin poisoning. From a clinical chemistry standpoint, HCC often presents with an elevated alpha-fetoprotein, which is not typically seen in patients with FLC. Finally, the male to female ratio of 2:1 – 4:1 seen in HCC (Liu et al., 2017) is not present in FLC, which has an approximate equal rate among males and females.

1.1.2 Epidemiology

FLC is a rare cancer that primarily affects adolescents and young adults with a median age of 21 (Lalazar & Simon, 2018). Its age-adjusted incidence rate is reported at 0.02 per 100,000 patient-years (El-serag and Davila, 2004). There are no known successful systemic chemotherapies for FLC, and thus, surgical resection is the mainstay of treatment. Due to the non-specific nature of the disease symptoms (e.g., weight loss, abdominal pain), FLC is often diagnosed at a fairly late stage, at which point the tumor has often metastasized and surgery is no longer an option. When the tumor is not surgically removed, the mortality rate is 100% by five years, with a median survival of just twelve months. When removed surgically, the patients fare better, with a five-year survival around 75% (Stipa et al., 2006). Overall, the five-year survival rate is only 34% (Eggert et al., 2013).

1.1.3 Histology

The hallmark of FLC is the lamellar fibrosis that surrounds and/or is interspersed among the tumor cells. But there are several other features that are seen in FLC tumors. The FLC cells are large and polygonal, with prominent nucleoli and granular eosinophilic cytoplasm, and in some cases the cytoplasm contains a white round structure on H&E, called pale bodies (Figure 1.1). On electron microscopy, you can clearly see the prominent nucleoli. In addition, FLC cells also typically have mitochondria that are larger than in normal hepatocytes and many of the cells are packed with these larger mitochondria (Figure 1.2).

Less commonly, some FLC tumors have a dark pink area within the cytoplasm, called hyaline bodies, and in some cases, pseudoglands can be seen within the tumor (Figure 1.3). Grossly, the tumors are usually large, yellow/tan in color with fibrous bands running through, and have a central scar (Figure 1.4).

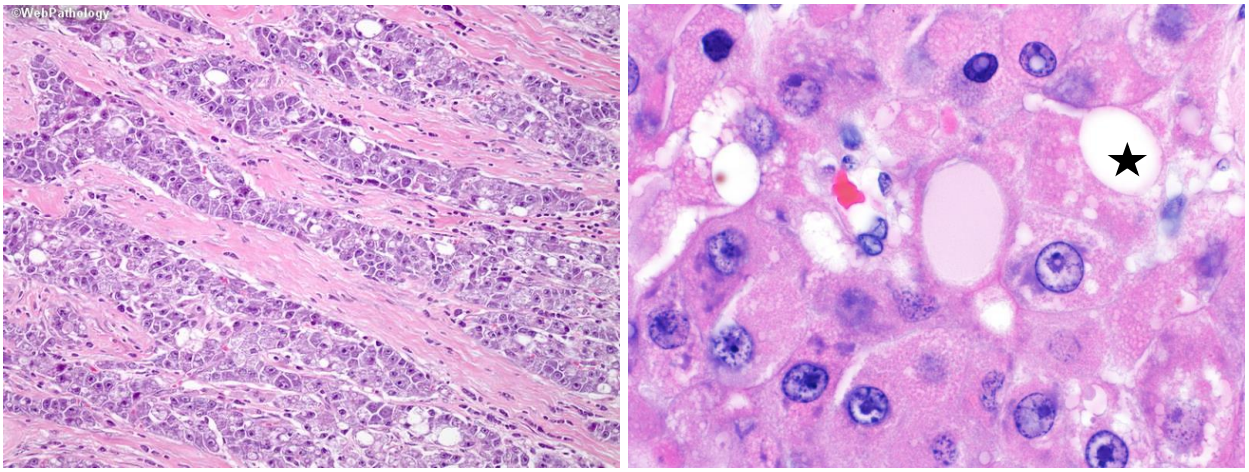

Figure 1.1 Typical features of FLC on H&E
Left - the fibrous bands (lamellae) of collagen running through the tumor give FLC its name (courtesy of webpathology.com). Right - higher magnification of FLC cells demonstrates the large polygonal cells, prominent nucleoli, and granular eosinophilic cytoplasm. A pale body in the cytoplasm of a cell can be seen in the top right of the image (star). Courtesy of Michael Torbenson, MD.

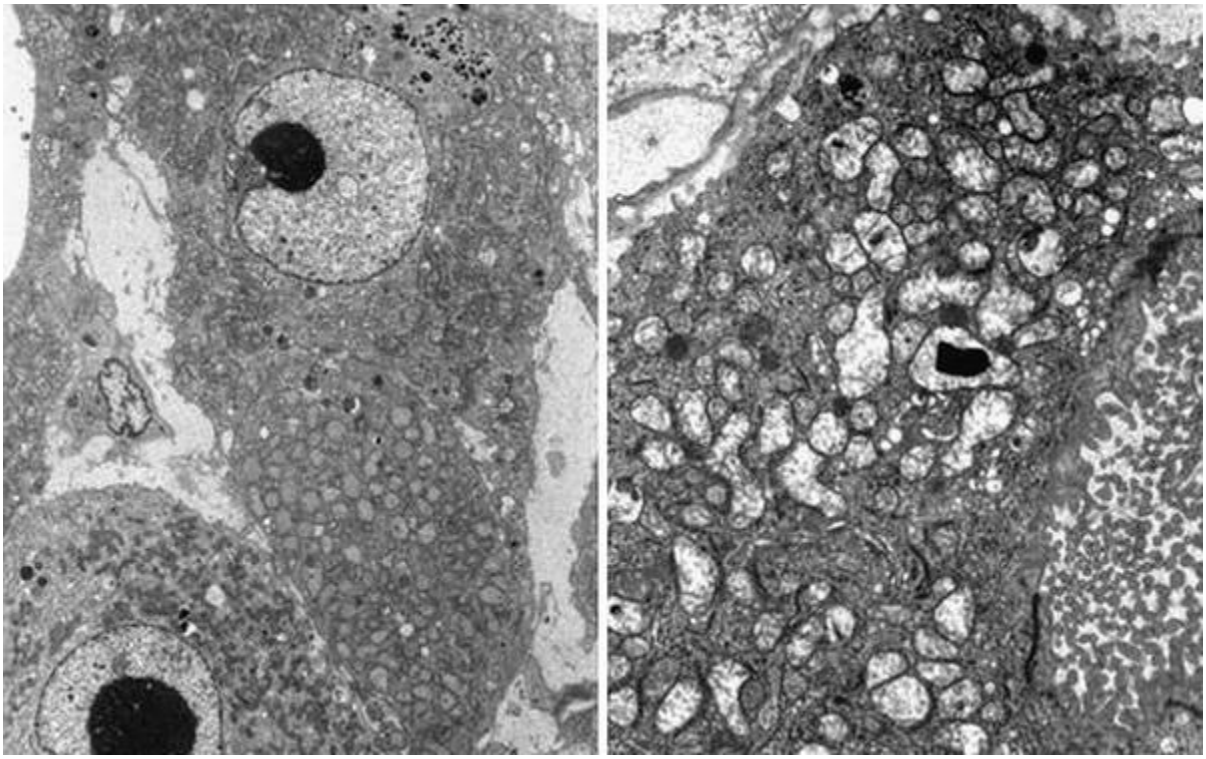

Figure 1.2 Features of FLC on electron microscopy
Left – round nuclei with prominent nucleoli. Right – abundant large mitochondria throughout the cytoplasm. From Matsuda et al., 2013.

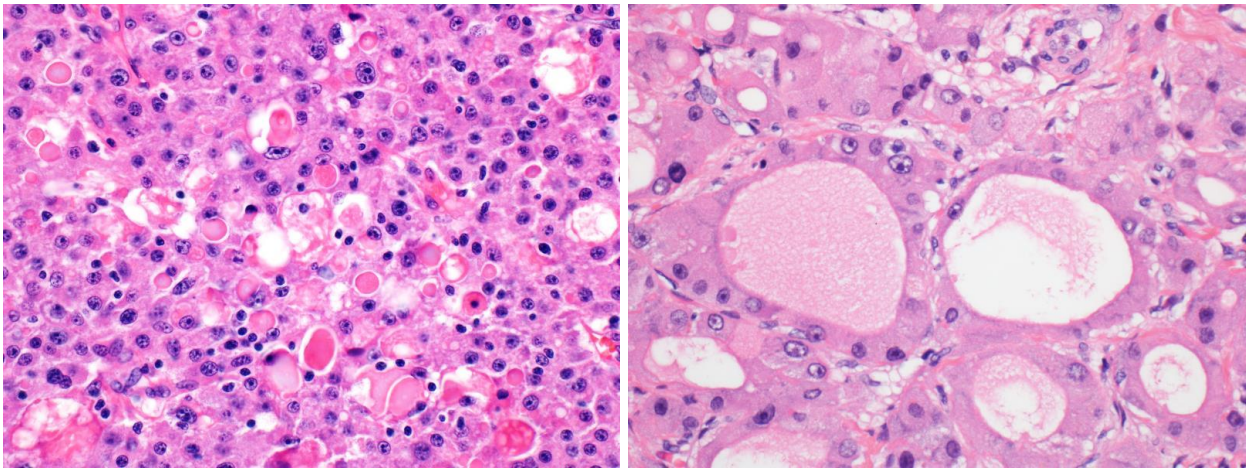

Figure 1.3 Other histological features seen in some FLC tumors
Left – hyaline bodies. Right – pseudoglands, which are surrounded by the neoplastic cells.
Courtesy of Michael Torbenson, MD.

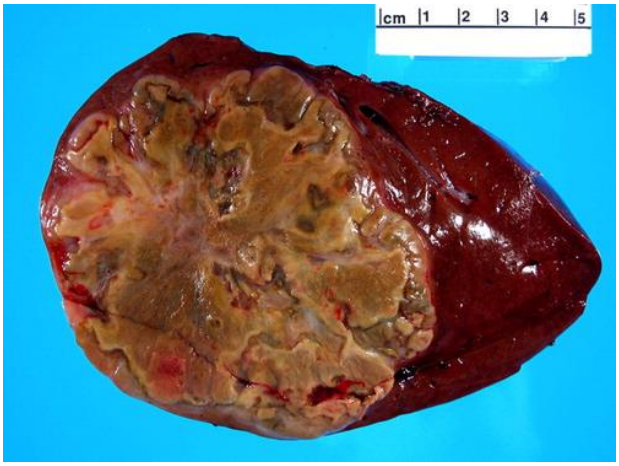

Figure 1.4 Image of an FLC tumor
From Smith et al., 2008.

1.1.4 Review of Recent Literature

While the histological characteristics of FLC and its classifications continued to progress, the field of FLC was relatively stagnant in terms of the understanding of the pathogenesis of this cancer until 2014, when our lab published its findings that FLC tumors consistently have the same genetic mutation: a genetic deletion of approximately 400 kilobases on chromosome 19. This deletion results in an in-frame fusion of two genes, *DNAJB1*, a member of the heat shock protein 40 family, and *PRKACA*, the catalytic subunit of Protein Kinase A. The two break points are in the first intron of *PRKACA*, and either the first intron of *DNAJB1*, or in the second exon of DNAJB1. Upon splicing, this results in a fusion transcript made up of exon 1 of *DNAJB1* and exons 2-10 of *PRKACA*. This chimeric transcript is translated into a chimeric protein

and has a mass of 47 kDa. Wild-type *PRKACA* has a mass of 41 kDa. For three of the tumors sequenced in this initial study, the break was far enough into second exon, that splicing results in two slightly different chimeric transcripts. The majority of transcripts were the same as the other patients: exon 1 of *DNAJB1* and exons 2-10 of *PRKACA*. They also expressed, at a lower rate, an additional chimera made up of the first and part of the second exons of *DNAJB1*, and exons 2-10 of *PRKACA* (Honeyman et al., 2014). Each of these transcripts were also translated into proteins. This has not been seen in any of the many dozens of other patients we have examined, and it is unknown if there is any physiological consequence of the second minority chimera.

Since this study was published, hundreds more tumors have been sequenced, with the vast majority of them testing positive for the chimera. Whole genome sequencing of ten FLC tumors revealed that there are no other recurrent deletions, amplifications, inversions, single nucleotide variants, or other structural changes in the genome (Darcy et al., 2015). RNA sequencing analysis revealed changes in expression of hundreds of transcripts with upregulation of many oncogenes (Simon et al., 2015).

Expression of the chimeric protein in the livers of mice by CRISPR deletion of the bases between *DNAJB1* and *PRKACA* on chromosome 8 (which is syntenic to chromosome 19 of humans) results in the formation of liver tumors with many of the histological features of FLC, including pale bodies, eosinophilic cytoplasm, and steatosis; however, lamellar fibrosis was not seen (Kastenhuber et al., 2017; Engelholm et al., 2017). These tumors also recapitulated many of the changes of the transcriptome observed in patients' tumors (Kastenhuber et al. 2017). Hydrodynamic tail vein injection of a transposon expressing the chimera also resulted in tumors that were histologically similar to FLC. This indicates that it is the formation of this chimeric transcript that is significant for pathogenesis, not the loss of the genes as a result of the deletion. A transposon encoding chimera with a point mutation that killed catalytic activity was expressed, but had no effect on the cells, demonstrating the importance of the kinase activity. Expression of a transposon expressing *PRKACA* resulted in the formation of atypical hepatocytes that did not fully recapitulate the oncogenic activity of FLC (Kastenhuber et al., 2017). This suggests that overexpression of the kinase activity alone is not sufficient and there is some additional gain of function in the chimeric protein.

While we now have a firm understanding of the genetic underpinnings of FLC, exactly how the presence of the chimera leads to oncogenic transformation remains poorly understood. To examine this, it is important to understand the activity of *PRKACA* in the context of the cell. *PRKACA*, which is the catalytic subunit of protein kinase A (PKA), is usually part of a holoenzyme with two catalytic subunits and two regulatory subunits. This has two effects. First, when the regulatory subunits are bound, they inhibit the catalytic activity. Second, there are four different regulatory subunits: *PRKAR1A*, *PRKAR1B*, *PRKAR2A*, *PRKAR2B*. Each of these regulatory subunits, in addition to engaging the catalytic subunit, also bind to different A Kinase Associate

Proteins (AKAPs). These affect the localization of the holoenzyme in the cell and are frequently found as part of a complex. This is elaborated further below in section 1.2.3.

A few recent papers have put forward speculations on how the chimeric kinase could contribute to pathogenesis. One study put forth some experimental evidence that the first exon of the chimera recruits HSP70, which is a normal partner for HSP40 proteins. The chimera/HSP70 binds with AKAP12, and this scaffold activates the RAF-MEK-ERK pathway (Turnham et al., 2019). However, the experimental design of this experiment calls their results into question: they used AML-12 cells, a non-transformed mouse liver line that was derived from mice overexpressing TGF-alpha (Wu & Fausto, 1994) which activates the RAF-MEK-ERK pathway. Another more recent paper claims that *PRKAR1A*, one of the isoforms for the regulatory subunits that binds to and inhibits *PRKACA*, exists in liquid droplets intracellularly, and that this keeps the enzyme activity localized. When the regulatory subunit was bound to the chimera, the droplet dispersed, which in theory, would result in unlocalized activity (Zhang et al., 2020). Another possibility that has been explored in our lab is that there may be a difference in substrate specificity between *PRKACA* and the chimera, which would potentially activate signaling pathways not typically activated by *PRKACA*. Finally, another possible contributor to transformation is that expression of chimera in FLC tissue is increased relative to normal levels of *PRKACA* (Honeyman et al., 2014), which results in increased catalytic activity (copy for copy, we tested recombinant *PRKACA* and chimera, and there was no significant difference in their activity when tested on a classic substrate of *PRKACA*, Kemptide). This increased expression is likely due to the chimera being driven by the promoter for *DNAJB1* and in normal liver, expression of *DNAJB1* is higher than *PRKACA* (Fagerberg et al., 2014).

1.1.5 Models for Studying FLC

Until recently, there has been a dearth of relevant models to study FLC. Slowly, as we begin to learn more and more of the genetics underlying FLC, several models have been made and are in use in our lab.

In vivo

The animal model created by CRISPR/Cas9 deletion that recapitulated the deletion seen in FLC is difficult to use in practice, given the length of time it takes for tumors to develop in those mice. In both of those studies, it took over a year from when the CRISPR was injected until formation of tumors was seen. In addition, since these tumors are intrahepatic, it is very difficult to know when the tumor has begun to form unless the mouse is sacrificed. Thus, without any further modifications to this protocol, this model is a difficult tool to use for many of the experiments. There is one additional, and critical constraint of this genetically engineered mouse model: It creates the mouse chimeric gene, the mouse transcript and the mouse protein. Much of the emphasis of this work will be on developing therapeutics that target either the human protein or the human transcript. Thus, this genetically engineered mouse model would not be helpful.

Another FLC mouse model, developed by Gadi Lalazar in our lab, is patient derived xenografts (PDX) formed by taking fresh tumor pieces from tumor resections and implanting them subcutaneously or intra-hepatically in immune compromised (NSG) mice. Many of the tumors that were collected from patients did not successfully grow in the mice, but after years of painstaking work, our lab now has several lines growing. As the tumor grows to a large size, the mouse is euthanized, and the tumor is cut up and re-implanted. The reimplanted tumors have a much greater rate of taking, so each line that we have in the lab, has continued for multiple passages.

Importantly, the PDX model has undergone many levels of validation to ensure that the tumors growing recapitulates FLC as much as possible. All of the lines have been validated as follows: by histological comparison with FLC (Figure 1.5), by probing for the presence of chimera at the transcript and protein level (Figure 1.6), and by RNA sequencing analysis comparing changes in the transcriptome to the changes seen in FLC (Figure 1.7).

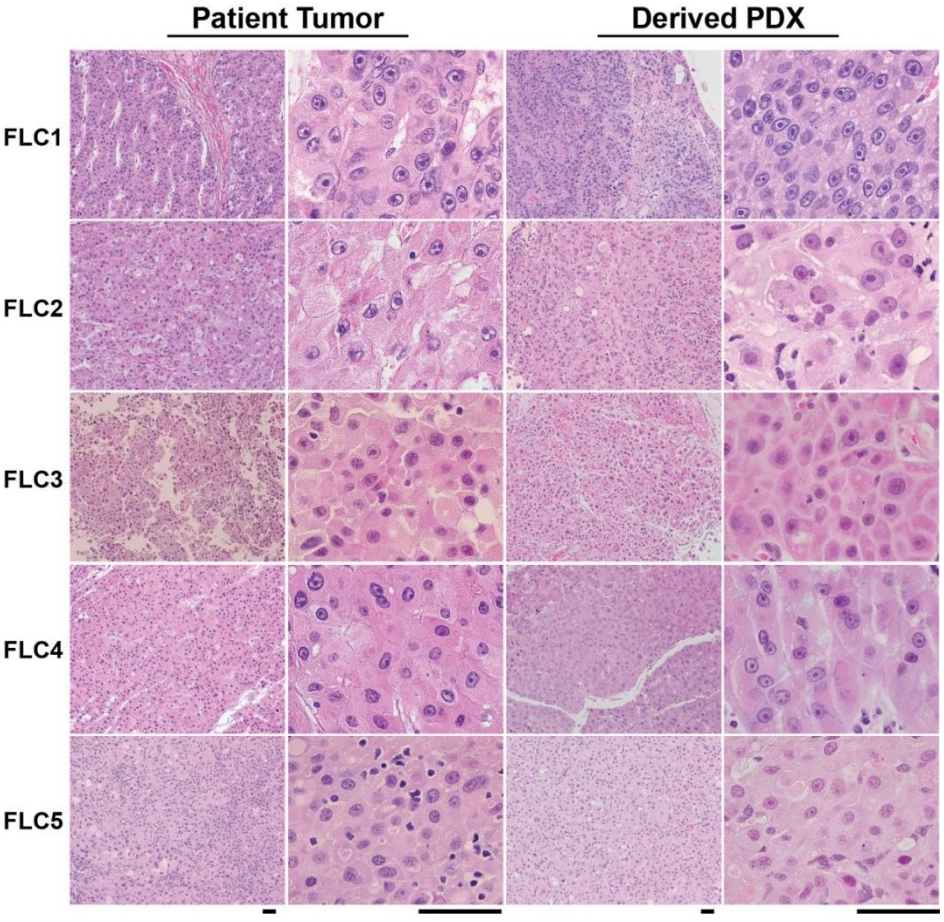

Figure 1.5 Histological comparison of PDX tumors to initial FLC tumors. Gadi Lalazar et al., manuscript in preparation.

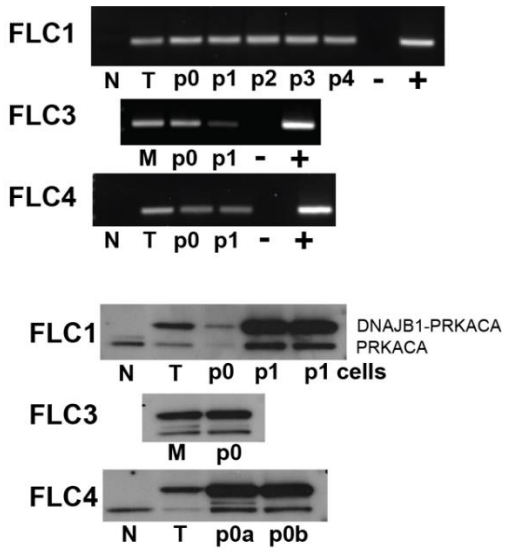

Figure 1.6 Chimeric transcript and protein is present in FLC PDX tumors
Top three are images of gels from RT-PCR with primers that flank the fusion junction. Bottom three are images from immunoblot with an antibody that probes for the c-terminus, which recognizes both *DNAJB1-PRKACA* and *PRKACA.*
Gadi Lalazar et al., manuscript in preparation.

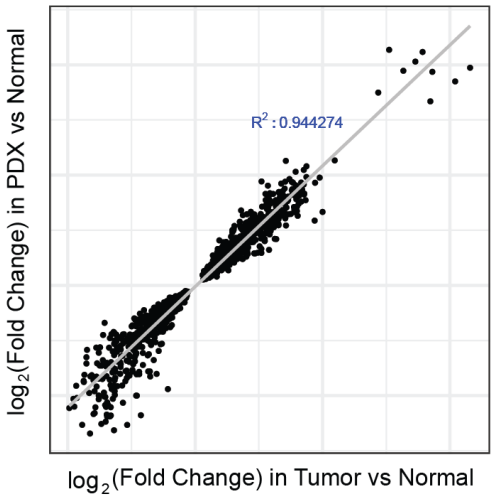

Figure 1.7 Transcriptomic validation of PDX tumors.
Gadi Lalazar et al., manuscript in preparation.

2D Culture

Our lab also has two FLC models for 2D cell culture. The first is an extension of the PDX model: the mouse is euthanized, the tumor is removed, cut up, and digested with collagenase, and the cells are plated on tissue culture plates that are coated with collagen. There are a few weak points with this model: tumor digestion is a very time-consuming process, and these cells do not typically grow in the culture, so passaging is

not possible and each experiment requires a new tumor digestion. In addition, the lack of growth can make it difficult to assess how closely these cells compare to FLC tumor in vivo.

Our second model is simply a liver cancer cell line, Huh7, which has been stably transfected with the chimera driver under the *DNAJB1* promoter. This model is incredibly easy to use, but its validity in recapitulating FLC has not been well characterized. However, the chimeric RNA and protein are expressed well in this line.

3D Culture (organoids)

Another FLC model that we use in our lab are organoids. Like the in vivo PDX models, these organoids are created directly from patient tumors that are collected in the operating room right after resection. The tumors are brought back to the lab, where they undergo digestion and dissociation into single cells. Many FLC tumors do not form organoids well, but through the painstaking work of Nikki Croteau in our lab, we now have several FLC organoid lines. These look morphologically different than normal organoids that are formed from adjacent normal tissue (Figure 1.8). The organoids have also undergone extensive validation and show similar transcriptomic changes as compared to FLC tumors with an R^2 of 0.82 (Figure 1.9).

From a technical standpoint, organoids are not difficult to use for experiments. They do require continued maintenance and passaging, but passaging an organoid culture is a relatively trivial affair. In addition, in contrast to the 2D FLC cells, these organoids grow at a relatively stable pace, which allows us to set up large experiments in a relatively short timeframe.

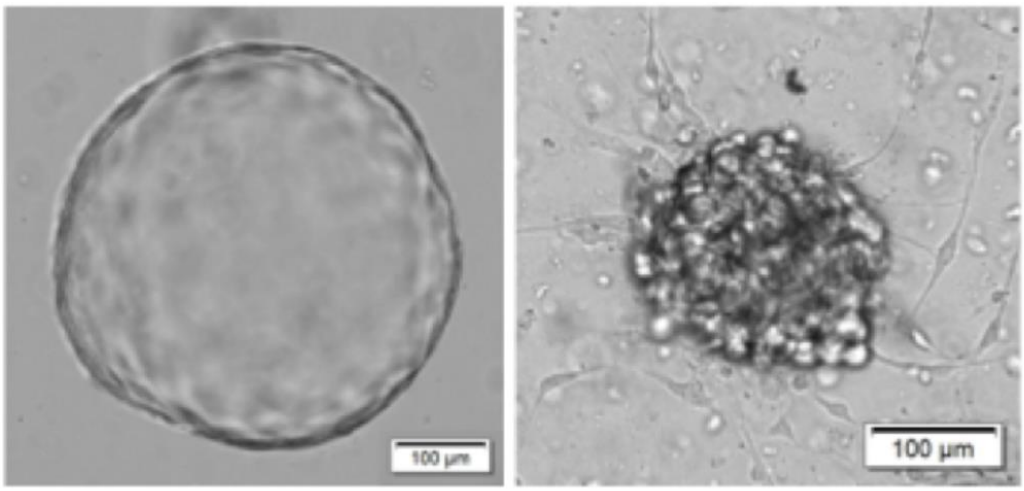

Figure 1.8 Brightfield image of organoids
Left – normal liver organoid. Right – FLC organoid. Nicole Croteau et al., manuscript in preparation.

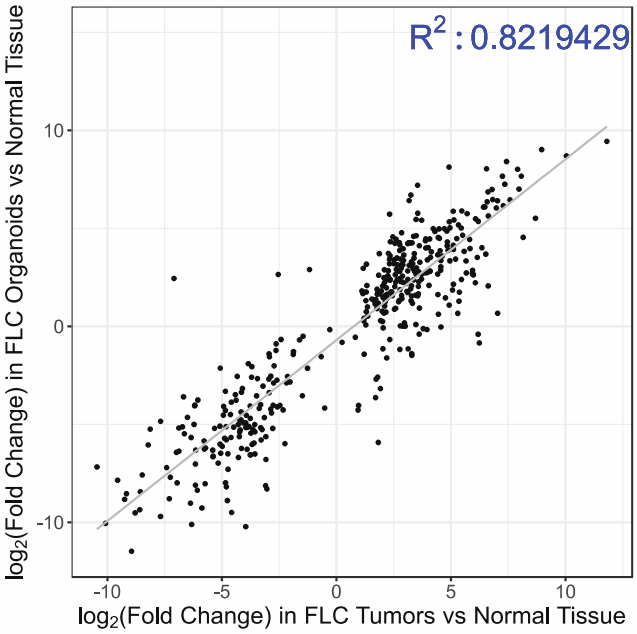

Figure 1.9 Organoid validation at the transcriptome level
Nicole Croteau et al., manuscript in preparation.

1.2 Proteomics

1.2.1 Mass Spectrometry

Mass spectrometry has proven to be a successful tool to probe the proteomic environment of biological tissue (Caldwell et al., 2005; Pardanani et al., 2002; Shruthi et al., 2016). Data from proteomic studies have shown unique proteomic signatures in different tissue, including cancerous tissue from the same organ. These studies can assist in elucidating the mechanism behind cellular transformation, and in some cases may help provide a targetable protein, especially in cases where the oncoprotein is unknown or is a non-feasible target. There are several experimental approaches for this type of study. The most straightforward is a shotgun proteomics experiment, where protein extracted from a tissue lysate is digested with a protease and the peptides are identified and correlated to specific proteins that contain the peptide. This approach allows for relative quantification of a specific protein between two tissues (e.g., cancer versus normal), which can reveal a protein that has a higher expression in the cancer over the normal adjacent tissue.

There are two primary approaches for a shotgun experiment: label free quantification (LFQ) and labelled quantification. In the former, each sample being studied is injected separately on to the liquid chromatography mass spectrometry (LC/MS) system. The samples injected are in peptide form, and they elute from the reverse-phase column by hydrophobicity. As the peptides elute form the column, they

enter the mass spectrometry instrument where they are ionized (via one of several mechanisms – e.g., electrospray), and the mass/charge of the peptide is detected (also via one of several mechanisms – e.g., time of flight). Different peptides may have similar mass/charge, such as peptides with the same amino acids, but with a different sequence. In addition, given the complexity of the sample, there is a lot of other noise on this spectrum (called MS1), which can confound accurate quantitation. Therefore, the peptides undergo a fragmentation event (via one of several mechanisms) and go through another detection. In this second detection (called MS2), each peptide is represented by several peaks – one peak for each fragment of the peptide. In other words, within a single MS1 peak, there are several MS2 peaks. The MS2 spectrum can be identified as a specific peptide based on the known fragmentation pattern of a peptide. This peptide to spectrum assignment is called a peptide spectrum match (PSM), and based on the relative intensity of the PSMs, we can determine the relative amount of peptide, which acts as a surrogate for the protein that contains that peptide. This process is known as LC/MS/MS or tandem mass spectrometry.

For labelled quantitation, I will focus on TMT technology, since that is what we used in our experiments. Tandem mass tags (TMT) are a set of molecules that all have the same chemical structure and the same overall mass. However, there is a different distribution of heavy and light carbons and nitrogens on the molecule (Figure 1.10). These tags have an NHS moiety, which binds irreversibly to primary amines. Once the sample proteins are digested into peptides, each sample is mixed with one of these tags, and then all samples are combined. This peptide mixture undergoes LC/MS/MS. For illustrative purposes, let us follow a peptide that is present in several of the samples. This tagged peptide has the same mass in all of the samples, so it will elute at the same time and it will show up as one peak on MS1. However, during the fragmentation stage, the TMT tag cleaves at a specific “weak spot” built into the molecule. Thus, a piece of the TMT tag is liberated, and at the same time, the peptide is fragmented and will be assigned to the peptide. The liberated piece of the tag (known as the reporter) has a mass that is slightly different between the samples, because the distribution of the heavy carbons on the tag was different between samples. Therefore, once we match the MS2 spectrum to a specific peptide (i.e., via PSM), we then look at the lower molecular weight area on the MS2 spectrum (the reporter area), and we will find peaks at the expected mass/charge of these liberated tags. The intensities of the reporters allow us to quantitate this peptide between the samples.

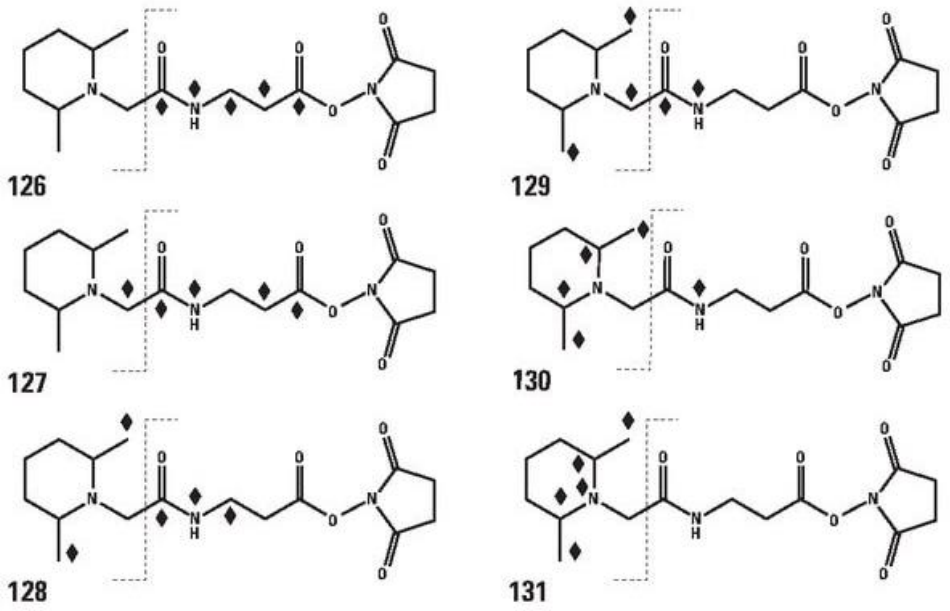

Figure 1.10 TMT tags chemical structure
Mass tags for the Thermo TMT 6plex system. Diamonds signify heavy atoms. Dashed lines signify the “weak spot” that is expected to fragment between MS1 and MS2 detection. The right side of the molecule is the amine reactive NHS moiety. The portion of the molecule to the left of the dashed lines is the reporter once the molecule is fragmented. Overall number of heavy carbons and nitrogens are the same on all 6 molecules; number of heavy carbons and nitrogens are different on the reporter part of the molecule. The numbers signify the expected mass/charge for each reporter.
Image from http://Fishersci.com

There is a slight confounder when we use TMT: other peptides that co-isolate at the same mass/charge on MS1 also have tags on them. Usually, we can ignore the peaks on MS2 that do not belong to the peptide assigned to that MS2. But here we are focusing on the liberated tags, and it is impossible to distinguish from which peptide the tag came from. For most peptides, this co-isolation issue is minor and doesn’t contribute much intensity to the tags; however, it is sufficient of a problem for some peptides, that a strategy has been created to overcome it, namely, MS3. For MS3 level quantitation, an n-terminal fragment with a tag that “survived” fragmentation (i.e., it still contains the intact tag) before MS2 analysis is selected and fragmented again. This filter that brings in this fragment to MS3 can filter on-the-fly (synchronous precursor selection) and only brings in fragments that meet its algorithm. At the MS3 level, only fragments from the peptide of interest (i.e., the peptide that has its PSM on the MS2 spectrum) that contain the full tag get fragmented and analyzed. Therefore, only the intensity of the reporters from this peptide gets analyzed. There is a cost to this approach, however: some peptides do not have fragments with tags that make it through the SPS filter, so there is a loss in sensitivity with this approach.

1.2.2 Absolute Quantitation of Proteins

While shotgun proteomics allows one to relatively quantify the amount of a protein between two different samples, this approach does not allow for quantification of different proteins in the same or other tissue, since different peptides ionize better than others, which would skew the intensity in favor of that peptide. There are many strategies available to overcome this and to accurately quantitate on an absolute level. I will introduce two of these techniques here.

In one strategy, we use peptide standards from the protein of interest. Peptide standards need to meet the following criteria: The sequence needs to be unique to the protein of interest, it needs to be a peptide that would result from digestion of the protein of interest, and it needs to be a peptide that ionizes and fragments well. The latter criterion can be assessed empirically from large proteomics dataset, though there are some tools that can assess this in silico. The chosen peptides are then synthesized with a lysine or arginine that is labelled with a stable heavy isotope. All peptides from a digestion have a lysine or arginine at the c-terminus since trypsin cleaves at the c-terminus of those residues.

A known amount of these heavy peptides is spiked into the sample. The stable isotope peptide can be detected separately from the peptide of interest even though they are mixed together, due to differences in mass/charge. As both peptides will be ionized with equal strength, the peptide of interest can be normalized to the known amount of the spiked heavy isotope labeled peptide. This quantification of the peptide, assuming the peptide is unique to the protein of interest, can be used as a proxy for the quantity of the protein of interest.

The second technique for absolute quantitation is conducted by using whole recombinant protein standards. These proteins are digested separately from the samples. The protein digests are then serially diluted, and each dilution is tagged with TMT. The protein digests from the samples are each tagged as well. They are then combined together and undergo LC-MS/MS-SPS-MS as described above.

1.2.3 Protein Kinase A

In the PKA system, as mentioned earlier, there are four isoforms of the regulatory subunit: RIα, RIβ, RIIα, and RIIβ. Each has variable expression in different tissues, with *PRKAR1A* having the highest expression globally, including in the liver. *PRKAR1B* and *PRKAR2B* have relatively low expression globally, though they do have tissue-specific increased expression in the brain and adipose tissue, respectively (Fagerberg et al., 2014). A more recent report has demonstrated that on the protein level, the dominant regulatory isoform in the liver is actually RIIα (Walker-Gray et al., 2017). This discordance between gene expression and protein level is not surprising, as gene expression in general does not necessarily correlate and cannot be used as an accurate marker for protein level (Shruthi et al., 2016). There are also four isoforms of the

catalytic subunit: Cα (the isoform that is in fusion with *DNAJB1* in FLC), Cβ, Cγ, and Cx. Cα and Cβ are the dominant ones in the liver. Cγ is primarily expressed only in the testes.

PKA holocomplexes are generally classified as Type I or Type II PKA complexes, where Type I refers to a complex with either RIα or RIβ and one of the catalytic subunits, and Type II refers to a complex with either RIIα or RIIβ and one of the catalytic subunits. Type I and Type II PKA complexes have distinct roles in the cell, and this uniqueness is maintained primarily via localization with specific AKAPs (A-kinase associated proteins), which are membrane-bound scaffolding proteins, that have stronger binding affinities to one of the regulatory subunit isoforms (Di Benedetto et al., 2008).

There are several studies concerning the question as to how the catalytic subunit remains localized to the PKA specific areas after it is dissociated from the regulatory subunits when cAMP binds to them. One study recently demonstrated with quantitative immunoblotting that the regulatory subunits are in ~17-fold molar excess of the catalytic subunits, which may contribute to the immediate recapture of the catalytic subunit immediately after it completes its catalytic activity (Walker-Gray et al., 2017).

Other mutations in the PKA system are seen in other tumors. For example, a mutation of L206 to arginine on *PRKACA* affects its binding to the regulatory subunit, thus causing the catalytic subunit to remain constitutively active (Goh et al., 2014). This has been shown to be an important pathogenic mechanism in adrenal adenomas, which is the mechanism behind Cushing's disease. In addition, mutations in *PRKAR1A* have been implicated in Carney complex, a multi-organ neoplastic disease (Kirschner et al., 2000). Notably, FLC has been seen as part of the complex in some patients. Indeed, an FLC sample from three patients with Carney complex has been shown to harbor the *PRKAR1A* mutation but not the fusion kinase described (Graham et al., 2018). That a mutation in two different subunits in the PKA system can lead to the same phenotypic disease leads us to hypothesize that at least some of the pathogenic transformation in FLC is a result of distorted ratios between the regulatory and catalytic subunit. Thus, one of the projects described in this thesis will measure the absolute quantities of the subunits of the PKA complex in FLC and in adjacent normal tissue.

1.3 Therapeutic Development

While understanding the underlying mechanism of any cancer is crucial, the ultimate need is a cure. There are none currently for FLC. Drug discovery by the pharmaceutical industry is unlikely for this infrequent cancer. Academic discovery, however, can play a significant role in developing therapeutics, especially in the initial discovery process.

1.3.1 Targeting the kinase protein

One strategy that has played a major role in therapeutic development in other kinase-driven cancers is focusing on discovering an oncoprotein-specific inhibitor. This has shown success in several diseases, with the first one shown to work against the fusion kinase that is expressed in chronic myelogenous leukemia (CML), BCR-ABL (Rowley 1973; Buchdunger et al., 1996; Druker et al., 1996). Structurally, there are three important similarities between *DNAJB1-PRKACA* and BCR-ABL at the protein level. First, each kinase has another protein fused to its amino terminus. Second, as a consequence of that fusion, their amino terminal glycine is not myristoylated. Third, a hydrophobic myristate pocket that is usually filled with the N-terminal myristate in the native kinase is unoccupied in the fusion kinase. Imatinib, a small molecular inhibitor of the active site of the BCR-ABL kinase, has shown incredible results in patients with CML: 5-year survival in patients with CML increased from about 60% in interferon-treated patients to 89% in imatinib-treated patients (Druker et al., 2006). Imatinib is specific for the mutated fusion kinase and does not inhibit the native ABL kinase. Unfortunately, the active site of the *DNAJB1-PRKACA* chimeric kinase is very similar to the active site of the wild type *PRKACA*, though there may be some subtle differences that may allow for the development of a specific inhibitor of the chimeric kinase. More recently, allosteric inhibitors of BCR-ABL (GNF-2, GNF-5, ABL001) have been developed that inhibits the kinase by binding in the hydrophobic myristate pocket (Adrian et al., 2006; Zhang et al., 2010; Wylie et al., 2017). This strategy may prove useful with *DNAJB1-PRKACA* as well.

1.3.2 Antisense oligonucleotides

There have been a number of recent successes of RNA targeting therapeutics, including the FDA approval of the siRNAs patisiran to treat hereditary transthyretin amyloidosis and givosiran for acute hepatic porphyria (Hu et al., 2020), and of several antisense oligonucleotides (ASOs) including mipomersen (familial hypercholesterolemia), etemplirsen (Duchenne's muscular dystrophy), nusinersen (spinal muscular atrophy), fomiversen (CMV retinitis), and inotersen (TTR Amyloidosis). Most recently, in an amazing feat, milosen was created as a targeted therapy for a single patient with a unique genetic mutation causing her particular case of Batten disease (Kim et al., 2019). These successes offer hope that they will facilitate the rapid translation of results from the bench to the bedside. Targeting RNA transcripts has been studied for several decades. It allows for very specific inhibition; even a single nucleic acid point mutation can be targeted, even if the encoded protein structure does not change significantly.

ASOs are single stranded oligonucleotides with a sequence that is antisense to the transcript of interest. There are two main mechanisms that can be employed to modify or inhibit the transcript from translation using ASOs; these include steric hindrance (occupancy-only mediated) and transcript degradation (occupancy-mediated

degradation) (Crooke et al., 2018). The latter is the ideal approach when dealing with deleterious proteins that are not wanted in the cell, such as oncogenes. Mammalian cells express RNase-H, which degrades RNA transcripts when they are bound in a heteroduplex with DNA (Liang et al., 2017); therefore, in theory, binding of a DNA oligonucleotide to the RNA transcript should result in degradation of the transcript (without cleavage of the DNA oligonucleotide). Indeed, there have been many attempts made at using ASOs for therapeutic intervention using this approach; however, there were many obstacles that took several decades to overcome. For one, oligonucleotides are unstable in human serum, due to the presence of exonucleases that rapidly degrade the oligonucleotide. In addition, unmodified oligonucleotides are poorly taken up by cells, thus making it an impracticable approach for intracellular RNA degradation. Over the years of research, these two problems have been reduced, and as mentioned, there are several ASO drugs in clinical use, and many more that are undergoing clinical trials.

The most effective ASO activity occurs when it can elicit RNAse-H mediated degradation, which requires a DNA-RNA duplex to degrade the RNA. Thus, the goal is to modify the ASO so as to optimize RNase-H mediated degradation, maximize resistance to exonucleases, and allow a high concentration of oligo to enter the cell. Therefore, there are several parameters that need to be optimized when selecting the type of ASO.

Length: Shorter ASO cross cell membranes more readily; however, the sequence design of shorter ASOs can be more difficult, since they are more likely to have an overlap, or at least a partial overlap with another existing coding or non-coding transcript. Fortunately, there are some nucleotide modifications that increase the specificity of the ASO to the point where even a single mismatch will result in a large decrease in binding. This allows for shorter ASOs to be used, assuming there are no perfect matches elsewhere in the human transcriptome.

Outer nucleotides: The outer nucleotides of the oligo are modified so as to make it relatively resistant to exonucleases. There are several options for this modification. They include modifying the ribose by adding an O-methoxyethyl or an O-methyl to the 2' carbon or adding an O-methylene bridge between the 2' and the 4' carbon of the ribose. The latter modification forces the sugar into a specific conformer (and is thus termed a locked nucleic acid), which has the advantage of increased potency and specificity; however, this form has shown to hepatotoxic in some cases (Swayze et al., 2007). More recently, the constrained ethyl modification has been developed, which adds a methyl group to the carbon in the O-methylene bridge (Crooke et al., 2018).

Inner nucleotides: The inner nucleotides remain unmodified DNA bases, which will allow it to form a DNA-RNA duplex with the target mRNA, activating RNAse-H degradation.

Distribution of modified and unmodified DNA nucleotides: An ASO that includes modified outer nucleotides and inner unmodified DNA nucleotides is known as a

“gapmer”. Of crucial importance is determining the optimal number of modified nucleotides that flank the inner DNA nucleotides in a gapmer ASO. Increasing the modified outer nucleotides may increase resistance against nucleases but will decrease efficiency of RNAse-H degradation, and vice versa. It has been shown that for a 20-mer ASO, a 5-10-5 distribution is an effective balance. The same has been shown for a 3-10-3 distribution on a 16-mer ASO. At a minimum, RNAse-H requires seven unmodified nucleotides.

Backbone: The backbones of ASOs are typically modified from phosphodiester bonds to phosphorothioate bonds. This modification decreases degradation to some extent and also allows the oligo to bind to plasma proteins (Brown et al., 1994), which has two advantages: it decreases renal elimination, and it helps the oligo cross the cell membrane and enter the cell.

As mentioned, there have been some reports of hepatotoxicity with LNA-modified ASOs. The mechanism of hepatotoxicity is unclear, with some studies reporting an off-target sequence dependent effect (Burel et al., 2016), and others reporting a general non-sequence dependent effect, such as binding of the LNA-modified ASO to hepatocellular proteins (Burdick et al., 2014). There are several LNA-modified ASOs that have been shown to be safe in vivo, including one against HIF-1alpha that underwent a pilot clinical trial with 10 patients; eight patients showed no hepatotoxicity, the other two did develop hepatotoxicity, although one of them had underlying liver disease (Jeong et al., 2014). Two studies have attempted to identify sequence motifs that may contribute to the hepatotoxicity using random-forest algorithms, and they have potentially identified some sequence motifs that are more likely to be problematic. One of these studies tested 236 LNA-modified ASO’s and found about half of them to cause hepatotoxicity (Hagedorn et al., 2013). The other study reported that of the 71 sequences they tested in mice, 51 were hepatotoxic. They found that all of their ASOs that contained the TGC or TCC motif caused hepatotoxicity; however, when they introduced these motifs into a non-hepatotoxic sequence, they only resulted in hepatotoxicity in three out of the five sequences generated, thus removing the possibility of an obligatory causative effect of these specific motifs (Burdick et al., 2014).

1.3.3 Small Interfering RNA

Small interfering RNA (siRNA) are another strategy to target a transcript for degradation. siRNAs take advantage of the mammalian RNA silencing strategy of microRNAs. Pre-miRNA, which are oligomers that usually have at least 42 nucleotides with some internal complementarity allowing for its characteristic stem-loop structure, are exported from the nucleus. In the cytoplasm, Dicer, a nuclease, processes it to a double stranded RNA, usually around 21 nucleotides per strand, with close (but not necessarily perfect) complementarity between the two strands. Dicer loads the “guide” strand (i.e., the strand that is complementary to the target transcript) and discards the other one. Dicer and several other proteins make up the RISC complex, which is now loaded with the guide strand, and when it finds the target RNA, cleaves it.

At a minimum, siRNA needs to be double stranded, so that Dicer can recognize it and load the guide strand. However, the length of the siRNA can be changed. The "classic" siRNA is a 21mer sense strand and a 21mer antisense strand with 19 base complementarity between the strands and 2 base overhangs at the 3' ends. There are two issues to address with this design: 1) Given the symmetry of the siRNA, it is difficult to ascertain which of the two strands will be loaded as the guide strand. Indeed, in most cases, they both will (in different Dicer enzymes); this decreases the number of Dicer enzymes available for loading of the guide strand and can also result in increased off-target inhibition (due to complementarity of off-targets to the sense strand). 2) The product of Dicer processing is a 21mer guide strand. If the siRNA is a 21mer to start with, Dicer will not need to enzymatically shorten the strands. It has been shown that when Dicer does not act as a nuclease, there is less loading of the guide strand to the RISC complex. One study characterized many length options and found that the ideal length for the antisense (guide) strand is 27 nucleotides (Kim et al., 2004). Another study found that if the sense strand is a 25mer and has two of its 3' nucleotides as DNA bases, it introduces a polarity into the siRNA, which forces the 27mer to be the strand that becomes the guide strand, and in addition, there is only a single 21mer product that is formed as the guide strand: When Dicer encounters one of these siRNAs (which are termed "Dicer substrate interfering RNA" (DsiRNA), it cleaves off 6 nucleotides on the 3' end of the 27mer guide strand, resulting in a 21mer strand that is loaded to RISC (Rose, 2005). Thus, we can predict exactly the final sequence loaded on RISC when we work with DsiRNAs.

One of the major differences between ASOs and siRNA with regards to drug development is that ASOs do not require any formulation. The ASO readily crosses cell membranes in vivo. In contrast, the double stranded siRNA cannot cross cell membranes effectively. In vitro, we can deal with this by using a transfection reagent, which is a lipid reagent that surround the siRNA and helps it cross the cell membrane. For in vivo use, however, another strategy needs to be used. Therefore, our siRNA work is done in collaboration with the Heller lab at Memorial Sloan Kettering, where they formulate liposomes to encapsulate the siRNA. Liposomes are an effective and safe formulation to get RNA into cells (Hu et al., 2020).

Chapter 2
Proteomic Analysis of FLC

In this chapter, I will discuss my efforts to characterize the proteome of FLC. All of the work in this chapter was done in collaboration with Soren Heissel and Henrik Molina in the Proteomics Resource Center.

In 2012, the Simon lab established the Fibrolamellar Tissue Repository. To date, this repository has collected tissue, and often serum, from over 130 patients with FLC. Considering how rare this disease is, having access to this tissue gives us and other labs the ability to push the FLC research field forward. Most of these samples are from patients who had resectable tumors and were gracious to allow a piece of the resected tumor to be used for research. In many of the cases, one or several of the members from the Simon lab went to the operating room where the surgery was taking place to ensure that once the samples were resected from the patient, they were immediately placed on ice, cut into small pieces, and either put in media on ice, flash frozen, or frozen in optical cutting temperature compound (OCT) and placed on dry ice for transport back to the lab. The experiments in this chapter were all made possible by the FLC tissue in this repository.

In section 2.1 of this chapter, I will present the proteomic landscape of FLC, which was done by comparing protein levels in tumor to the protein levels in adjacent non-transformed liver taken directly from patients. Since it does not have detectable chimeric transcript, it will be referred to as normal. In addition, since the hallmark of FLC is a fusion kinase, the phosphoproteome was also analyzed and will be presented here. In both cases, a distinct proteomic and a phosphoproteomic signature can be detected by unsupervised clustering analysis.

In section 2.2, a more targeted approach of mass spectrometry was conducted. The purpose here was to quantitatively account for all of the components of the PKA system, in particular, the isoforms of the kinase, the isoforms of the regulatory subunits, and the isoforms of endogenous inhibitors. We hypothesized that finding the quantitative ratio of kinase:regulatory/inhibitor subunits in FLC tumor as compared to adjacent normal liver tissue can provide insight into the pathogenesis. I will present results for one technique that was used to quantify this system and describe potential pitfalls of this technique. Then, I will demonstrate the process of a newer, more robust technique that is underway in the lab. This newer technique requires the purification of all the proteins that are being quantitated, so I will present progress to date on this front.

2.1 The proteomic and phosphoproteomic landscape of FLC

2.1.1 The proteome

For this experiment, we chose tumor and adjacent normal liver samples from eight patients. We avoided samples that we knew were not placed on ice immediately

after resection. We used TMTpro 16plex technology (see Chapter 1.2.3), which allowed us to analyze all 16 samples in a single experiment. Following digestion, reduction, and alkylation of all 16 samples, the peptides were TMT-tagged and then combined into a single sample, which was run through a metal affinity column for phosphopeptide enrichment. The flowthrough from this enrichment was used for proteomic analysis. The elution was used for phosphoproteomic analysis, described in section 2.1.2. A schematic of this process is illustrated in Figure 2.1.

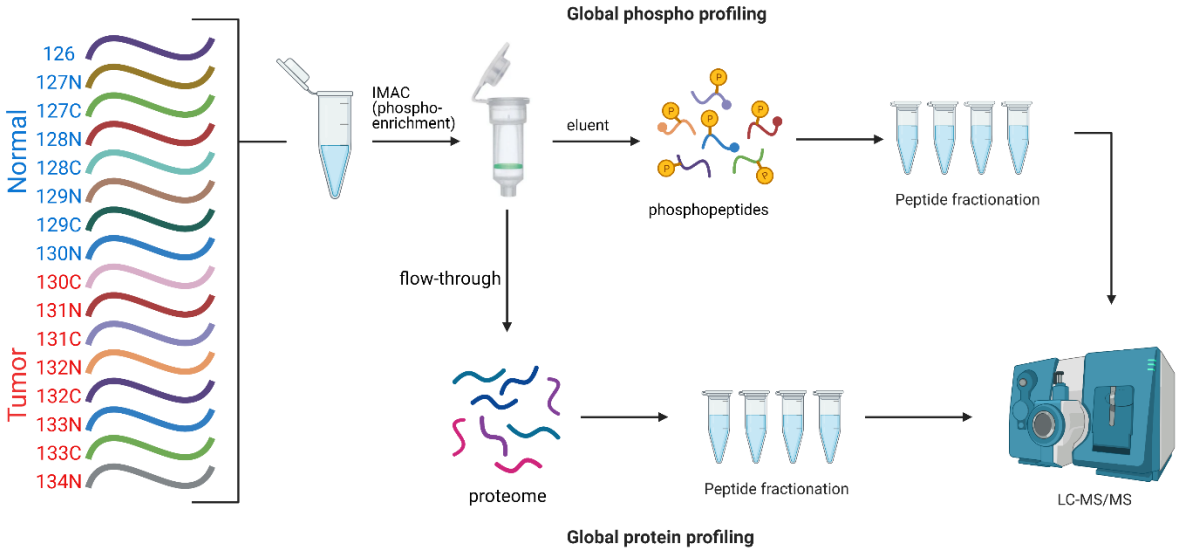

Figure 2.1 Schematic of experimental protocol for proteomic analysis
Peptide digests from eight tumor and eight normal samples are tagged with TMT tags and combined. The sample undergoes phosphopeptide enrichment. The flowthrough is analyzed as the unmodified proteome. The eluent is analyzed for phosphopeptides. Image is modified from Navarrete-Perea et al., 2018.

Principal component analysis revealed two clear distinct clusters which were predominantly tumor and normal (Figure 2.2). However, there was one exception: the tumor sample from patient 4 was within the cluster of normal samples. When I joined the lab, I started to routinely test every sample of tumor, and when available, the adjacent tissue, with RT-PCR for the presence of the chimeric transcript of DNAJB1-PRKACA. Given that this sample came into the tissue repository before I joined the lab, it did not have the RT-PCR validation. Therefore, I performed our standard validation on this sample, and the sample was negative for the fusion kinase (Figure 2.3). The other tumor samples were positive for the chimera, either by RT-PCR (Figure 2.4) or for some of the older samples, by RNA sequencing analysis. Upon reaching out to the facility where this sample was collected, we learned that upon subsequent histopathological

analysis of the patient's tumor the tumor was deemed to be HCC and not FLC. We had collected the sample prior to this analysis. For all future analyses on this proteomics dataset, sample 4T was excluded.

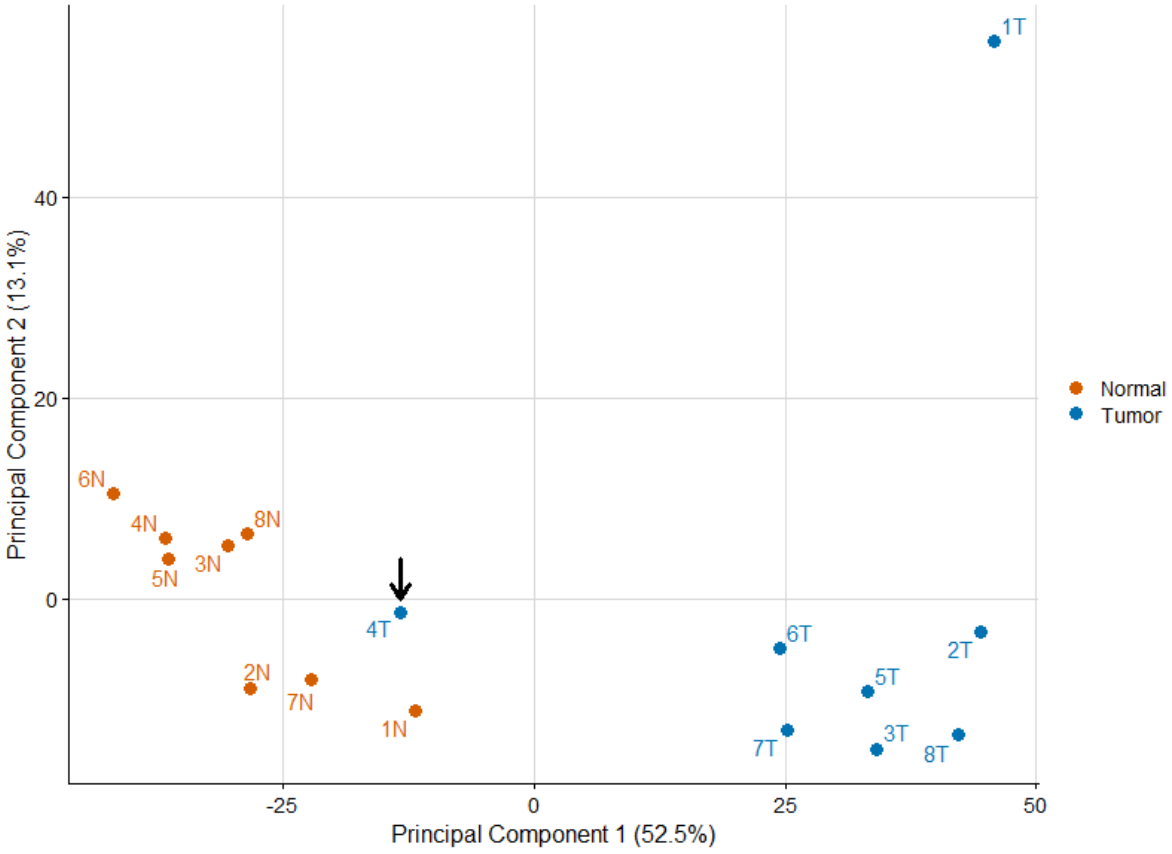

Figure 2.2 Principal component analysis of the proteome
Two distinct clusters can be seen. Sample 4T (arrow) was found to be negative for the *DNAJB1-PRKACA* fusion transcript.

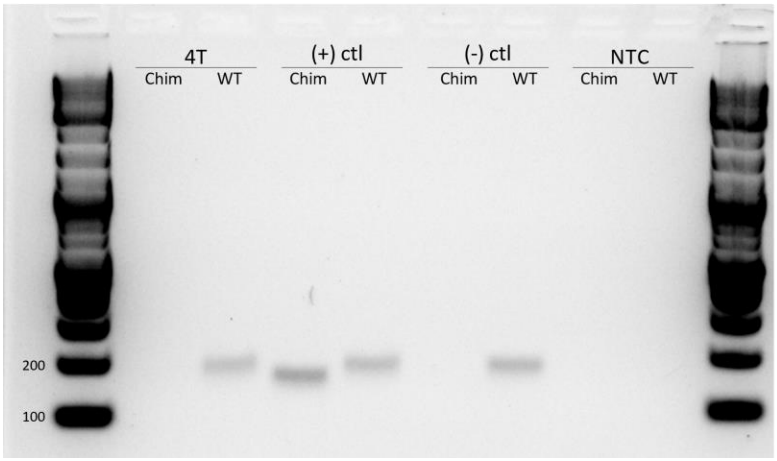

Figure 2.3 RT-PCR of the tumor sample from patient 4.
(+) ctl is RNA from a PDX tumor sample. (-) ctl is RNA from a normal liver sample from a non-FLC patient. NTC is a no RNA template control. Chim is RT-PCR for *DNAJB1-PRKACA* (expected amplicon: 160 bp), WT is RT-PCR on *PRKACA* (expected amplicon: 184 bp)

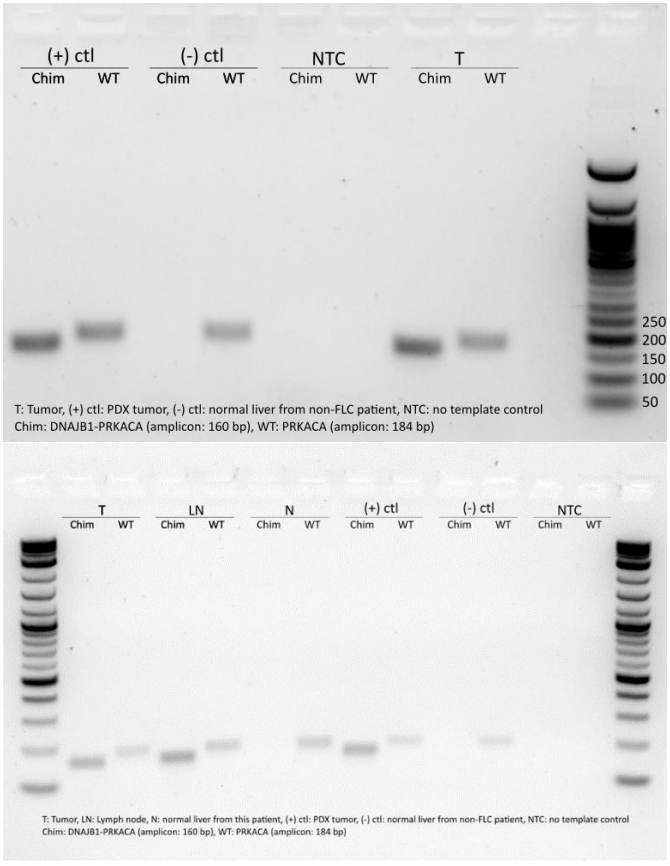

Figure 2.4 RT-PCR of tumor samples from two other patients.
(+) ctl is RNA from a PDX tumor sample. (-) ctl is RNA from a normal liver sample from a non-FLC patient. NTC is a no RNA template control. LN is lymph node. N is the adjacent non-transformed liver (Normal). Chim is RT-PCR for *DNAJB1-PRKACA* (expected amplicon: 160 bp), WT is RT-PCR on *PRKACA* (expected amplicon: 184 bp)

The total cumulative number of proteins detected among all 15 samples was 4650. For differential protein expression, when including proteins that have a $\log_2$ fold change of 0.585 (fold change of 1.5) or greater, and an adjusted p-value less than 0.05, 15% (703 proteins) were increased in expression in tumor samples and 18% (838 proteins) were decreased in expression in the tumor relative to the adjacent normal liver samples (Figure 2.5).

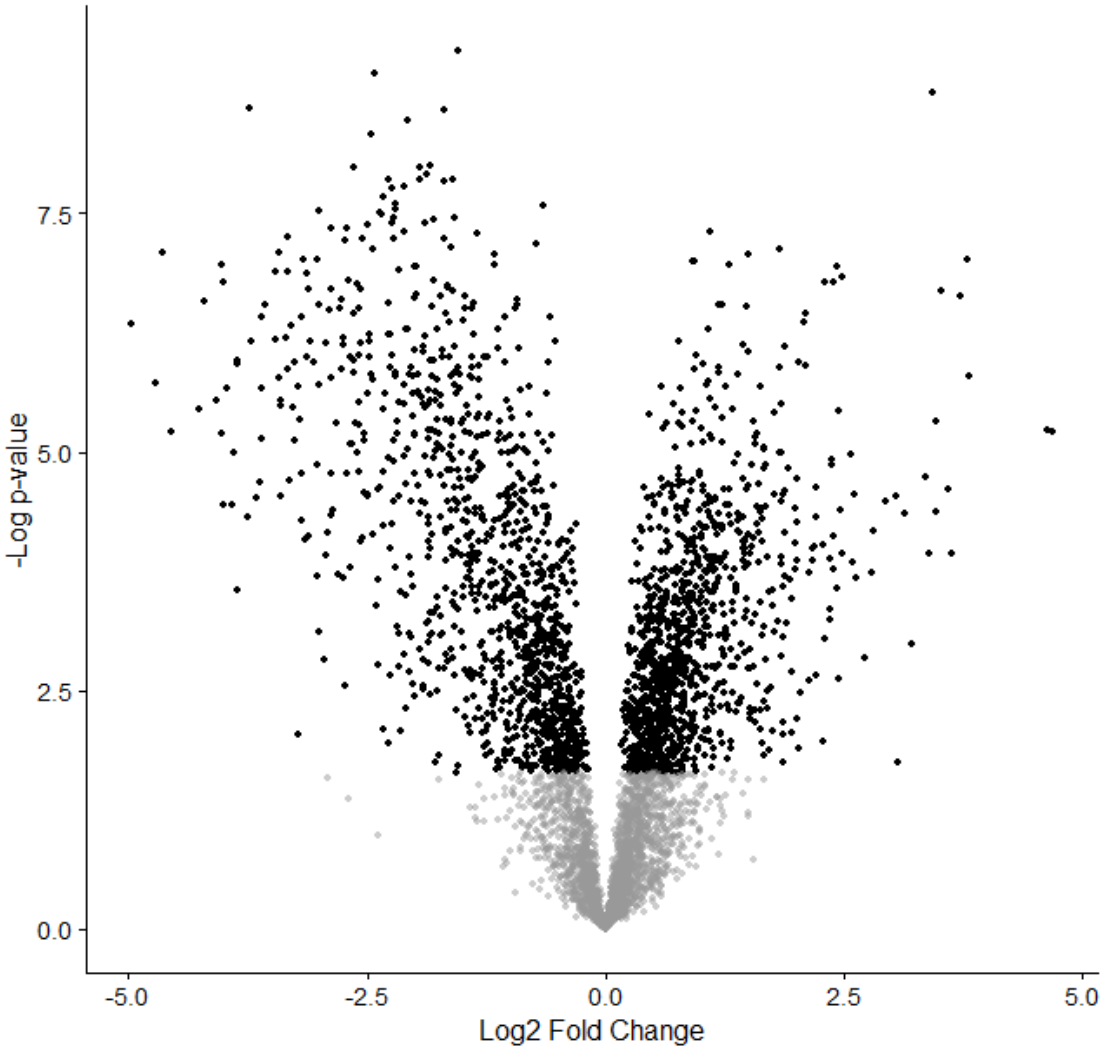

Figure 2.5 Volcano plot showing differential protein expression
Each point represents a protein. Black points are those that are significant at an FDR of 0.05. The proteins on the right have a higher expression in FLC tumor; those on the left have a higher expression in normal liver.

Of the many proteins that are deregulated in FLC, there are several that belong to a particular pathway that is of clinical interest to FLC: the urea cycle. One common cause of morbidity and mortality in patients with FLC is hyperammonemic encephalopathy, a condition that results from a buildup of ammonia in the blood. Ammonia is a breakdown product of proteins and it is usually metabolized in the liver, by conversion to a compound, carbamoyl phosphate, which then combines with ornithine to make citrulline. Through a series of reactions, the ammonia molecule is released from arginine as urea, which is water soluble and excreted by the kidneys.

Ornithine has three fates: 1) It can join carbamoyl phosphate to make citrulline via ornithine transcarbomylase and contribute to the urea cycle, 2) it can convert to Pyrroline-5-carboxylate (P5C), which is an intermediate in one pathway to form glutamate or proline, and 3) it can be used in the synthesis of polyamines, like spermine and putrescine, via ornithine decarboxylase (Figure 2.6). Of the 17 proteins that were upregulated with a log2 fold change greater than 2.5, three of them were centered around P5C (OAT, PYCR1, and PRODH) (Figure 2.7).

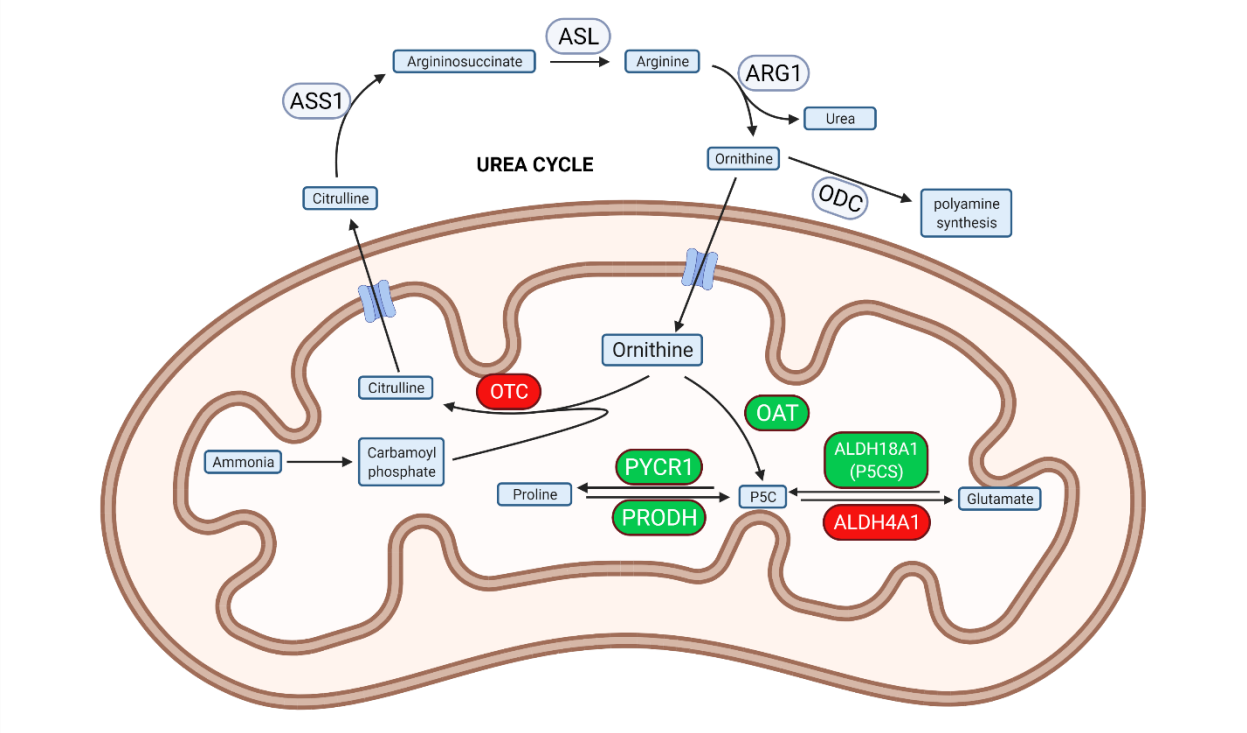

Figure 2.6 The urea cyle and related pathways
Enzymes in green and red are upregulated and downregulated in the proteomics dataset, respectively. Enzymes not highlighted by color are either not significantly differentially expressed (ASS1, ASL, ARG1), or weren't detected in this experiment (ODC).

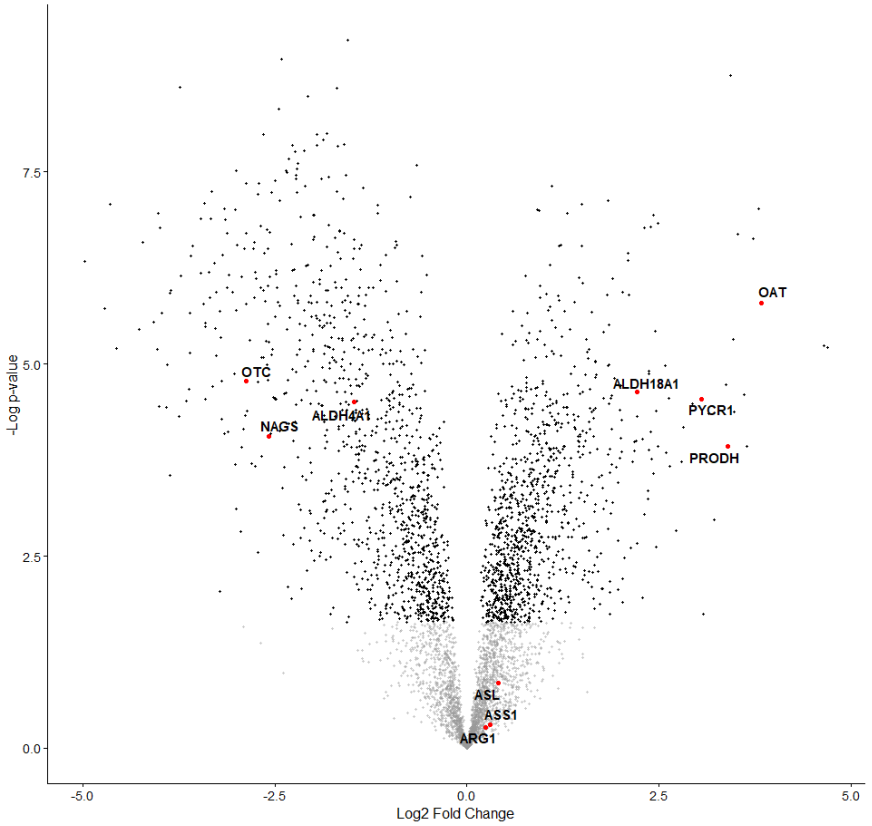

Figure 2.7 Volcano plot with urea cycle enzymes highlighted

ODC may be acting as a sink to divert ornithine away from the urea cycle in the rest of the liver. It has been proposed that since ODC is upregulated by c-myc, which is upregulated by PRKACA, this may be the mechanism for hyperammonemia in FLC (Surjan et al., 2018). However, we do not have the data to show whether ODC is higher on the protein level. Our RNA sequencing data shows a non-significant difference of ODC between tumor and normal. Given the greatly increased OAT in this experiment, OAT can also be acting as a sink to divert ornithine away from the urea cycle.

Unsupervised hierarchical clustering of the proteins that were significantly up or downregulated was consistent with the PCA (Figure 2.8): all of the tumor samples clustered together and away from all of the normal samples.

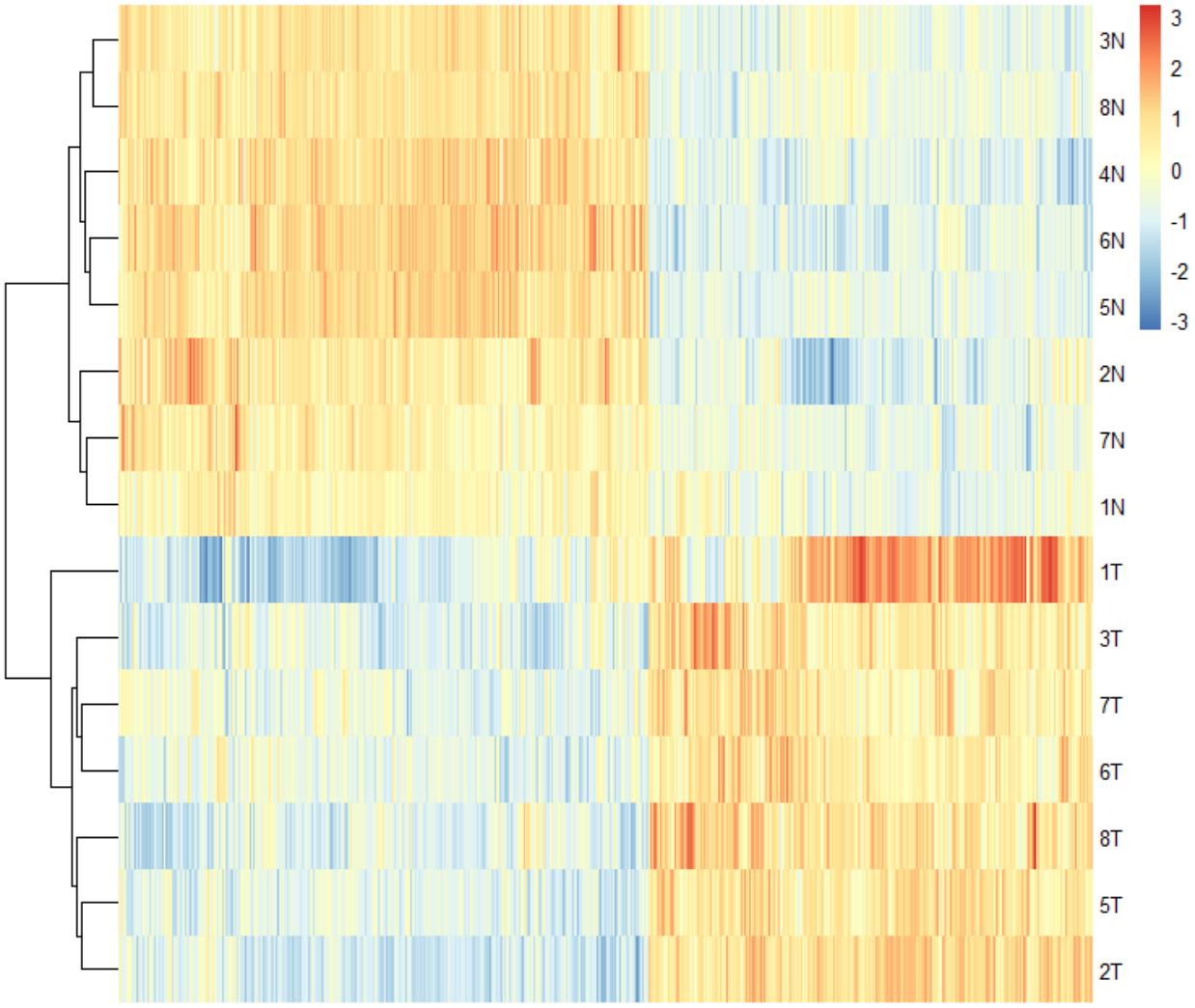

Figure 2.8 Hierarchical clustering of proteins deregulated in FLC

2.1.2 The phosphoproteome

The metal affinity column binds to phosphopeptides and the elution from the column was analyzed separately from the other peptides with LC-MS/MS. Among all samples, 6661 phosphopeptides were detected from 2637 proteins. At an FDR of 0.05, 1050 phosphosites were up in tumor and 1030 phosphosites were down (Figure 2.9). Principal component analysis again shows clustering of tumor and normal samples among themselves (Figure 2.10), with the exception, as with the proteome, of sample 4T. The phosphome of tumor 4T, as with the proteome of 4T, clustered with the normal tissue. Since we had shown that 4T was not fibrolamellar, it was excluded from subsequent analyses. However, it raises the interesting possibility that both the proteome and phosphohome of FLC are distinct from not only normal but also from HCC.

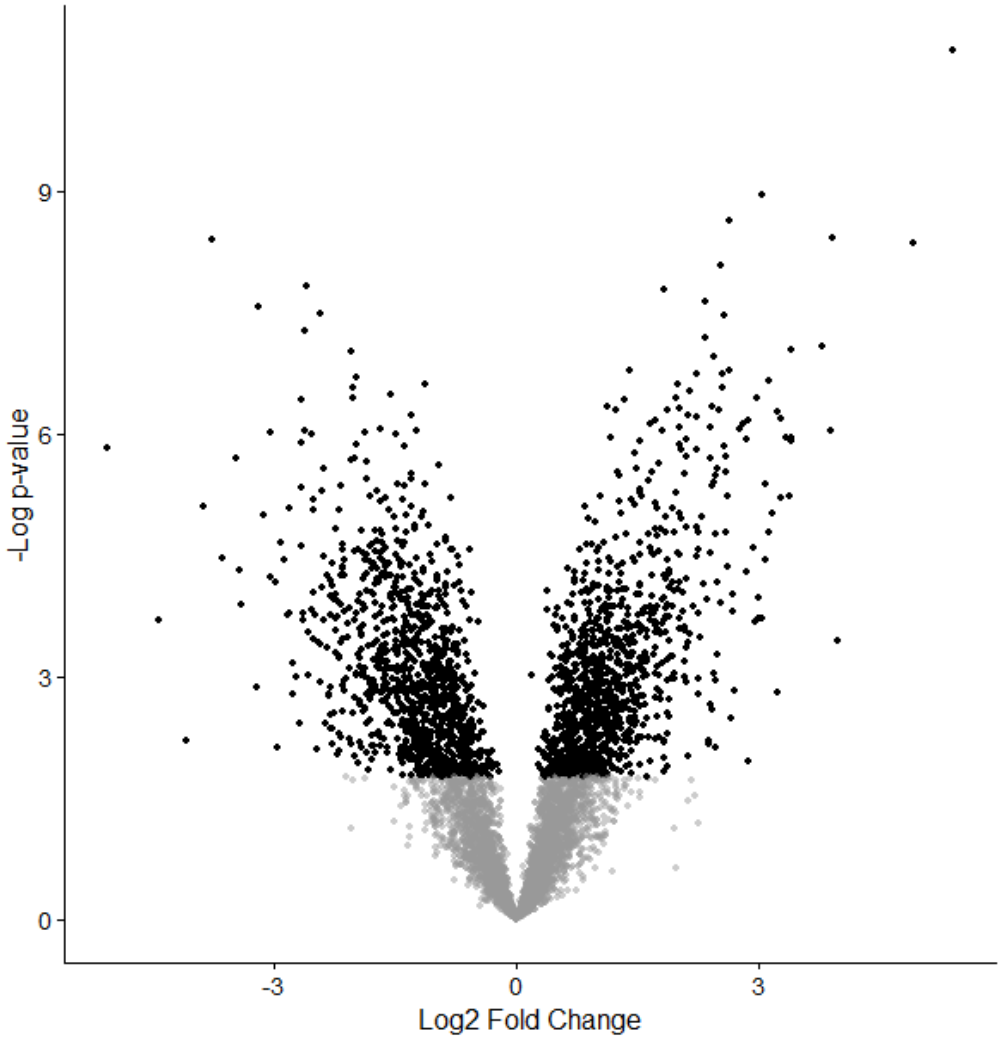

Figure 2.9 Volcano plot showing phosphosite deregulation in FLC
Each point represents a phosphopeptide. Black points are those that are significant at an FDR of 0.05. The phosphopeptides on the right are higher in FLC tumor; those on the left are higher in normal liver.

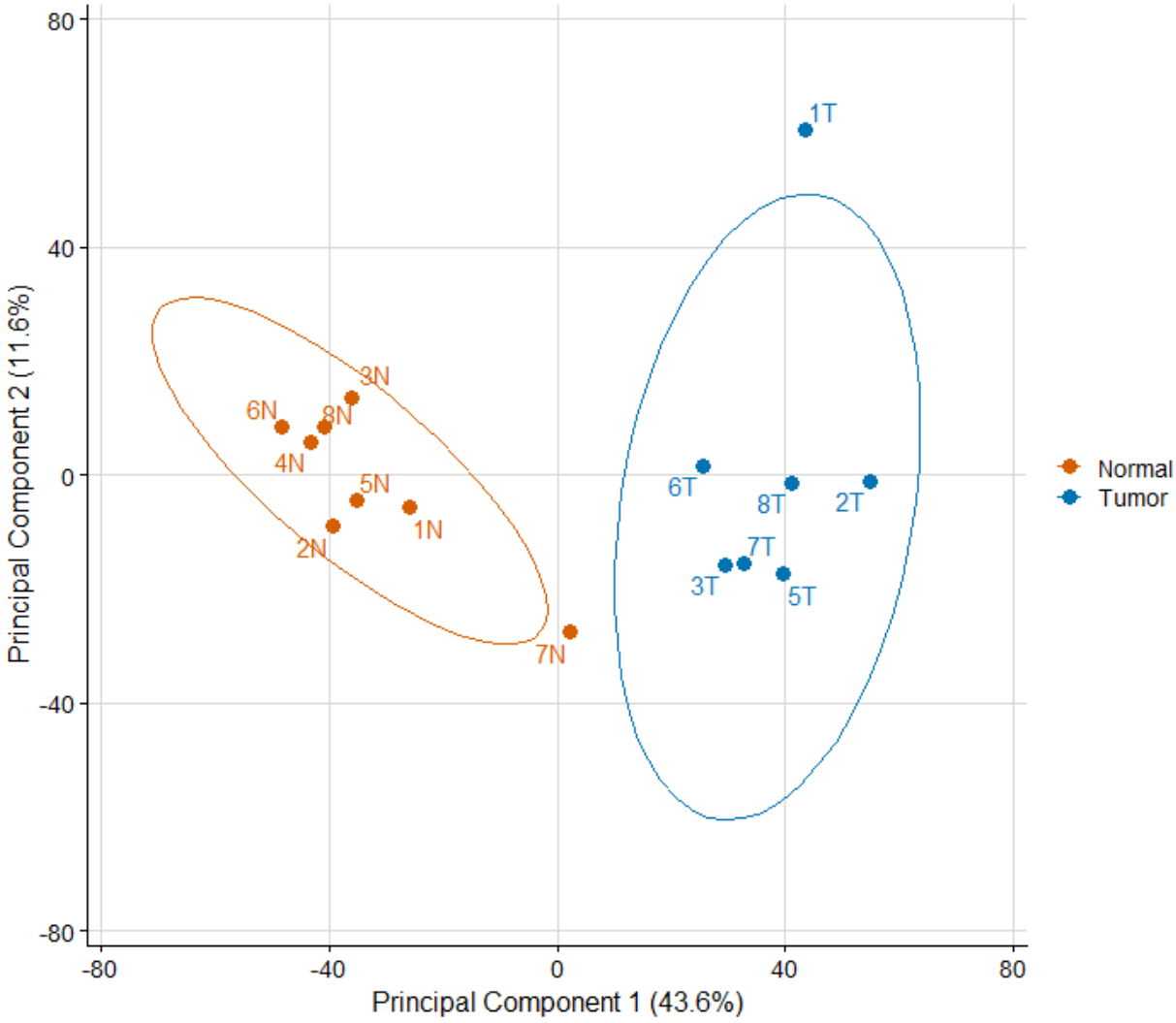

Figure 2.10 Principal component analysis of phosphosites in FLC and normal liver

An increase in the detection intensity of a phosphopeptide of a protein could reflect an increase in phosphorylation of that phosphosite. Alternatively, it may reflect an increase in the cellular levels of that protein, either as a result of increased transcription, more efficacious translation, or decreased degradation. Conversely, a decrease in the detection intensity of a phosphorylated phosphosite of a protein can reflect increased phosphatase activity, or decreased protein levels as a result of increased protein degradation, decreased transcription or decreased efficiency of translation.

The altered levels of phosphosites may be consequential for the pathophysiology, independent of mechanism. To further characterize these changes, I evaluated the levels of phosphorylation of the phosphosites as a function of the levels of expression of the protein in the FLC tumor and in the adjacent non-transformed tissue. In general, there was a positive correlation between extent of phosphorylation and level of protein expression. By linear regression, we see a positive correlation with an R^2 of 0.50 (Figure 2.11).

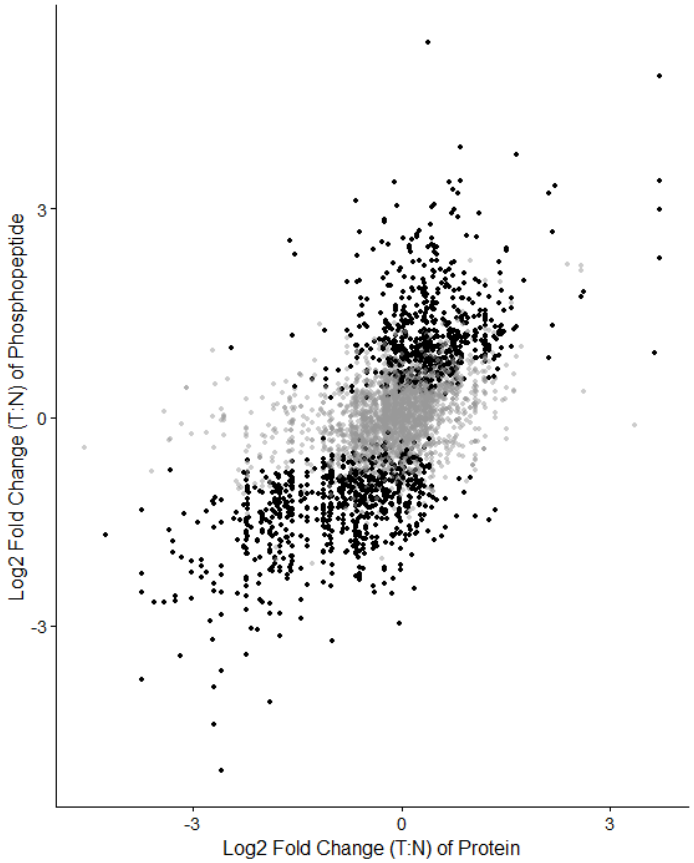

Figure 2.11 Scatterplot of phosphosites versus protein differential expression
This plot compares changes in detected phosphorylation by mass spectrometry for individual proteins to changes in the levels of the proteins that contain that phosphosite. The grey points are phosphosites that were not significantly different at an FDR of 0.05. These phosphosites were excluded from the correlation analysis. Several vertical lines of points can be seen; these are phosphosites that belong to the same protein and therefore have the same x-value, but there was differential change in the phosphorylation of different sites.

I used three proteins to illustrate these different relationships between protein levels and number of phosphopeptides (Figure 2.112). For VCAN, four phosphopeptides were detected and were upregulated in tumor relative to normal. However, upon analysis of the proteome, the VCAN protein was upregulated by a similar amount. While there is clearly an increase in the number of phosphopeptides, which may affect physiology, it appears to be the result of increased amount of protein In contrast, WARS^{Ser467} was the phosphosite with the greatest increase in the detection intensity in the whole dataset with a $\log_2$ fold change=5.4 and an adjusted p-value of 1.8E-11. At the protein level, however, there is no significant change in expression of WARS between tumor and normal. Finally, CFL2^{Ser23} is an upregulated phosphosite in tumor ($\log_2$ fold change of 2.34), while the CFL2 protein is expressed at a lower level in tumor relative to normal ($\log_2$ fold change of -1.54).

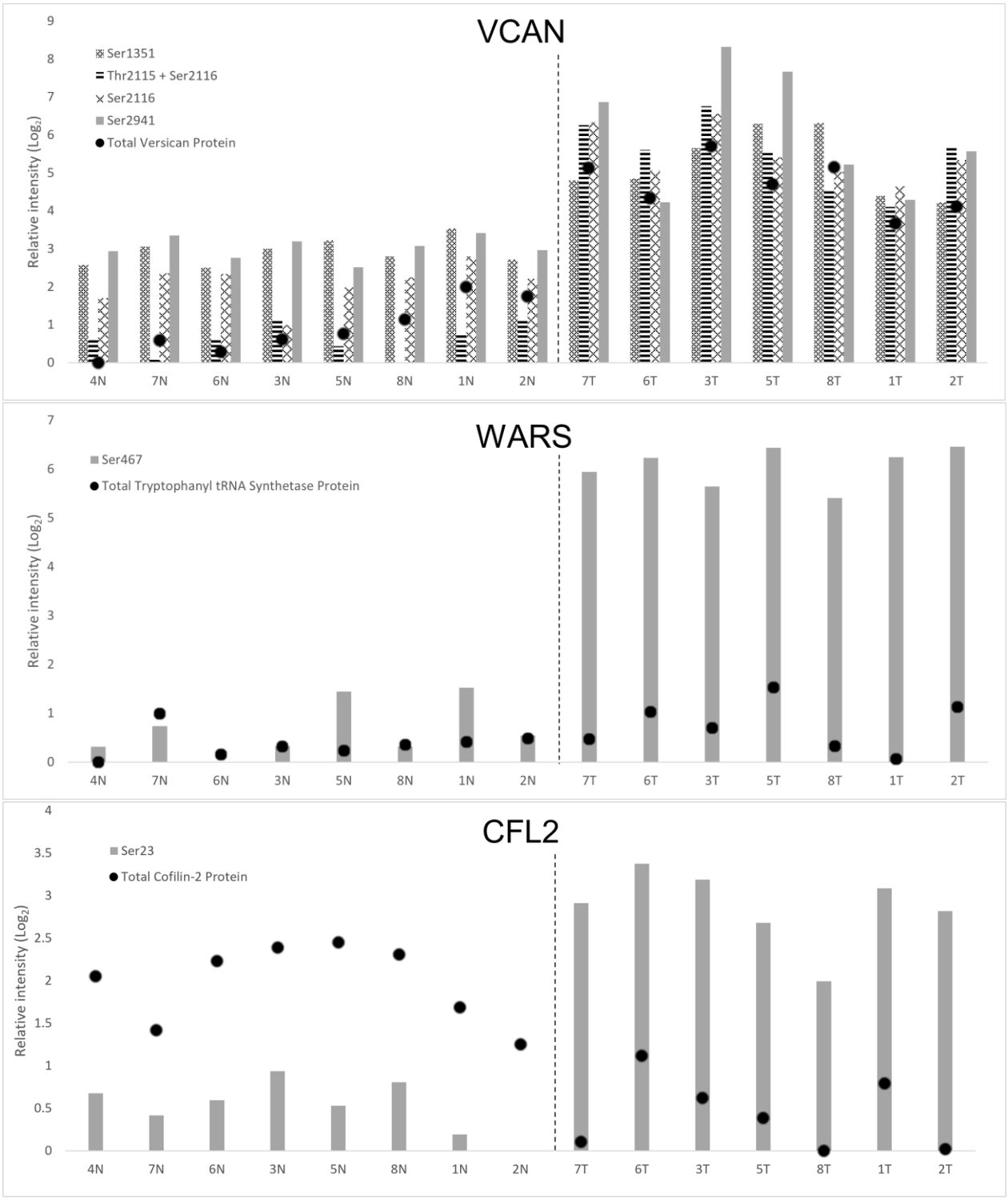

Figure 2.12 Relationship between phosphosite(s) and protein expression for 3 proteins For versican, four phosphopeptides were detected. One of them was diphosphorylated at Thr2115 and Ser2116. That same peptide was detected with only Ser2116 phosphorylated. Note: The relative intensities for total protein were calculated separately from the relative intensities for phosphopeptides and should not be compared to each other.

I further characterized the phosphoproteome by creating a PCA graph on the normalized intensity values (Figure 2.13). I did this normalization by subtracting the $\log_2$ intensity value for each protein from the $\log_2$ intensity value for all phosphosites of that protein for each of the 15 samples. The PCA for this matrix looks similar to the PCA for the non-normalized phosphosites (Figure 2.10). However, sample 1T, which was separated from the tumor cluster in the second component, clusters with the other tumor samples far better in this new analysis. It is possible that the separation of 1T in PC2 is due to a difference in protein expression, but from a phosphorylation standpoint alone, 1T is more similar to the other tumor samples. This would explain why 1T is separate from the other tumor samples when analyzing the proteome (Figure 2.2). Another possibility is that the phosphosites not included in this analysis (due to the proteins not being detected in the non-phosphorylated proteome experiment) were a cause of this second component separation of 1T from the rest of the tumor samples.

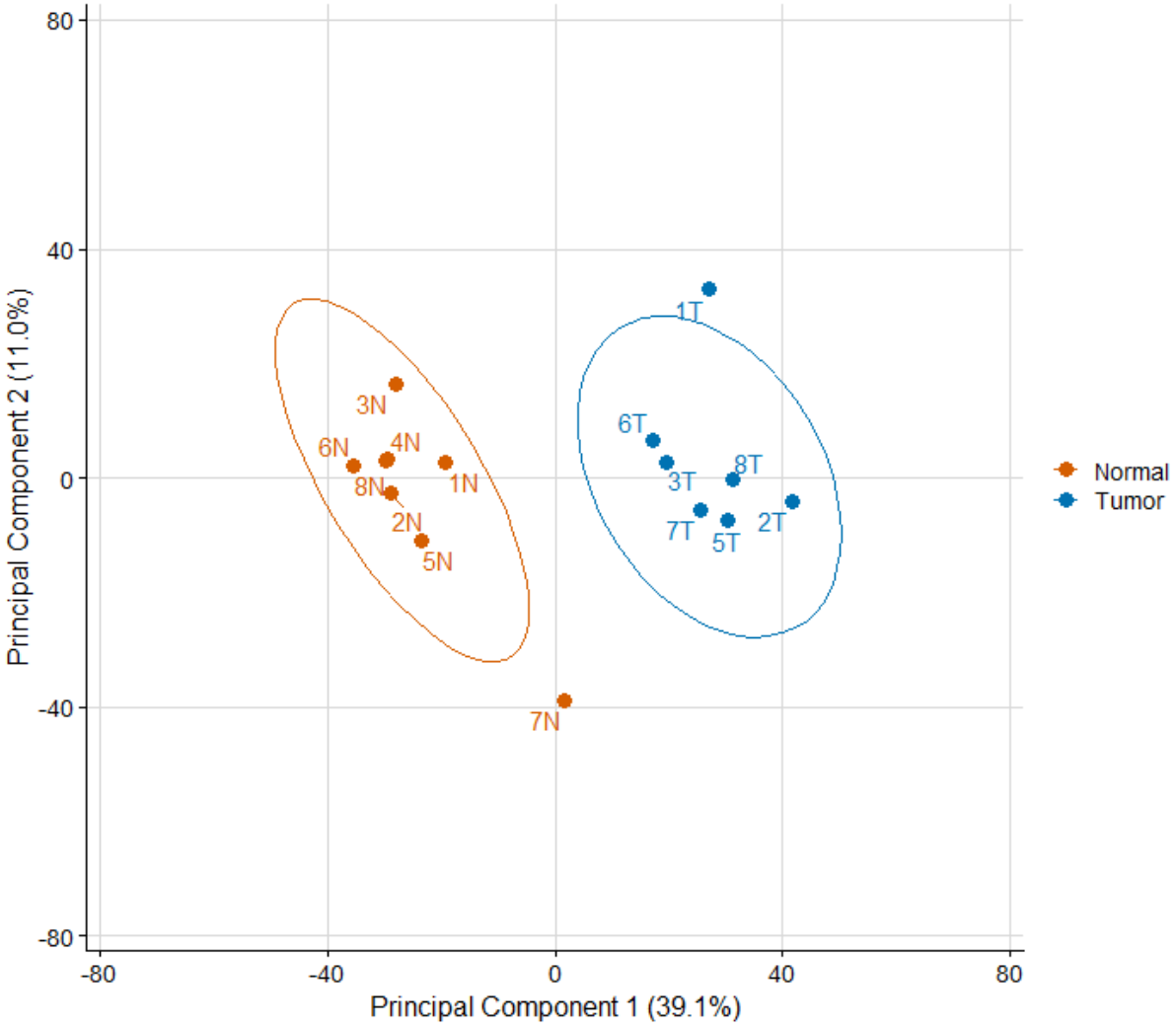

Figure 2.13 PCA of phosphosite intensities normalized to protein intensities

To determine which phosphosites were up- or down- regulated when normalized to the protein expression, I calculated the differential intensities of these normalized values. Of the 4202 phosphosites included in this analysis (the rest of the phosphosites were not detected in the proteome experiment), at an FDR of $\leq$ 0.05, 693 were higher in tumor with a $\log_2$ fold change greater than 0.585, and 363 were lower in tumor with a $\log_2$ fold change less than -0.585. Many phosphosites were "demoted" once normalized (such as VCAN described earlier), but many others were promoted or unchanged, including phosphosites on CFL2 (cofilin-2), WARS (tryptophanyl tRNA synthetase), and ABAT (4-Aminobutyrate Aminotransferase) (Figure 2.14). The latter is an enzyme that catalyzes the catabolism of GABA and is important for the metabolism of some amino acids. More recently, a study found that ABAT it is essential for mitochondrial dNTP salvage (Besse et al., 2015). This particular phosphosite has been detected in a large proteomics dataset, but has not been reported in the context of regulation of this protein.

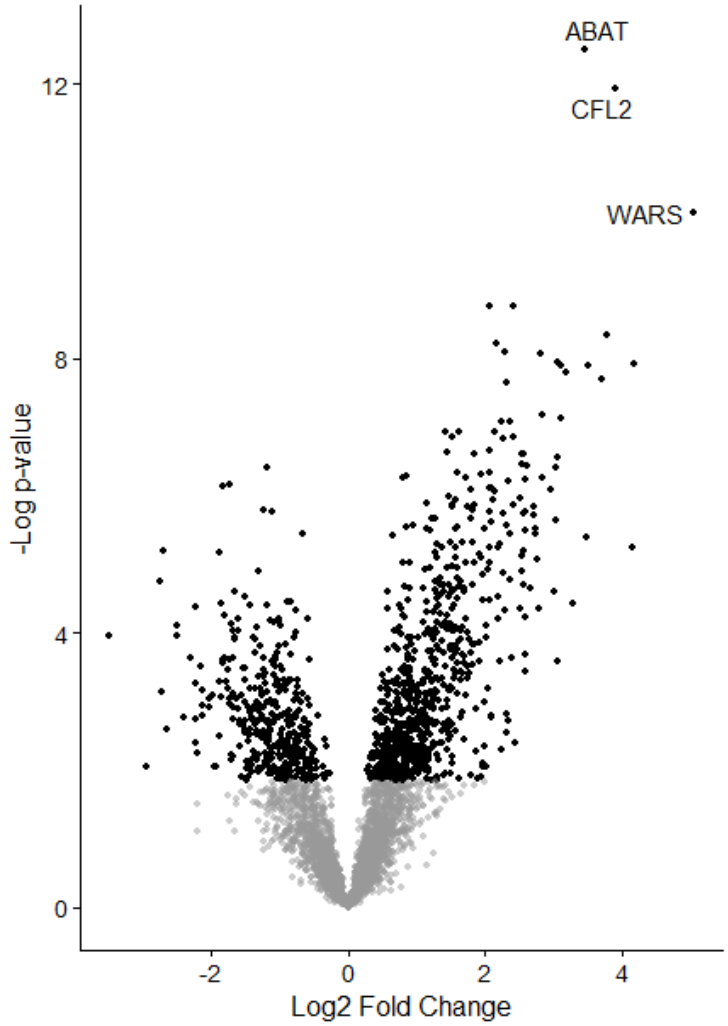

Figure 2.14 Volcano plot showing normalized phosphosite deregulation in FLC
Black points are those that are significant at an FDR of 0.05. The phosphosites on the right are higher in FLC tumor; those on the left are higher in normal liver.

2.2 Absolute quantitation of PKA subunits

One cannot use the data generated in a typical shotgun proteomics experiment to compare relative values of different proteins to one another. This is because some proteins are detected better than others via mass spectrometry (due to differences in ionizability of peptides). The data can only be used to compare the same proteins to each other in different samples. When analyzing the data for the subunits of PKA, we find that many of them are differentially expressed in tumor as compared to normal (Table 1). However, since these components regulate one another, we hypothesized that the ratio between them could provide insight into the pathogenesis of FLC (see Chapter 1.2).

Table 1 Expression difference of PKA subunits between FLC and normal tissue

Gene Name	Log_2 Fold Change in tumor relative to adjacent tissue	P-value (adjusted)
PRKACA	1.30	9.13E-6
PRKACB	0.812	0.86
PRKAR1A	1.19	3.52E-5
PRKAR1B	1.00	0.00162
PRKAR2A	-0.559	0.00104
PRKAR2B	-1.09	0.00496

In addition to the subunits of the PKA holoenzyme, we were interested in quantifying the isoforms of Protein Kinase Inhibitor (PKI). There are three isoforms of PKI: PKIA, PKIB, PKIG. All three of them are small with a little more than 70 residues, and they all bind to the active site of the catalytic subunit of PKA. The key question that we are probing here is whether, on a stoichiometric level, there is enough inhibitor in FLC tissue to overcome the overexpression of the catalytic subunits, PRKACA and chimera. The inhibitors include the regulatory subunits and the PKIs, and potentially some other endogenous inhibitors that are unknown or understudied. ARHGAP36 is one such inhibitor that was recently found.

Besides for acting as a PKA inhibitor, the regulatory subunits have another important role in the regulation of PKA: localization within the cell. The regulatory subunits have a domain that binds to A-kinase associated proteins (AKAP), and AKAPs have a domain that bind to membranes. Once PRKACA is released from the regulatory subunit after cAMP stimulation, exactly how the catalytic subunit remains localized is not well understood.

In normal tissue there is a large stoichiometric excess of endogenous inhibitor (regulatory subunits and PKIs combined) relative to catalytic subunit. A recent study theorized that the high ratio of regulatory subunits to catalytic subunits, provides a mechanism for capture very shortly after it is released (Walker-Gray et al., 2017). The question to be addressed here is whether in tumor, where the catalytic subunit is

increased in expression, is there is enough endogenous inhibitor to keep the catalytic subunits localized, or at least inhibited.

There are several approaches to absolutely quantify the amount of a specific protein in a complex protein mix, such as in tissue lysate. One method is with heavy labelled peptide standards. These peptides are called AQUA (absolute quantitation) peptides. The other method is with protein standards that are tagged with tandem mass tags (TMT). We performed the first method, though at the time, we were only focused on regulatory subunits and therefore did not quantify the PKIs. We are in the process of conducting the second method to quantify the regulatory subunits and the inhibitory proteins.

2.2.1 Quantification with AQUA peptides

For this approach, we chose peptides from each protein of interest that we previously detected in our shotgun experiments. For our shotgun experiments, we used a combination of Trypsin, a protease that cleaves at the c-terminus of arginines and lysines, and Lys-C, a protease that cleaves at the c-terminus of lysines only. In previous shotgun experiments from our lab, the fusion peptide of chimera was detected, but only the form that was not cleaved at arginines. In other words, the peptide REIFDRYGEEVK was detected, but not YGEEVK. Since there are arginines in this detected peptide, the peptide most likely came from the aliquot that was digested with Lys-C. Therefore, we used Lys-C for this experiment, to make sure that we were able to detect this peptide, since it is the only unique peptide for chimera.

We selected peptides for synthesis with the following criteria: Peptides were detected in a previous mass spectrometry experiment (thus, is ionizable), peptides were Lys-C peptides (i.e., they have a lysine at the c-terminus, but no other lysines), and peptides were unique to the protein of interest. Given the significant homology between PRKACA and PRKACB, and the regulatory subunits among each other, the latter criterion severely restricted our choices, and for many of the proteins we were left with a single peptide. Each peptide was then synthesized (Thermo) with a heavy isotope labelled lysine at the c-terminus and underwent amino acid analysis to provide accurate quantitation of the synthesized peptides.

The mass difference between the heavy lysine peptide and the endogenous cleaved peptide is 8Da. The chemical properties, like hydrophobicity, are identical. Therefore, both peptides elute at the same time from the liquid chromatography column. This is important so that we can select a time window in which we expect the peptide to elute, which allows us to focus solely on the peptides of interest and decreases noise. Once the peptides are eluted and ionized, they are detected at different mass/charge, and all downstream analyses (like SRM transitions, see Chapter 1.2.4) are detected identically. In other words, the peptide ion detectability will be the same between the

peptides. Therefore, the amount of endogenous peptide can be calculated based on the signal from the heavy peptides.

For this experiment, we analyzed 3 FLC samples and 3 normal liver samples, and we used synthetic heavy labelled lysine peptides for PRKACA, PRKACB, PRKACG, PRKAR1A, PRKAR1B, PRKAR2A, and PRKAR2B. Two peptides were used for PRKAR1A and PRKAR2A. The chimeric fusion peptide was not detected in the normal samples and were detected in all tumor samples (Figure 2.15).

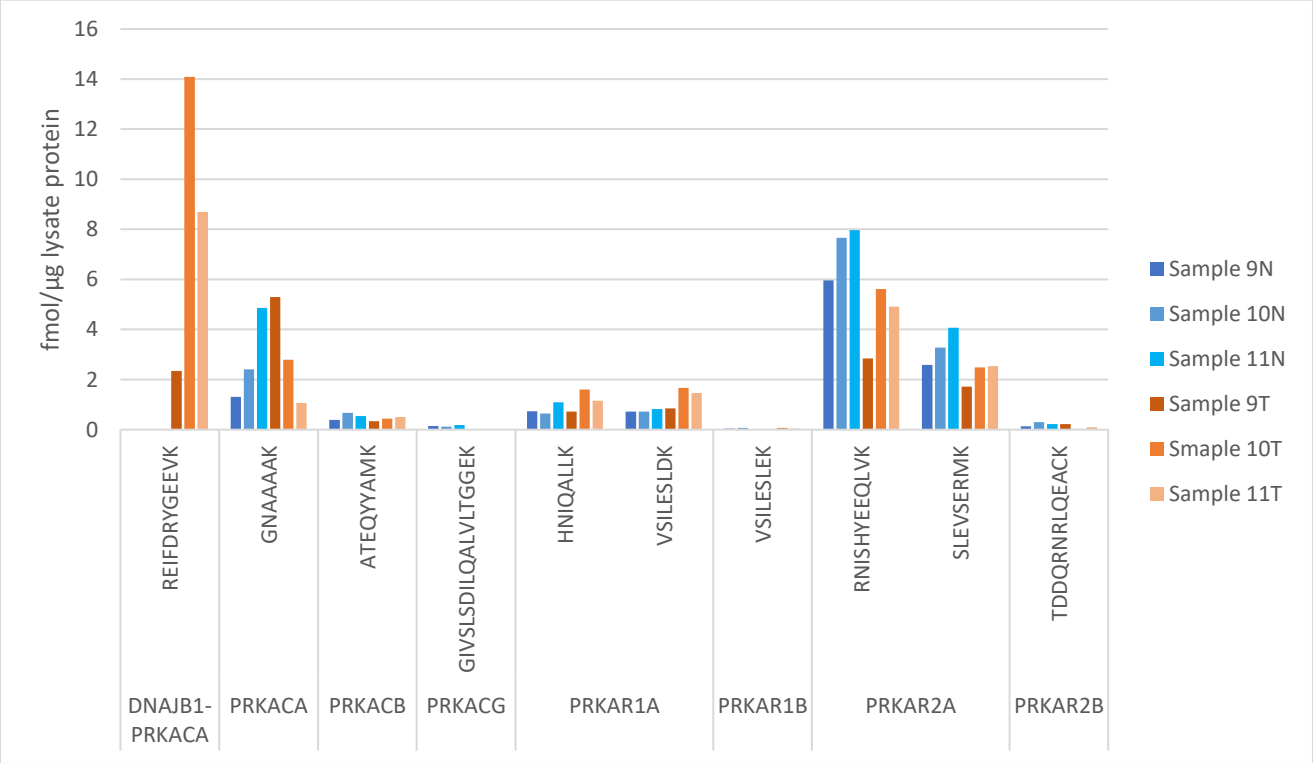

Figure 2.15 Absolute quantitation of peptides of PKA subunits

The sum of the quantity of peptides of all the catalytic subunits was compared to the sum of the quantity of peptides (or average of peptides for PRKAR1A and PRKAR2A) of all the regulatory subunits. The result shows a shift in the ratio of regulatory:catalytic from excess regulatory subunit in normal tissue to excess catalytic subunit in FLC tissue (Figure 2.16).

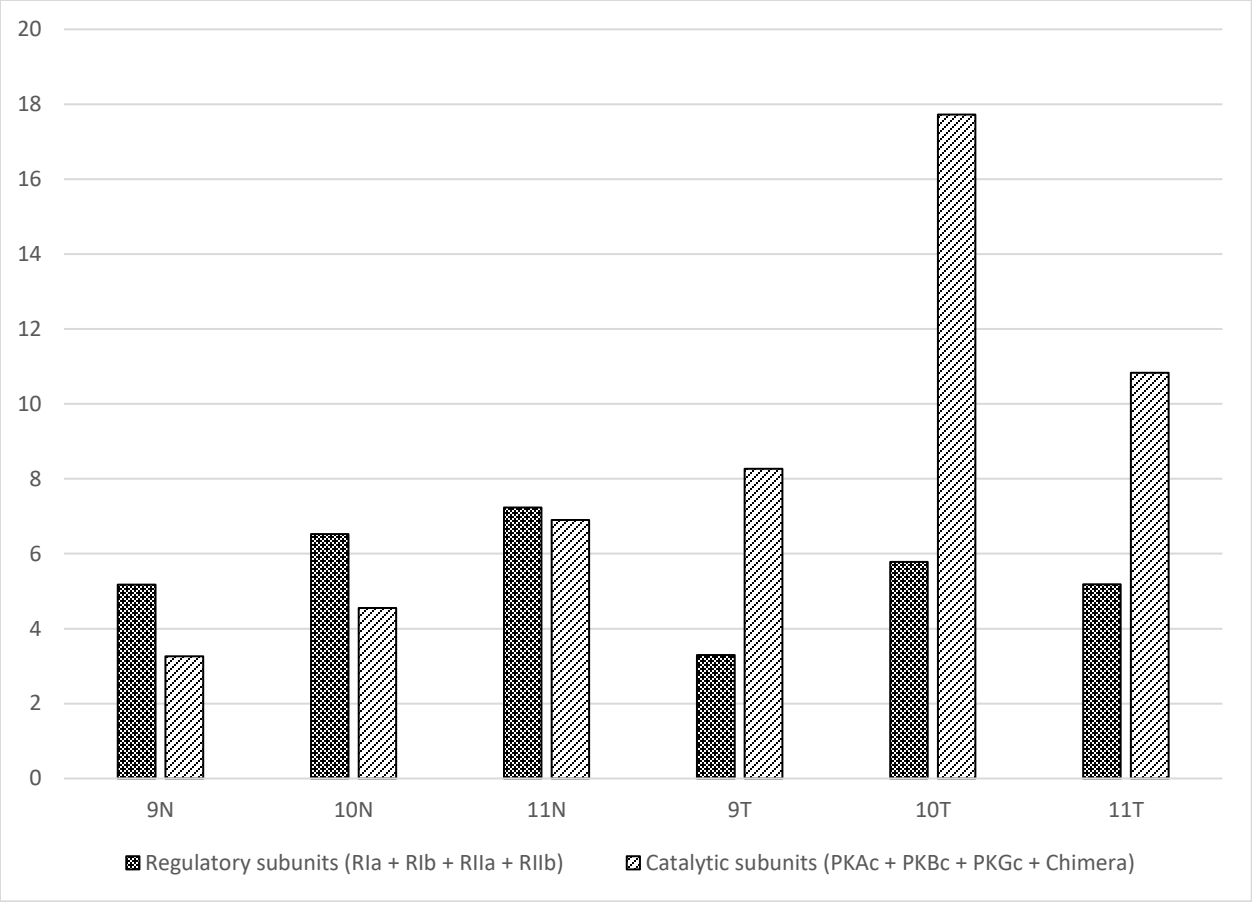

Figure 2.16 Comparing sum of catalytic subunits to sum of regulatory subunits

There are several potential issues with this method. Firstly, the endogenous proteins get digested with Lys-C, and the number of moles of peptide that is created per mole of protein is dependent on the efficiency of that digestion. Digestion efficiency may depend on the sequence directly surrounding the peptide (Gershon, 2014). Since we are using those digested peptides as a surrogate for protein, this efficiency directly translates to accuracy of quantification, because the peptide standards do not undergo this digestion. A second issue that we discovered after this experiment was completed is that per the manufacturer, lyophilized peptides have varying degrees of solubilization efficiency due to their tendency to form colloids during the lyophilization process, and in some cases (~5% of peptide sequences) only 10% of the peptide is properly solubilized. The issues described here can lead to the following results for quantitation: Poor digestion efficiency would underestimate the amount of protein in the tissue, poor peptide standard solubility would overestimate the amount of protein in the tissue.

For PRKAR2A, there were two peptide standards. The quantification based on these standards yielded quantities of PRKAR2A that were different from one another in each sample. This ~2-fold difference between the two peptides was remarkably consistent in all six samples (see Figure 2.13), supporting the robustness of this

approach overall, though the difference itself is concerning and may be explained by the issues mentioned above. In addition, the lack of other peptides for most of the other proteins quantified does not allow us to analyze any other potential problems. For a typical AQUA experiment, 2-3 peptides per protein are recommended.

A recent study quantified the PKA subunits in several organs of the Sprague–Dawley rat with calibrated immunoblotting (Walker-Gray et al., 2017). Their quantification values as compared to the quantities from the normal livers in our AQUA experiment are shown in Table 2. Of particular concern are the catalytic subunits, which have a 5.7-15 fold increase in our experiment relative to theirs. This can be explained by the potentially low solubility of the PRKACA peptide standard, which was myristoylated at the n-terminus. For PRKAR2A, the quantification from the second peptide ("Peptide 2" in Table 2) is 1.4-2.3 fold higher than their experiment, a more reasonable change that can be attributable to technical variation between experiments or interspecies variation.

Table 2 Quantification of PKA subunits

	Walker-Gray et al. (fmol/µg ± SEM)	This experiment (fmol/µg ± SEM)
PRKACA + PRKACB	0.29 ± 0.03	2.86 ± 1.05
PRKAR1A + PRKAR1B	1.41 ± 0.26	0.88 ± 0.07
PRKAR2A	1.86 ± 0.31	Peptide 1: 7.20 ± 0.62 Peptide 2: 3.31 ± 0.43
PRKAR2B	0.52 ± 0.06	0.22 ± 0.05

For the catalytic subunits, Walker-Gray et al. used an antibody that probes both PRKACA and PRKACB. For the regulatory subunits, they used three antibodies: one that recognized both PRKAR1A and PRKAR1B, and one for each of the PRKRA2s.

Given the issues with our AQUA approach, a new method to absolutely quantitate these proteins is underway and is described in the next section.

2.2.2 Quantification with whole proteins and TMT

In this approach, we will use whole proteins as the standards. Since the standard proteins will undergo the same digestion as the endogenous proteins, sequence context-dependent digestion efficiency will not matter. Solubility differences will also not be an issue here. All of the recombinant proteins will undergo amino acid analysis for accurate quantification. The proteins from the tissue lysates of five patients (ten samples total) will be digested and also undergo amino acid analysis. An equimolar amount of each protein standard will be combined, digested with Lys-C, and undergo a serial dilution to create a six-member dilution series. This dilution series and the ten protein extracts from patient tissue (also equimolar) make up 16 samples. Each of these samples will be tagged by tandem mass tags using the TMTpro 16plex Label Reagent.

All of the samples will be combined, fractionated, and each fraction will undergo LC-MS/MS. Since these are fractionated, a larger amount of protein extract will be able to be loaded and will allows us to detect low amount of protein (such as PRKAR2B) more accurately. The proteins analyzed in this experiment include the same ones analyzed in the AQUA experiment, in addition to PKIA, PKIB, PKIG.

Currently, we have purified recombinant chimera, PRKACA, PKIA, PKIB, PKIG, PRKAR1A, PRKAR1B, and PRKAR2B (Figure 2.17). All of them are at >90% purity by densitometry analysis. Purification of PRKAR2A and PRKACB is currently underway. Given the extremely low expression of PRKACG, based on RNA sequencing and on our AQUA experiment, we will not be including it in this experiment.

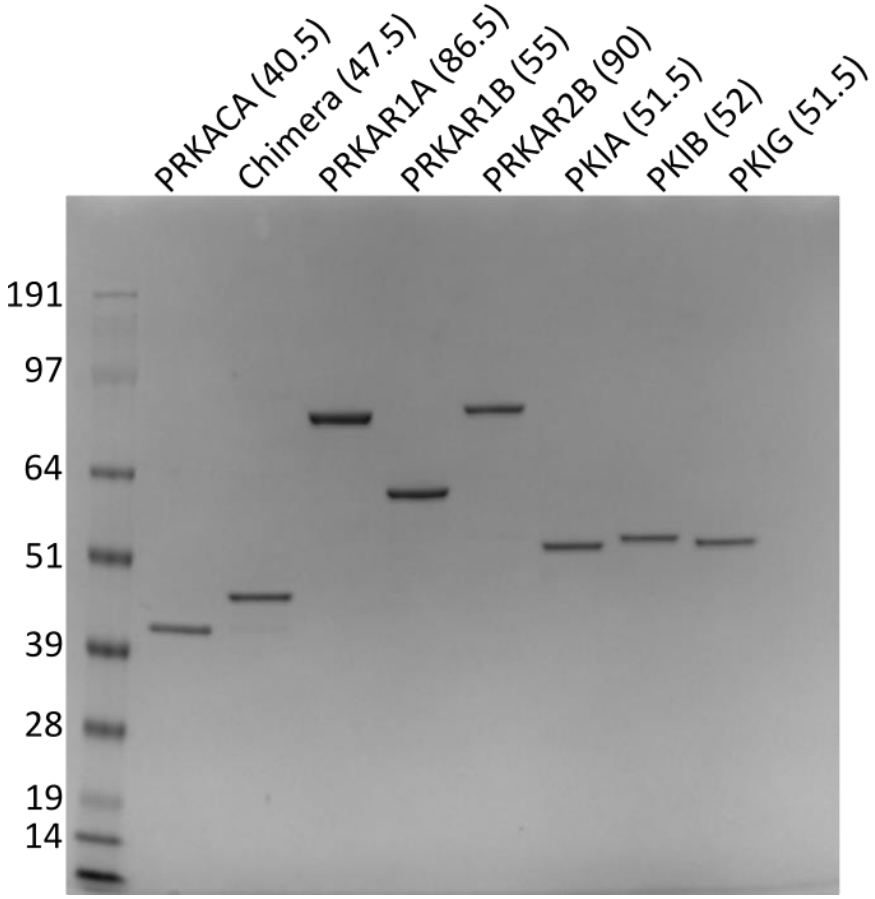

Figure 2.17 Purified proteins for quantification of PKA and PKI subunits
Coomassie stained gel of the recombinant proteins that have been purified for this experiment. The affinity tags for these proteins have not been cleaved. The expected molecular weights of the proteins with their affinity tags are in parentheses.

Chapter 3
Therapeutic Development for FLC

In this chapter, I will discuss my efforts to develop the first systemic chemotherapeutic for FLC. I used three approaches: targeting the protein with a small molecule, targeting the RNA with antisense oligonucleotides, and targeting the RNA with siRNA.

In section 3.1, I will discuss my initial efforts, in collaboration with Lavoisier Espiritu-Ramos in the High-throughput Screening Center, to screen for a small molecular inhibitor that is specific for the DNAJB1-PRKACA protein. This entailed developing a protocol for the purification of this chimeric protein on a large scale, and then assaying a library of almost 400,000 small molecules to find inhibitors of the protein.

Next, I began working on developing an ASO that would result in degradation of the chimeric transcript. This was successful but led to some problems when tested *in vivo*. I am still working on designing an ASO that is safe for *in vivo* use. This is discussed in section 3.2.

Finally, a more recent effort to develop an siRNA against the chimeric junction was started. I will present the initial results of the siRNA study in section 3.3.

3.1 High-throughput screen for DNAJB1-PRKACA inhibitors

3.1.1 Developing a method for large-scale protein purification

For the high-throughput screen, we needed to express and purify large amount of the chimeric protein for the primary screen. All hits from the primary screen were assessed with dose-response curves and ultimately tested against wild-type PRKACA. We were concerned about purifying these two proteins with an affinity tag, given preliminary results that showed a decrease in activity of the protein with a scar at the terminus. Thus, I used a method that took advantage of a known cellular protein, Protein Kinase Inhibitor (PKI), that binds specifically in the substrate binding pocket of the catalytic subunit of the kinase, PRKACA. In normal physiology, this 70 amino acid protein binds to the free catalytic subunit in the nucleus inhibiting the ability to bind substrate (see chapter 1.2.2). A 20 amino acid segment of this peptide still has nanomolar affinity to PRKACA and discriminates against all other cellular proteins. By conjugating this peptide to a resin in a column, the PRKACA can be purified in a single step from a bacterial expression system with greater than 95% purity by densitometry analysis (Figure 3.1). Using this system, I was able to purify >5mg of pure protein per 1L e. coli culture.

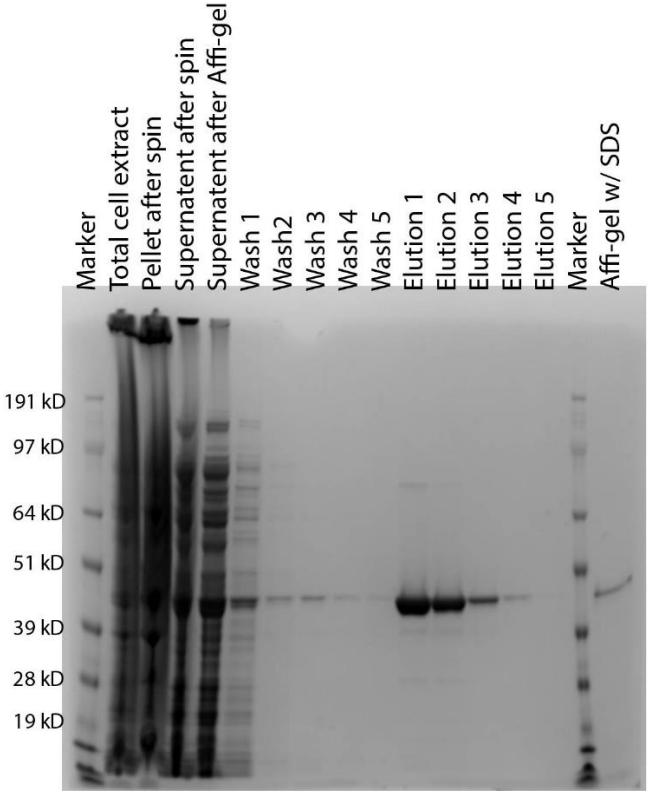

Figure 3.1 Purification of DNAJB1-PRKACA protein
Coomassie stained gel of the recombinant untagged DNAJB1-PRKACA protein (47 kDa)

3.1.2 High-throughput screen

We then established a quantitative assay for the activity of PRKACA using Promega's ADP-Glo Luminescent Assays together with kemptide (LRRASLG), a substrate for PKA. Using the purified protein, we conducted a screen of 378,981 small molecules (Figure 2). In the screen we used 10 μM H89 as a positive control and DMSO as a negative control and each compound was evaluated on a Normalized Percentage Inhibition (NPI) Luminescence, where H89 is 100 and DMSO is 0. A standard of a Normalized Percentage of Inhibition (NPI) ≥ 15 with z-score of ≥ 3.5 yielded 134 compounds.

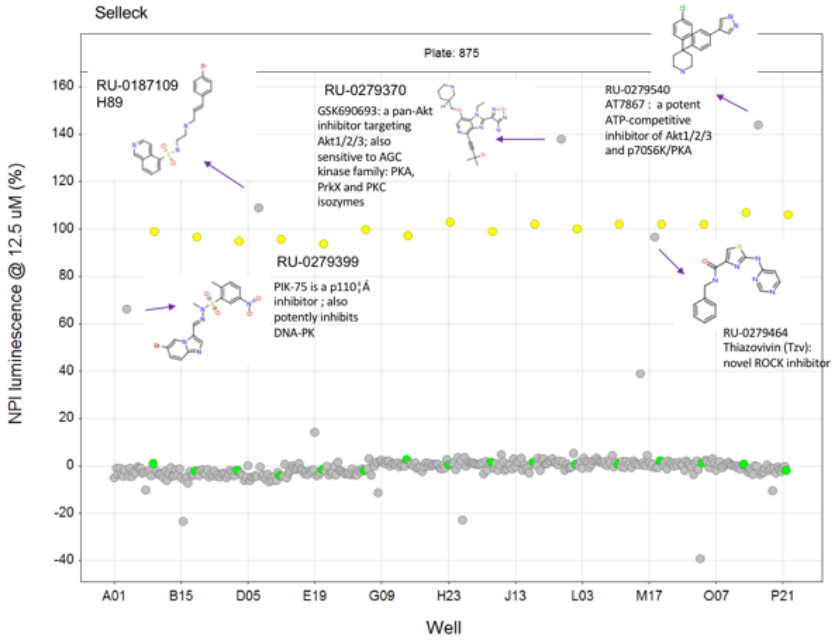

Figure 3.2 Example of a 384-well plate from the high-throughput screen
Each point represents the luminescence (negatively correlated with kinase activity) in a single well. The yellow is the positive control (H89) and green was the negative control. A few of the positive hits are shown.

There were five small molecules with a K_i < 10 nM and an additional six with a Ki < 50 nM. The best hit, RU-0240400, has a K_i of 1.08 nM against DNAJB1-PRKACA (Figure 3). Unfortunately, it did not show selectivity to DNAJB1-PRKACA over PRKACA. While there were a few compounds that did show some specificity for chimera over the native kinase, they did not have as good potency.

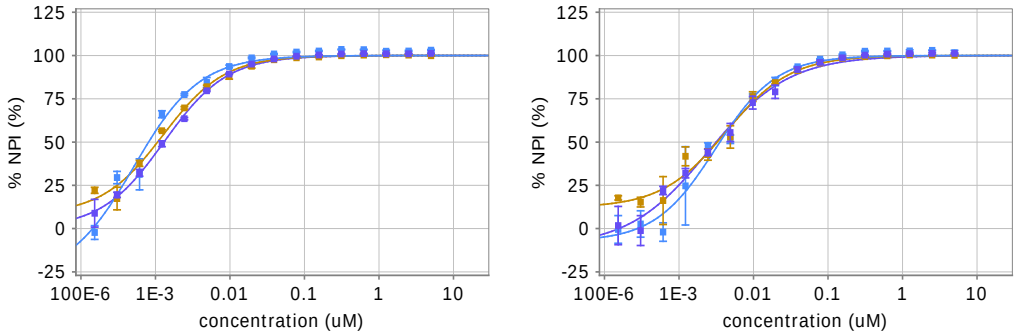

Figure 3.3 Dose-response curves of PKA inhibition
RU-0240400 (left) and RU-0422540 (right) for DNAJB1-PRKACA (1.08/2.5 nM), PRKACA (1.06/4.3 nM) and non-myristoylated PRKACA (4.29/3.1 nM). The first number is the IC_{50} for RU-0240400 and the second number by RU-0422540.

We currently have crystal structures and molecular dynamics simulations for some of these inhibitors. In collaboration with the lab of Nathanael Gray, we are using these to develop selectivity for the *DNAJB1-PRKACA* fusion over *PRKACA*.

3.2 Antisense Oligonucleotides

As an alternative strategy for inhibiting the chimera, I shifted to developing antisense oligonucleotides (ASOs), since specificity is easier to achieve on the DNA or RNA level. Given our understanding of ASO chemistry and the success of specific ASO chemistries in the clinic (see Chapter 1.3.1), we chose to use ASOs that are modified with a phosphorothioate (PS) backbone and locked nucleic acids (LNA) for my experiments. The initial design of these ASOs were 3-10-3 “Gapmers”, which have ten central unmodified DNA nucleotides, and three LNA nucleotides at each flank. The backbone was consistently PS throughout the oligonucleotide. In an effort to find the optimal sequence, I performed a one-nucleotide gene walk along the *DNAJB1-PRKACA* junction and tested each of those ASOs (Figure 3.4).

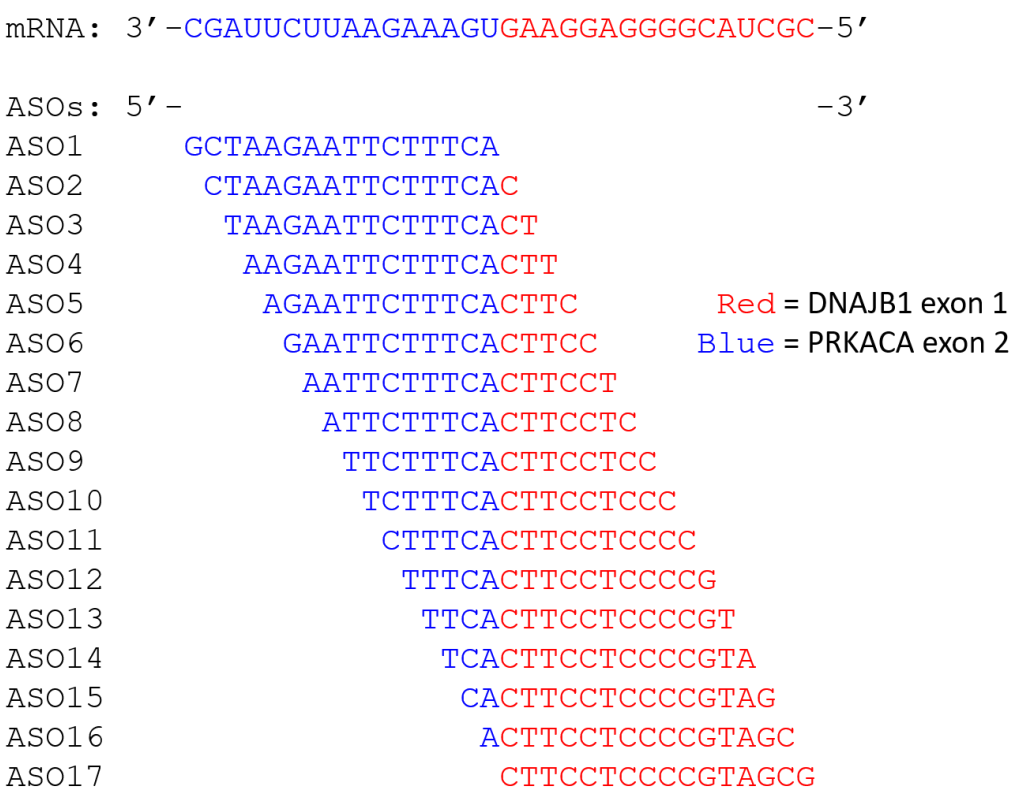

Figure 3.4 Single-nucleotide gene walk across the DNAJB1-PRKACA junction
Every possible 3-10-3 Gapmer sequence along the junction was synthesized for the initial experiment, including one ASO completely within the PRKACA sequence (ASO1) and one completely within the DNAJB1 sequence (ASO17).

These ASOs were tested on cells that were dissociated from one of the FLC patient-derived xenografts (PDX) implanted in a mouse. The cells were treated with 10μM in Kubota's StemCell Growth Media. Cells were incubated for 72 hours at 37°C with 5% pCO_2 and 5% pO_2. A scrambled ASO, which was a scramble of ASO8, was also included. The cells were harvested for RNA, and expression levels were checked for *DNAJB1-PRKACA*, *PRKACA*, and *DNAJB1* by one-step qRT-PCR (Figure 3.5). The results showed that several ASOs caused successful knockdown of the chimeric transcript. There was a strong knockdown (>95%) of the chimera with ASO9, ASO10, ASO11, ASO12, ASO13, ASO14) with only minimal effect on the expression of either parental molecule, DNAJB1 or PRKACA. The only ASO which affected an endogenous transcript was ASO17, which is completely within the *DNAJB1* transcript. This ASO also reduced the expression of the chimera to below 1% relative to PBS treated cells. *PRKACA* expression was relatively stable for all ASOs.

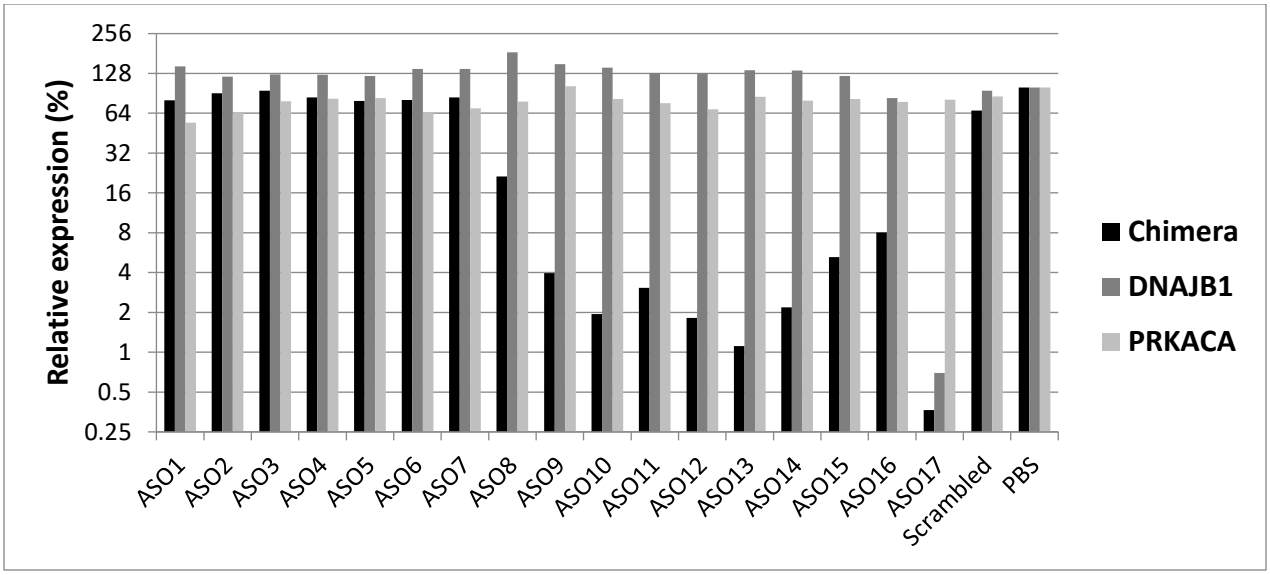

Figure 3.5 Quantitative PCR of RNA expression in ASO-treated FLC cells
Relative mRNA expression levels measured via qRT-PCR of the chimera, *DNAJB1*, and *PRKACA* transcripts after treatment of 10 μM ASO for 3 days.

Several of these ASOs were retested at several doses in the same model system. For ASO17, significant knockdown is seen for both chimera and *DNAJB1* transcripts, with IC50s in the low nanomolar range (Figure 3.6). Although avoiding *DNAJB1* knockdown is manageable by appropriate choice of ASO, it may not be of major concern as an off-target effect. There is considerable redundancy of the HSP40 gene family, of which DNAJB1 is a member. Indeed, deletion of DNAJB1 has no effect on the viability of mice (Uchiyama et al., 2006).

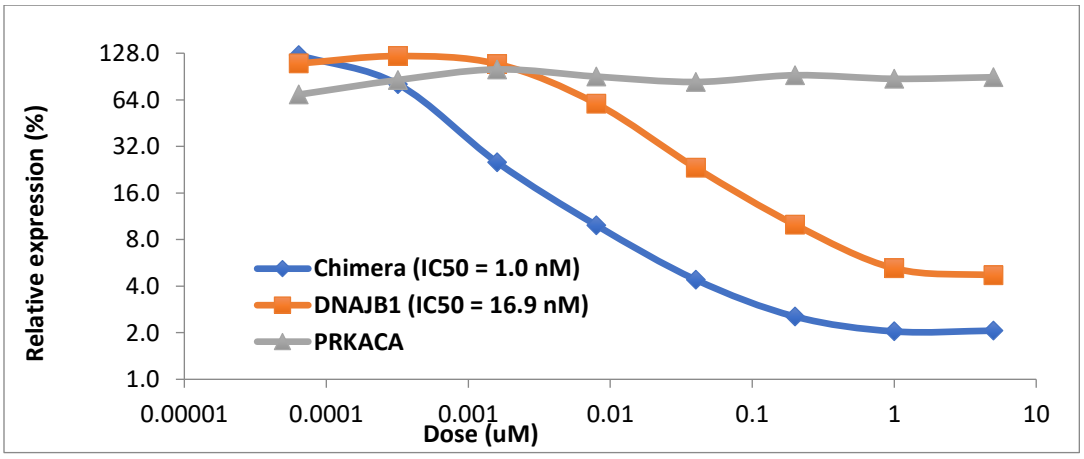

Figure 3.6 RNA Knockdown Dose-response Curves for FLC Cells
Cells were dissociated from PDX mice, treated with ASO17, and harvested for RNA 72 hours later. Chimera, *PRKACA*, and *DNAJB1* transcripts were quantified from total RNA via qRT-PCR.

To test these on another model system that is more likely to resemble the in vivo characteristics of an FLC tumor, the dose response with ASO17 was repeated on organoids. These were formed directly from dissociated cells from patient tumors and were validated based on their expression of the transcript for DNAJB1-PRKACA, for their expression of DNAJB1-PRKACA fusion protein, and for recapitulating the transcriptome of the FLC tumor in the patients.

The dose-response on the organoids showed very similar results to the results of the 2D system. Significant knockdown of both DNAJB1-PRKACA and DNAJB1 was seen, with IC50's also in the low nanomolar range (Figure 3.7)

Given the success of RNA knockdown by ASOs in the organoids, even without any transfection reagent, we utilized the organoids to check knockdown of the protein level (Figure 3.8). We detected significant dose-dependent knockdown of the fusion protein when the organoids were treated with ASO17, but not when treated with the scrambled ASO, relative to organoids treated with PBS.

In our 2D cell model system, I have not seen knockdown of protein, even when the cells were treated with ASO for a considerable length of time (up to 17 days). This finding, or lack thereof, has spurred considerable discussion in our lab (see Chapter 4.3). However, despite this lack of protein knockdown, when the cells in monolayer were treated with a much higher concentration of ASO17, it did result in cell death as early as six days after the initiation of treatment, while the same concentration of the scrambled ASO did not affect viability (Figure 3.9). This same concentration of ASO17 did not seem to have any significant effect on primary human hepatocytes (received from the Rice Lab). I did not successfully test for knockdown of the chimeric protein in the cells at this high concentration, due to the early death of these cells. A more fine-tuned time series, with more frequent timepoints and more concentrations, might be essential for this purpose.

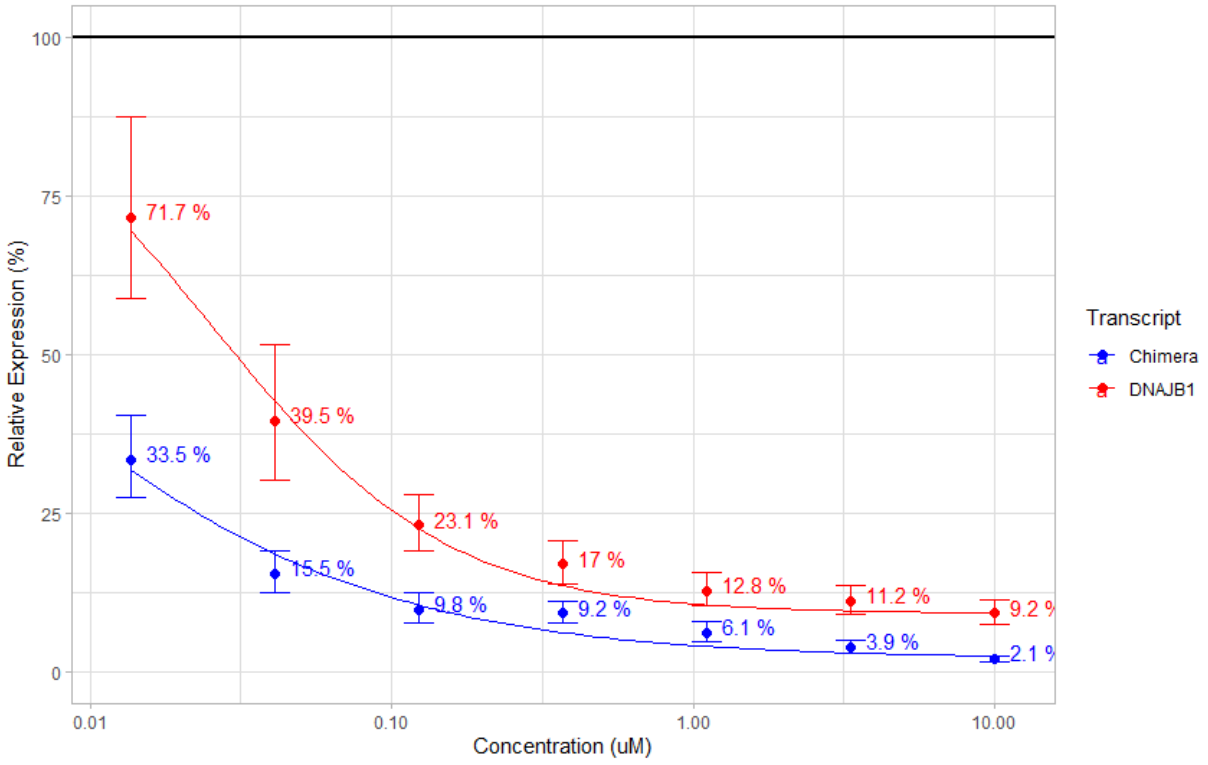

Figure 3.7 RNA knockdown dose-response curve for FLC organoids
Organoids were treated with ASO17 and harvested for RNA 48 hours later. Chimera and DNAJB1 transcripts were quantified from total RNA via qRT-PCR. The calculated IC_{50} for chimera is 4.2 nM and for DNAJB1 is 25.3 nM.

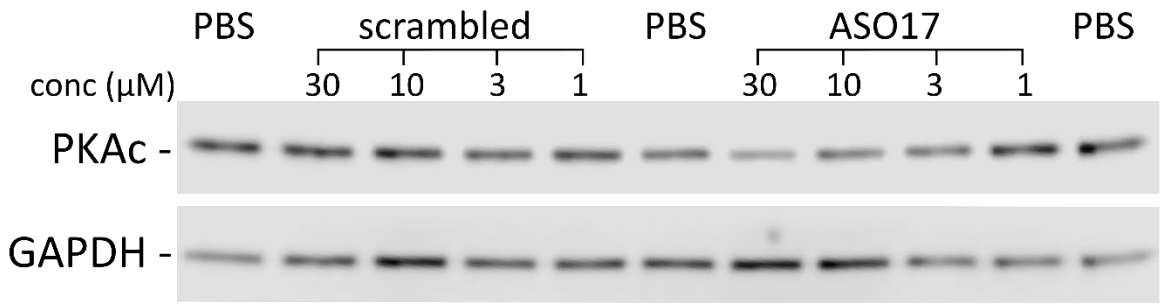

Figure 3.8 Western blot of organoids treated with ASO17
Organoids were treated with ASO17 and harvested for protein three days later. The PRKACA antibody recognizes the c-terminus of PRKACA, and therefore recognizes both wild-type PRKACA and the chimera (which migrate at different speeds on the gel). There were no changes in PRKACA in this experiment.

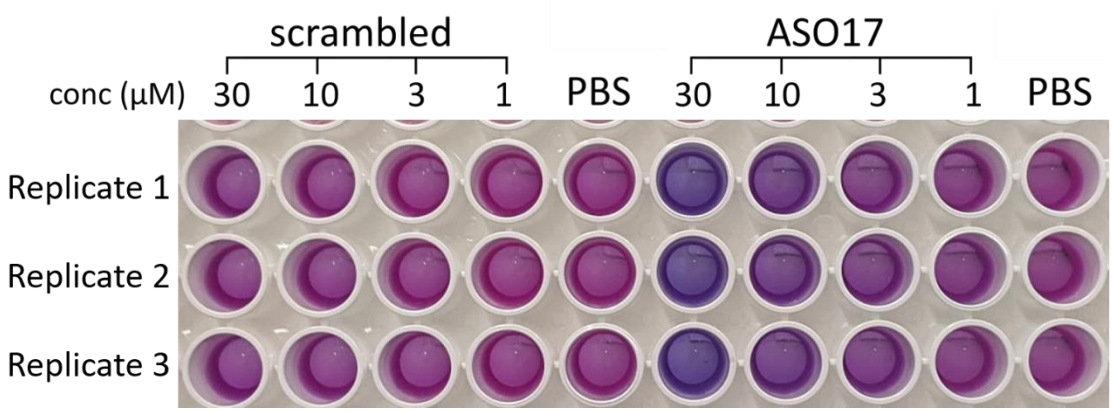

Figure 3.9 Viability of FLC cells treated with ASO
Viability (resazurin) assay of FLC cells treated with ASO17, vehicle, or a scrambled control. The color of the assay changes from blue to pink with increasing reducing potential. Wells with decreased viable cells have decreased capacity to reduce resazurin and remain blue.

Following these experiments, I moved forward with a pilot in vivo experiment in collaboration with the Antitumor Assessment Core Facility at the Sloan Kettering Institute. Many ASOs (in particular, those that contain LNAs) have been found to be hepatotoxic (see Chapter 1.3.2). Thus, the goal with this experiment was to assess whether any of the ASOs that were shown to be successful in knocking down the chimeric transcript (ASO8-ASO17) were not hepatotoxic and have the potential to move forward with higher dosing studies to test efficacy. This experiment was conducted on NSG mice since those are the mice that our PDX are implanted in and would be used for future efficacy studies. The experimental plan was to treat the mice with 20 mg/kg on days 0, 2, 4, 7, and 10, and to sacrifice on day 14. This protocol is a slightly modified from the protocol conducted by Pfizer in a study attempting to determine potential sequence motifs that are associated with hepatotoxicity (discussed below), and is significantly lower than the doses used in other ASO studies targeting other oncogenes (Ross et al., 2017). All ten ASOs in addition to a scrambled negative control (scrASO) and a vehicle control (PBS) were given as treatments to three NSG mice each. For this experiment, I used a new “scrambled” control that was taken from another study, where it was used to knock down the HBV RNA in mice (Javanbakht et al., 2018). Given that this study did the controls to ensure that there were minimal off-target effects within the human genome, and there was no toxicity apparent in the mice treated, I decided to use it as my scrambled ASO.

On day four of the experiment, all the mice treated with ASO9 or ASO13 were found dead in their cage. In addition, all the mice treated with ASO11, ASO12, and ASO14, and one mouse treated with ASO17 were deemed unwell (sluggish) and were sacrificed early. On day 7, the mice treated with ASO8, and ASO10, and the rest of the mice treated with ASO17 were all sacrificed for similar reasons. Only the mice treated

with ASO15, ASO16, scrASO or vehicle made it to the end of the study. However, the ALT and AST levels of all mice treated with an ASO were significantly increased, including the group treated with scrASO, albeit to a lesser extent (Table 3).

Table 3 Clinical status and liver markers of mice treated with ASO

	Animal #	ALT (U/L)	AST (U/L)	Clinical status
ASO8	1	-	-	Found dead – day 7
	2	-	-	Found dead – day 7
	3	-	-	Found dead – day 7
ASO9	1	-	-	Found dead – day 4
	2	-	-	Found dead – day 4
	3	-	-	Found dead – day 4
ASO10	1	-	-	Found dead – day 7
	2	-	-	Found dead – day 7
	3	-	-	Found dead – day 7
ASO11	1	828	2509	Euthanized – day 4
	2	111	502	Euthanized – day 4
	3	330	923	Euthanized – day 4
ASO12	1	606	829	Euthanized – day 4
	2	408	814	Euthanized – day 4
	3	396	582	Euthanized – day 4
ASO13	1	-	-	Found dead – day 4
	2	-	-	Found dead – day 4
	3	-	-	Found dead – day 4
ASO14	1	358	594	Euthanized – day 4
	2	1442	1674	Euthanized – day 4
	3	400	609	Euthanized – day 4
ASO15	1	1400	703	Good
	2	1130	1379	Good
	3	1190	1624	Good
ASO16	1	2576	740	Good
	2	2094	699	Good
	3	3566	870	Good
ASO17	1	3127	1977	Euthanized – day 7
	2	1805	2631	Euthanized – day 4
	3	1235	2834	Euthanized – day 7
scrASO	1	451	420	Good
	2	1708	2346	Good
	3	235	265	Good
Vehicle	1	35	97	Good
	2	20	54	Good
	3	21	48	Good
Reference	-	27-195	54-77	-

Mice with clinical status of “Good” were euthanized at end of study (day 13)

In all the ASO sequences that were studied in this in vivo experiment, there is a TCC motif (ASO8-ASO17, see Figure 3.1). This motif is one of two motifs that have been shown to be correlated with an increased likelihood of causing hepatotoxicity (Burdick et al., 2014). The sequence of the scrambled ASO, taken from the HBV study, includes a TGC motif, which is the other motif that is purported to be associated with increased risk of causing hepatotoxicity. However, the study that uses this ASO to decrease HBV antigenemia in mice reported no increase in the levels of AST and ALT in the mice treated. In retrospect, I did not appreciate that the dose that they used in their HBV study was significantly lower than the dose I used in our study. Per my correspondence with the author of that study, they did not test this ASO at higher doses than they published.

The tumors from the mice treated were harvested. The tumors from two of the mice from the groups treated with ASO12, ASO15, ASO16, scrASO and vehicle were analyzed. The RNA was extracted from these tumors and analyzed for knockdown of chimera, *PRKACA*, and *DNAJB1*. Chimera was knocked down for all of these samples, except for those treated with scrASO and vehicle. No significant knockdown was seen with *PRKACA* and *DNAJB1* (Figure 3.10). The RNA was then analyzed with RNA sequencing for transcriptomic changes. Principal component analysis revealed that the tumors for ASO12 clustered away from the rest of the tumors in the first component Figure (3.11).

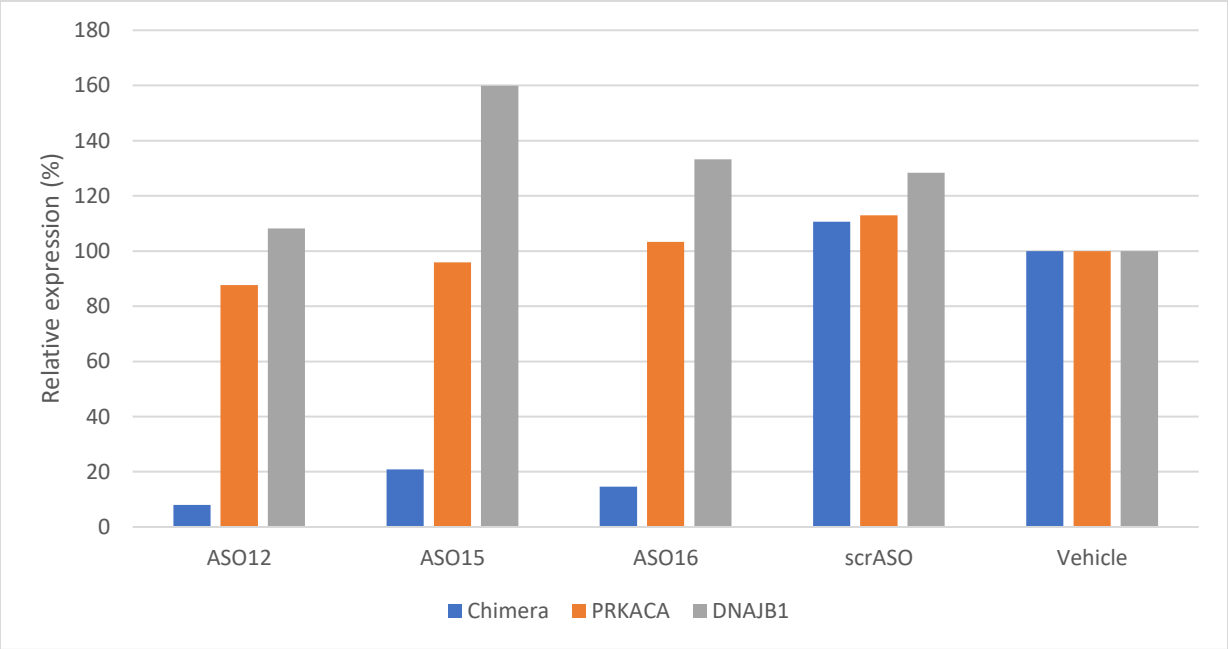

Figure 3.10 RNA levels in tumors treated with ASO in vivo
Levels of chimera, PRKACA, and DNAJB1 transcripts in tumors treated with the ASOs indicated. For ASO12, tumors were harvested four days after the initial treatment. The rest of the tumors were harvested two weeks after the initial treatment.

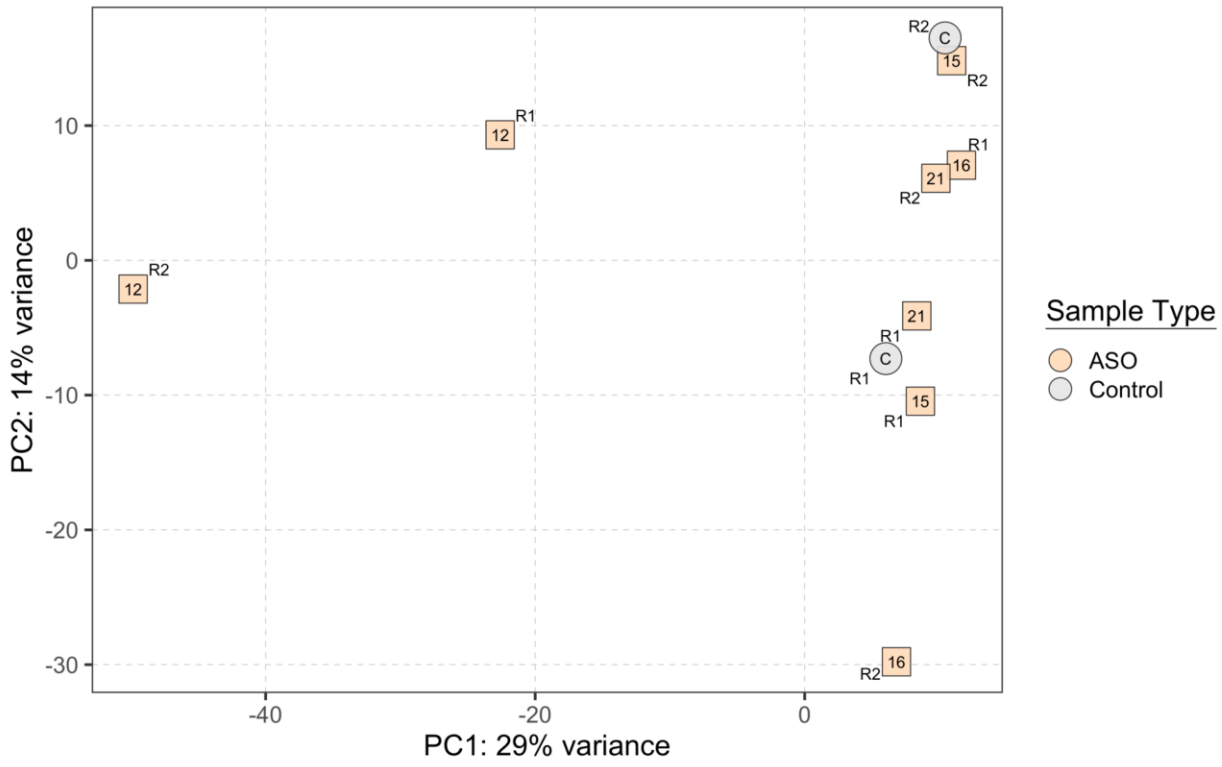

Figure 3.11 PCA of RNA sequencing of the tumors treated with ASO
R1 and R2 represent the two replicates: There were three mice per group, but only two of them underwent RNA sequencing. 21 refers to the scrambled treated tumors. C refers to the vehicle treated tumors

Given the separation of the tumors treated with ASO12 from the tumors treated with the other ASOs, we then checked which genes are the biggest contributors to PC1 and we found that the top contributor is KFL9 (Figure 3.12). KFL9 is overexpressed in cells undergoing oxidative stress and promotes reactive oxygen species related death (Zucker et al., 2014). The average $\log_2$ normalized count for tumors treated with ASO12 is 12, as compared to an average of 9.4 for the other tumors.

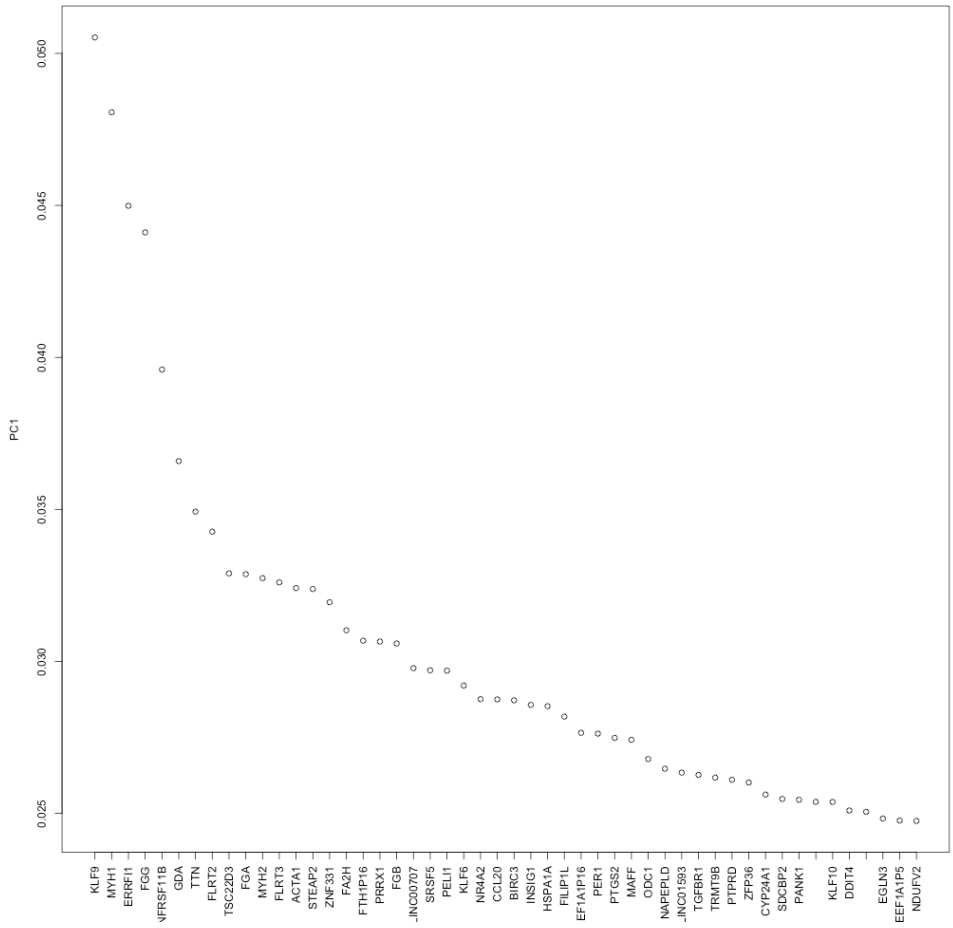

Figure 3.12 Transcripts with the highest contribution to PC1

Given the hepatoxicity shown in this study, I designed other ASOs with sequences that did not contain a TCC or TGC motif. ASO1 through ASO5 do not contain either of these motifs. However, these did not result in any knockdown in the initial screen (Figure 3.1).

Current public mathematical models do not accurately calculate the melting temperature (Tm) of LNA-modified oligonucleotides binding to RNA; however, some tools, such as IDT's OligoAnalyzer, provide a rough estimate. Using this calculator on the sequences of ASO1-17, it is clear why the ASOs closer to PRKACA did not do well: The Tm of the ASOs as you move towards PRKACA steadily decreases. The ASOs that resulted in greater than 80% knockdown in the initial screen all had Tm's greater than 50 °C, compared to the ASOs that did not knock down as well, which all had Tm's lower than 50 °C (Table 4). One study attempting to optimize the ideal melting temperature of ASOs for knockdown concluded that the ideal Tm is around 55 °C (Dieckmann et al., 2018).

Therefore, for the next iteration of this experiment, I designed ASOs based on the sequences of ASO3, ASO4, and ASO5, but increased the Tm by increasing the length of the ASO and by increasing the number of LNA-modified nucleotides. Table 4 lists these ASOs, and Figure 3.7 shows the transcript knockdown results of a one-day experiment on Huh-7 cells expressing the chimera. Since these ASOs targeted the PRKACA side of the junction, levels of DNAJB1 were not tested.

ASO5, based on Figure 1, seems to have 4 bases that are specific to DNAJB1. However, the last base of the first exon of PRKACA (cytosine) is the same as the last base of the first exon of DNAJB1. Therefore, with ASO5, there are only 3 bases that are specific to DNAJB1, which makes the ASO slightly less specific to the chimeric transcript over PRKACA. In other words, ASO5 is a 13/16 match for wild-type PRKACA. ASO3 is a 15/16 match. While LNA modifications significantly decrease off-target effects even when there are only small differences in the sequence, Figure 3.8 shows that at as we lengthen the ASO (and therefore increase the percentage match for wild-type PRKACA), we increase the probability that wild-type PRKACA will be knocked down. This can be seen very well from the ASOs that are modified from ASO5.

Table 4. Sequences and estimated melting temperatures of ASOs

Sequence Name	Sequence	Tm (°C)
ASO1	GCTAAGAATTCTTTCA	38.9
ASO2	CTAAGAATTCTTTCAC	37.3
ASO3	TAAGAATTCTTTCACT	38.9
ASO4	AAGAATTCTTTCACTT	38.2
ASO5	AGAATTCTTTCACTTC	41.6
ASO6	GAATTCTTTCACTTCC	45.1
ASO7	AATTCTTTCACTTCCT	45.2
ASO8	ATTCTTTCACTTCCTC	47.2
ASO9	TTCTTTCACTTCCTCC	52.5
ASO10	TCTTTCACTTCCTCCC	56.9
ASO11	CTTTCACTTCCTCCCC	57.7
ASO12	TTTCACTTCCTCCCCG	59.2
ASO13	TTCACTTCCTCCCCGT	62.7
ASO14	TCACTTCCTCCCCGTA	63
ASO15	CACTTCCTCCCCGTAG	61.1
ASO16	ACTTCCTCCCCGTAGC	64
ASO17	CTTCCTCCCCGTAGCG	62.4
scrASO	AGCGAAGTGCACACGG	54.9
ASO3.18.6-7-5	GCTAAGAATTCTTTCACT	51.1
ASO3.19.6-8-5	GGCTAAGAATTCTTTCACT	54.1
ASO4.19.6-7-6	GCTAAGAATTCTTTCACTT	51.7
ASO5.19.6-7-6	CTAAGAATTCTTTCACTTC	50.5
ASO5.20.5-10-5	GCTAAGAATTCTTTCACTTC	50.9
ASO5.20.5-9-6	GCTAAGAATTCTTTCACTTC	51.8
ASO5.20.6-8-6	GCTAAGAATTCTTTCACTTC	53.1
ASO5.21.6-8-7	GGCTAAGAATTCTTTCACTTC	56
ASO5.21.7-8-6	GGCTAAGAATTCTTTCACTTC	56.9
ASO5.22.7-8-7	TGGCTAAGAATTCTTTCACTTC	58.4

ASOs listed after scrASO were tested during the second iteration. The naming scheme for those ASOs is as follows: The first part of the name describes the starting position of the 5’ end of the ASO on the chimeric transcript. The second number indicates the length of the ASO. The third number (x-x-x) describes the gapmer design. For example, ASO3.18.6-7-5 has the same starting position as ASO3, is 18 nucleotides long, and has 7 unmodified DNA bases in the center, but is flanked by 6 and 5 LNA-modified nucleotides on the left and right sides, respectively.

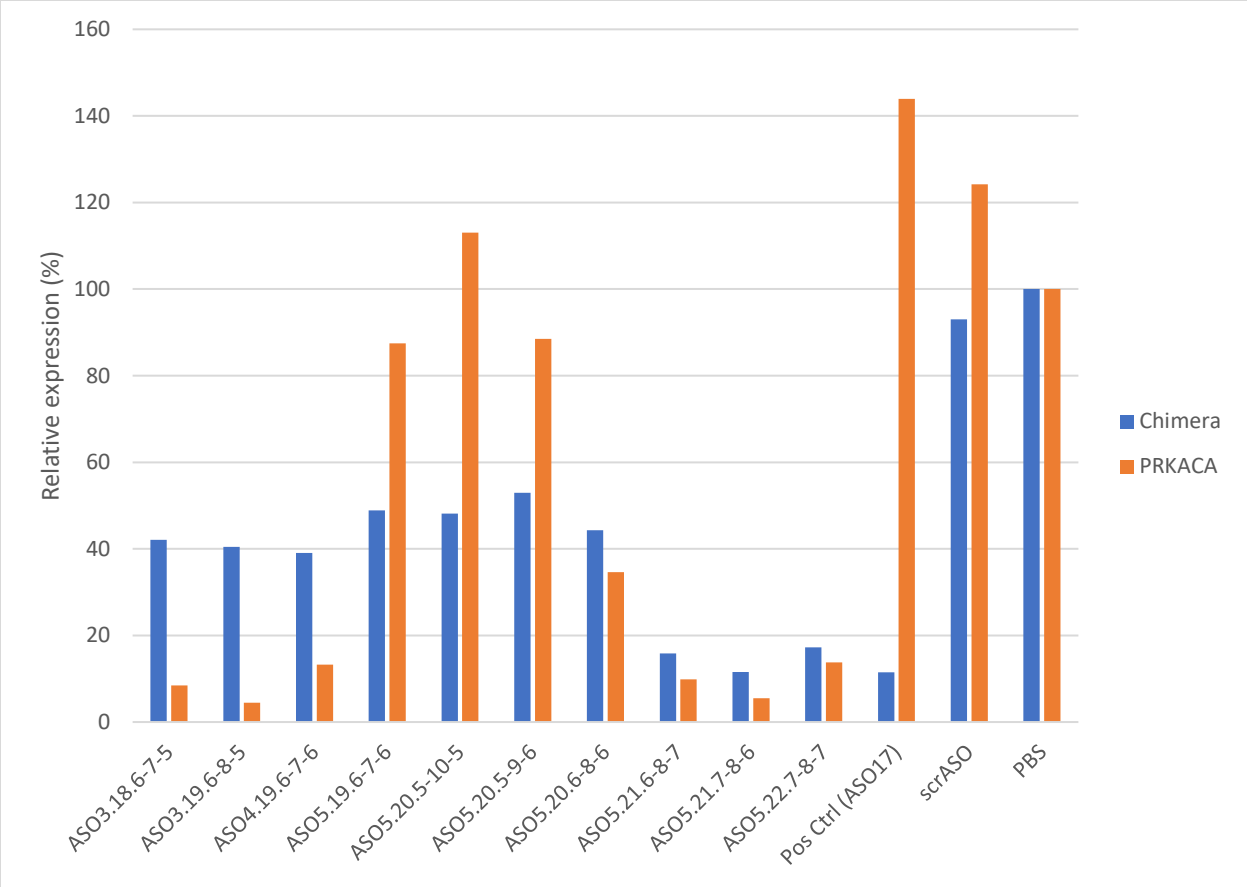

Figure 3.13 RNA knockdown in ASO-treated chimera-positive Huh7 cells
Relative mRNA expression levels measured via qRT-PCR of the chimera and *PRKACA* transcripts after treatment of 20 µM ASO for 1 day.

Given the difficulty I had with hepatotoxicity (in iteration 1) and specificity (in iteration 2), we decided to conduct a very similar experiment, but with siRNA instead of ASOs. In chapter 4, I will discuss our plan for next steps for the ASOs.

3.3 siRNA

There are many modifications and permutations that can be used for siRNA oligonucleotides (other than the sequence itself). As discussed in section 1.3, dicer substrate siRNA (DsiRNA) has several advantages over regular siRNA, and therefore, we used them for our experiments thus far. We had every DsiRNA from across the fusion junction synthesized (Figure 3.12). For our initial experiment, to assess the ability of the DsiRNAs of knocking down the chimera, I tested them against our Huh7 line that expresses the chimera. All 22 of the DsiRNAs resulted in knockdown in chimera. DsiRNA1-10 also resulted in knockdown of *PRKACA* (Figure 3.13).

```
mRNA: 3′-  GAAACCGAAACCGAUUCUUAAGAAAGUGAAGGAGGGGCAUCGCCAGCU-5′
      5′-                                                   -3′
siRNA1      cuuuggCUUUGGCUAAGAAUUCUUUCA
siRNA2       uuuggcUUUGGCUAAGAAUUCUUUCAC
siRNA3        uuggcuUUGGCUAAGAAUUCUUUCACU
siRNA4         uggcuuUGGCUAAGAAUUCUUUCACUU
siRNA5          ggcuuuGGCUAAGAAUUCUUUCACUUC
siRNA6           gcuuugGCUAAGAAUUCUUUCACUUCC
siRNA7            cuuuggCUAAGAAUUCUUUCACUUCCU
siRNA8             uuuggcUAAGAAUUCUUUCACUUCCUC
siRNA9              uuggcuAAGAAUUCUUUCACUUCCUCC
siRNA10              uggcuaAGAAUUCUUUCACUUCCUCCC
siRNA11               ggcuaaGAAUUCUUUCACUUCCUCCCC
siRNA12                gcuaagAAUUCUUUCACUUCCUCCCCG
siRNA13                 cuaagaAUUCUUUCACUUCCUCCCCGU
siRNA14                  uaagaaUUCUUUCACUUCCUCCCCGUA
siRNA15                   aagaauUCUUUCACUUCCUCCCCGUAG
siRNA16                    agaauuCUUUCACUUCCUCCCCGUAGC
siRNA17                     gaauucUUUCACUUCCUCCCCGUAGCG
siRNA18                      aauucuUUCACUUCCUCCCCGUAGCGG
siRNA19                       auucuuUCACUUCCUCCCCGUAGCGGU
siRNA20                        uucuuuCACUUCCUCCCCGUAGCGGUC
siRNA21                         ucuuucACUUCCUCCCCGUAGCGGUCG
siRNA22                          cuuucaCUUCCUCCCCGUAGCGGUCGA
```

Blue = PRKACA exon 2
Red = DNAJB1 exon 1

Figure 3.14 Gene walk across the DNAJB1-PRKACA junction for siRNA design
Every possible DsiRNA sequence along the junction was synthesized for the initial experiment, including one DsiRNA completely within the PRKACA sequence (siRNA1) and one completely within the DNAJB1 sequence (siRNA22). The bases in lowercase are the ones that are predicted to be cut out by Dicer before being loaded on to the RISC complex.

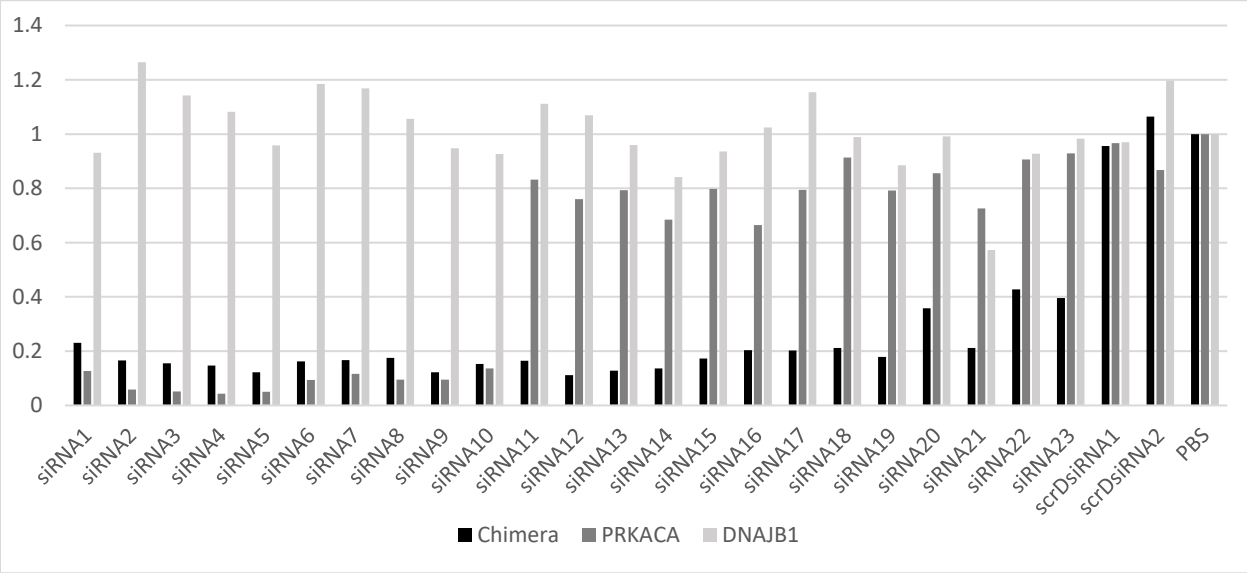

Figure 3.15 RNA knockdown in DsiRNA-treated chimera-positive Huh7 cells
Relative mRNA expression levels measured via qRT-PCR of the chimera, *DNAJB1*, and *PRKACA* transcripts one day after DsiRNA transfection.

Chapter 4 Implications and Future Directions

4.1 Discussion on proteomics

The proteomic data acquired in this study provides the first large dataset quantifying proteins for FLC. To my knowledge, there has been only one smaller dataset that have been published as a means to correlate differential protein expression as an orthogonal confirmation of other experimental data, e.g., RNA sequencing (Simon et al., 2015). But the data presented here is a resource that can be used for future questions related to protein expression. Given the rarity of FLC, the seven FLC tumors used in this experiment provides for strong statistical significance.

Interestingly, we found that the proteomic signature of FLC is unique from normal liver and HCC, though we only analyzed one tumor of the latter. While FLC has been considered a variant of HCC for a long time, with our current understanding of the genetic basis of FLC, it is not surprising to see that the proteomic signature is different between the two cancers.

For the phosphoproteome we expected the differential levels of the many phosphosites. This is part because the oncogene is a kinase. Similarly to the proteome, the phosphome for the FLC tumors clustered together and away from the adjacent non-transformed tissue, but also away from the HCC sample. This suggests a distinct phosphorylation signature in the FLC cells that is different from both the adjacent normal, but even other liver tumors. The results were essentially the same whether the phosphome or proteome were characterized by LFQ or by TMT, suggesting that this si a robust observation. There are two classes of proteins whose increased phosphopeptides will be of interest for further analysis. Some proteins, such as VCAN have increased phosphopeptides as a result of being over expressed. Still the increased level of phosphopeptides could be significant for cell signaling. Some proteins, such as WARS, do not change in the level of expression, but have a significant increased phosphorylation. Both of these are worth exploring. It will be important to pursue both a bioinformatic approach and biochemical approach. Bioinformatics can analyze the kinase pathways. Experimentally, we can try expressing some of the most interesting candidates in the tumor cells in a form where the serine cannot be phosphorylated (e.g. a serine to alanine mutation) to see if that affects the phenotype. Conversely, we can express the protein in a phosphomimetic form (aspartic acid instead of serine) in normal primary human hepatocytes and then probe how that affects the phenotype.

4.2 Discussion on PKA quantification

We pursued the calibration of the levels of protein kinase A, and its regulatory proteins, because we believe that this information is important for testing some

hypotheses for the pathogenesis of FLC. It is important to note that classically the regulatory subunit *PRKAR1A* has been thought to be the predominantly expressed isoform in the liver, based on RNA sequencing data. However, when quantified at the proteome level, both the data presented here and the data from Walker-Gray et al. show that the predominant isoform on the protein level is *PRKAR2A.*

One potential contributor to the pathogenesis of FLC (more extensive discussion in chapter 1.1.4) is that there is an increase in catalytic subunit relative to regulatory subunit in the FLC tumor. In normal liver, there is a stoichiometric excess of the regulatory subunits. This was reported by Walker-Gray, and we reproduced this in our data presented here, albeit, the excess is not as large as in their study. In their study, there is more *PRKAR2A* alone than *PRKACA*. In our cells we also find that in the normal tissue there is an excess of regulatory subunits. Thus, most of the catalytic subunit is inhibited, except when the is signaling by cAMP that releases it from the regulatory subunit. In contrast, in the FLC tumors, we found a stoichiometric excess of catalytic subunit. This would suggest that there is free, uninhibited catalytic subunit in the tumor. This is something that we are currently testing in the lab by measuring how much free catalytic activity is in tissue extract and how much is cAMP stimulated. This increased activity could contribute to much of the pathogenic activity. However, it may not account for everything since expression of PRKACA alone in mouse liver did not fully recapitulate the tumor phenotype. It would be interesting to test if these relative levels holds true in patient with *PRKAR1A* mutations that result in Carney complex or Cushing's disease. Either way, the decrease in active *PRKAR1A* in those cases is going to skew the catalytic:regulatory ratio and may favor decreased localization of cAMP mediated signaling.

A second potential contributor is an alteration in the localization of the chimeric catalytic subunit relative to the localization of the native catalytic subunit. One recent report found that the R1α subunits, both as monomers and when bound to the catalytic subunits, form liquid droplets which keep them localized to specific compartments with in the cell. When they had R1α bound to the chimeric protein, the liquid droplet dispersed, and they hypothesized that the lack of localization due to the chimera is a contributing factor for FLC. Interestingly, this study was conducted with *PRKAR1A* and not *PRKAR2A* (Zhang et al., 2020). Based on our quantification data, the ability of *PRKAR1A* to stay localized may not be that relevant, since there are not enough regulatory subunits to contain all of the catalytic subunits in the first place.

4.3 Discussion on therapeutic development

Developing a therapeutic for FLC has been the primary focus of my research years in the lab. Unfortunately, but not surprisingly, this area of my research hit many obstacles along the way. That said, given the very limited room within the fusion transcript to target for degradation and remain specific to the chimera over *PRKACA*

and *DNAJB1*, it is fortunate that several of the ASOs initially treated resulted in very significant and specific knockdown of the chimera. Once we had several ASOs that resulted in transcript knockdown, we ran into a very odd problem not solved to this day. I did not see any chimeric protein knockdown when I tested the ASOs on FLC cells, which are the same cells that I saw this very significant RNA knockdown. I tried many different concentrations and long time points with no success. I termed this RNA-protein dissonance, and it has sprouted all kinds of theories. The simplest is that the half-life of the chimera is too long, so that while there is no new RNA to form new protein, the existing protein sticks around for many days. This is possible but not likely given that *PRKACA* has a reported half life of 55 hours in non-dividing primary hepatocytes (Mathieson et al., 2018). Of course, chimera may have a longer half-life than *PRKACA*, and it is also possible that overall protein turnover in FLC is lower than in primary hepatocytes. Interestingly, a recent SILAC experiment in FLC primary cells in our lab resulted in very poor incorporation of heavy isotope labelled amino acids, suggesting that overall protein turnover may indeed be low in FLC cells. It is important to note that all of these experiments were done on the FLC cells that we had dissociated from PDX tumors. None of these cells could be propagated and none of them grew very long in vitro. Thus, these cells, once removed from the host mouse, may be in a static state with little to no protein turnover.

Another fortunate event during my time in the lab was that the FLC organoids were successfully starting to grow around this time. This was the result of years of work done by Jamie Saltsman followed by Nikki Croteau. A paper published by the Clevers lab, experts in organoids, suggested a new media recipe, which Nikki implemented and thereafter, several lines of FLC organoids were created. Given that these organoids do grow and multiply, I theorized that they are much more likely to recapitulate the normal protein half-life overall. Indeed, when I tested an ASO on them, it resulted in protein knockdown after only 3 days. Unfortunately, Nikki returned to her clinical duties, so there is no longer anyone maintaining any live organoids. However, in the very near future, I plan to revive several of the organoids for future experiments.

The hepatoxicity seen in vivo with the ASOs was a devastating result. Given that about half of LNA modified ASOs result in hepatotoxicity, we were hopeful that we would find several that were not toxic. However, as discussed in chapter 1.3.2, there are several studies that have shown that there are sequence motifs that are more likely to result in hepatotoxicity, with one study showing that the tri-nucleotide motif of TCC, which is a motif present in all of the sequences tested in vivo, is highly correlated with increased rates of toxicity.

This in vivo hepatoxicity raises several questions: One, was the cell death seen when the FLC cells were treated a direct result of chimera knockdown (i.e., the FLC cells have oncogenic dependence on the chimera), or was it a more general result due to the inherent toxicity of the compound? The second question is related to the first: Is the upregulation of several oxidative stress transcripts in the tumors of the mice treated

with ASO12 a result of the cells' response to the loss of chimera, or again, are those the result of the inherent toxicity? There are several ways to answer these questions that I am currently pursuing: Several slides of these tumors are currently awaiting TUNEL staining. The TUNEL assay is specific for apoptotic cells, so we expect that if the cells are undergoing stress due to chimera depletion, then they are more likely to be undergoing apoptosis and will have positive TUNEL staining. In contrast, ASO mediated toxicity results in necrosis and is expected to be TUNEL negative. I will contrast this with the livers from these same mice, where I expect to see no increase in TUNEL staining compared to the mice treated with vehicle. As an orthogonal experiment to this same question, I will immunoblot protein extract from the tumors to assess levels of cleaved caspase.

The results of these experiments may answer whether the FLC tumor cells have an oncogenic addiction to the chimera, which will confirm that the chimera is an important target for FLC drug development. However, new drugs must be designed to overcome this toxicity problem. I am pursuing two broad approaches: designing more ASOs and using siRNA.

For ASOs, I will be avoiding any sequence that has any of the motifs that have been reported to have increased risk of hepatotoxicity. However, this leaves very little room at the fusion junction since there are two TCC motifs in that general area. The area of the junction that does not have those motifs have low GC content, resulting in low Tm ASOs, which don't work well. Therefore, I am designing several new ASOs in that area that are larger and have more LNAs, thus increasing their Tm. The initial results of these ASOs were shown, and there were some efficacious ASOs, but none of the successful ones were specific to the chimera over PRKACA. I am designing several more in that area. At the same time, I will design several more ASOs that are completely with in the *DNAJB1* region of the chimera. These ASOs are likely to result in knockdown of *DNAJB1* as well, but fortunately, complete knockout of *DNAJB1* in mice results in viable and fertile mice with no obvious abnormalities (Uchiyama et al., 2006). When the peritoneal macrophages from these mice were compared to wild-type peritoneal macrophages, the only difference found was decreased thermotolerance in the early phase for the cells from the knockout mouse. There was no difference between the cells in terms of resistance against apoptosis-reducing agents. Therefore, we don't anticipate toxic effects in human, especially with transient knockdown.

We now have a pretty good understanding of the ideal Tm necessary for adequate knockdown, so this next iteration of ASO designs will be in areas of *DNAJB1* that result in an ideal Tm with a typical 3-10-3 LNA gapmer.

At the same time, I will be forging ahead with testing the siRNAs in collaboration with the Heller lab. As mentioned above, I will be reviving some organoids, and I will test the siRNAs that resulted in chimeric RNA knockdown in the Huh-7 cells on the organoids. We do not know whether liposomes will successfully cross through the Matrigel and get into the cells in the organoids, but a recent study detailed a method for

organoid transfection using commercial transfection reagents, so we will follow that protocol if the liposomes do not work on the organoids. Ultimately, the siRNA liposomes will be tested in vivo. siRNA has a better safety profile than LNA modified ASOs. There certainly has been some cases of toxicity, though in most of those cases, it is due to activation of the immune system and not a frankly hepatoxic compound (Hu et al., 2020).

Chapter 5 Materials and Methods

5.1 Mass spectrometry

Patient tissue processing

Tissue preparation protocol was modified from Mertins et al. (2018). Liver samples for proteome or transcriptome analysis were placed on dry ice immediately after resection and stored at -80 C. For tissue lysis, small pieces (2-5 mm in diameter) were cut from the specimen and placed in Eppendorf tubes. The tube was placed in a liquid nitrogen cooled mini mortar and pestle set that accommodates Eppendorf tubes (Bel-Art; catalog # H37260-0100). The tissue was pulverized over liquid nitrogen. Ice cold lysis buffer (8 M urea, 75 mM NaCl, 50 mM Tris (pH 8.0), 1 mM EDTA) supplemented with cOmplete EDTA-free protease inhibitor (Roche), and PhosSTOP phosphatase inhibitor (Roche) tablets was added to the pulverized tissue. The tube was then vortexed at max speed for 15 seconds, incubated on ice for 15 minutes, and then vortexed again at max speed for 15 seconds. The sample was then spun at 30,000 x RCF for 30 minutes. To avoid the lipid layer, the Eppendorf tube was punctured near the bottom (above the pellet) and the supernatant flowed into another Eppendorf tube until the lipid layer reached the level of the hole. All spins were performed at 4 °C. The lysate was assayed for protein concentration using the BCA assay (Pierce).

Digestion

Proteins were precipitated with the chloroform/water/methanol method (Folch et al., 1957) to remove remnant lipids. Pellets were dissolved in 8M urea (GE Healthcare), 50 mM ammonium bicarbonate (AMBIC. Fluka Chemicals), 10mM dithiothreitol (EMD Chemicals) in water, and disulfide bonds were reduced for 1 hour at room temperature with vigorous shaking. Iodoaceamide (Sigma) was added to 20mM and alkylation proceeded for 1 hour at room temperature in the dark. Samples were diluted with 50 mM AMBIC and digested with lysyl endopeptidase (Wako) overnight at room temperature. The concentration of urea was adjusted to 1.5M using 50mM AMBIC, and the samples were further digested for six hours at room temperature, using sequencing grade modified trypsin (Promega). Digestion was stopped by acidification using either formic acid (FA, Fluka) or trifluoroacetic acid (TFA, Thermo), and peptides were purified using high-capacity 30 mg Oasis HLB cartridges (Waters), according to manufactorer specifications. Peptides were then tagged with tandem mass tags from the TMTpro 16plex Label Reagent Set (Thermo) following the manufacturers instructions.

Phosphopeptide enrichment

Peptides were subjected to a two-step phosphopeptide enrichment, first by in-house constructed titanium dioxide microtips as described by Larsen et al. (2005) with minor modifications followed by High-Select Fe-NTA Phosphopeptide Enrichment Kit (Thermo Scientific), according to manufacturer specifications.

LC-MS/MS-SPS-MS analysis for nonmodified peptides

The nonphosphorylated peptide fraction (flow-through from the phosphopeptide enrichment) was fractionated using a Dionex 3000 Ultimate loading pump equipped with a 2.1*150mm 3.5µm Xbridge C18 column (Waters). Solvent A consisted of 10mM ammonium hydroxide (Sigma-Aldrich) in water, pH 10 and solvent B consisted of 10mM ammonium hydroxide, 90% acetonitrile (ACN) in water, pH 10. Peptides were separated across a 60-minute gradient and 96 fractions were collected and concatenated for a total of 24 fractions. Fractions were analyzed using a Fusion Lumos mass spectrometer with SPS-MS3 acquisition. Data was analyzed using Proteome Discoverer v.2.3. Spectra were queried against the human proteome with a 1% false discovery rate. 80% SPS matches were required for a hit to be included.

LC-MS/MS analysis for phosphopeptides

Solvent A was 0.1% formic acid in water and solvent B was 0.1% formic acid, 80 % acetonitrile (ACN) in water. All LC-MS solvents are of LC/MS purity and purchased from Fisher Chemical. Enriched phosphopeptides were separated using an Easy 1200 nLC (Thermo Scientific). Separation was achieved directly using a 75µm*120mm pulled-emitter nanocolumn without trap column loading. Solvent B went from 0% to 30% over 70 minutes and to 60 % over 10 minutes followed by a sharp 5-minute increase 175 to 90% where it was kept for 15 minutes. Peptides were analyzed using a Orbitrap Fusion Lumos mass spectrometer (Thermo Scientific). Data was recorded in positive mode with Top 20 DDA acquisition and quadrupole isolation and HCD fragmentation (30% CE). MS1 resolution was set to 60 000 and an MS2 resolution of 30 000. AGC targets of 1e6 (MS1) and 8e4 (MS2) were applied.

Database searching

Acquired RAW files for the phosphopeptides were analyzed in the MaxQuant framework (v. 1.6.0.13). Spectra were queried against the human proteome and searched with a 1% false discovery rate on both PSM and protein level. Carbamidomethylation of C was applied as a static modification and oxidation (M), acetylation (Protein Nterminus) and phosphorylation (S, T or Y) were applied as variable modifications. A maximum of 5 modifications was allowed on each peptide. Matching between runs was enabled.

Data analysis

Initial data analysis was performed within the Perseus framework. Intensities were log2 transformed and normalized by subtraction of the median in each experiment. Missing values were imputed by low-abundant random signals. The resulting intensities were imported and further analyzed in R v4.0.2 and Rstudio v1.3.1073 using base R statistics. Significant differences in intensities were determined by Student’s t-tests, and p-values were adjusted with the Benjamini-Hochberg algorithm. Graphics were created with the ggplot2 package.

AQUA quantitation

Proteins were precipitated with ice-cold acetone. Pellets were dissolved in 8M urea, 50mM ammonium TEAB, 10mM DTT. Reduction and alkylation (IAA) was carried out at room temperature for 1 hour each. Alkylation was carried out in the dark. Proteins were digested with LysC and spiked with isotopically labeled AQUA peptides to a concentration of 11fmol peptide / microgram of lysate. Samples were purified by RP-microcolumns and analyzed by LC-MS/MS using a Q-Exactive HF mass spectrometer operating in positive ion PRM mode (PRM method designed from injections of AQUA peptide without background). Peak area quantitation was performed using the Skyline software platform.

5.2 RT-PCR validation of the chimera

RNA patient tumors and non-tumor liver was extracted using RNeasy Mini Kit (Qiagen). Liver and tumor tissues were embedded in OCT, and frozen curls of 10 µm were lysed with RLT buffer. RNA concentration was measured using NanoDrop 2000c (Thermo Scientific). All RNA samples were diluted to an equal concentration for the reverse transcription reaction. The LunaScript RT SuperMix Kit (NEB) was used to convert RNA into cDNA according to the manufacturer's instructions. Platinum PCR SuperMix High Fidelity (Invitrogen) was used for PCR with the following conditions for each reaction: 22.5 µL of supermix, 1.5 µL of cDNA, and 0.5 µL of each primer at 10 µM (final primer concentration: 200 nM). Reactions were performed on a C1000 Thermal Cycler (Bio-Rad) as follows: 2 minutes at 94 °C, followed by 30 cycles of 30 seconds at 94 °C, 30 seconds at 55 °C, and 20 seconds at 68 °C. The PCR product was run on a 2% agarose gel with SYBR Safe (Invitrogen) powered with a PowerPac (Bio-Rad) set at 100V for 60 minutes. Gel was imaged using Gel Doc EZ imager (Bio-Rad).

Primer sequences: DNAJB1-PRKACA forward – GCCGAGGAGAAGTTCAAGGA, reverse – CTGTGTTCTGAGCGGGACTT, expected amplicon – 160 kb. PRKACA forward – GAGCAGGAGAGCGTGAAAGAA, reverse – TCATGGCATAGTGGTTCCCG, expected amplicon – 184 kb.

5.3 Protein purification

PRKACA and chimera

pET151-chimera and pET151-PRKACA were gifts from Sergio Botero in our lab. The plasmids were transformed into BL21 (DE3) e. coli cells. The cells were grown until and OD600 of 0.8, and then induced with 0.4 mM IPTG and the cells were grown at 18 °C overnight. The cells were spun down and frozen at -80 °C. The cells were lysed with BPER reagent (Thermo). The lysate was clarified by a spin of 20 minutes at 20,000 x RCF. Purification was modified from Olsen and Uhler (1989): The clarified lysate was incubated with PKI5-24 peptide that was ligated to Affi-gel10 resin (Bio-rad) for 1-2

hours. The resin was washed five times with a wash buffer () and then eluted in an arginine elution buffer ().

PRKAR1A, PRKAR2B, PKIA, PKIB, PKIG

PKRKAR1A and PRKAR2B genes were cloned from Addgene (#23741 and #23667). PKIA, PKIB, and PKIG genes were synthesized by IDT. These genes were cloned into the pMAL-c6T plasmid (NEB) with HiFi (NEB). For PKAR1A and PRKAR2B, the proteins were expressed in BL21 CodonPlus RIL cells (Agilent). For PKIA, PKIB, and PKIG, the proteins were expressed in NEB Express Competent E. coli cells. Cell growth, IPTG induction, and purification were conducted as per NEB instructions using the amylose resin.

PRKAR1B

This gene was cloned from Addgene (#23376) into a pET151 vector with a his-tag at the n-terminus and a SUMO protease recognition site between the tag and the protein. Protein was expressed in BL21 CodonPlus RIL cells (Agilent), and protein was purified using nickel resin.

5.4 Cell culture

FLC cells

2mm pieces of PDX tumor tissue were placed into 50ml Falcon tubes with RPMI, collagenase 4 (Worthington) and DNAse, and digested while rotating at 37C until digestion was complete (Benchmark scientific Roto-therm). All following steps were done on ice or at 4C. The digested tissue was passed through a 200um strainer using a syringe plunger for remaining pieces, and then through a 100um strainer (Fisher). The cells were spun down at 300g for 5 minutes at 4C and the pellet subject to red blood cell (RBC) depletion by a 10 second exposure to 1ml of water followed by the addition of 49ml of PBS. The cells were then subjected to mouse cell depletion according to the manufacturer's instructions (Miltenyi Biotec). Cells were kept at 37°C with 5% pCO_2 and 5% pO_2.

Huh7 cells

Huh7 cells were maintained in DMEM supplemented with10% FBS and grown at 37 °C in a 5% CO2 setting.

5.5 ASO treatment of cells

For the initial screen, ASOs were synthesized by Microsynth. Subsequent experiments were done with ASOs synthesized by IDT. For the initial screen, the cells were treated with 10μM ASO, and cells were harvested for RNA after 72 hours. For the dose-response on the cells, the cells were treated at the indicated concentrations for 72 hours and harvested for RNA. For the dose-response on organoids, the organoids were

treated at the indicated concentrations for 48 hours and then harvested for RNA. For the protein knockdown assessment on organoids, the organoids were treated at the indicated concentrations for 72 hours.

5.6 ASO treatment of mice

NSG mice were implanted with FLC cells in Matrigel subcutaneously. 2 weeks after implantation the mice were treated with 20 mg/kg subcutaneously on days 0, 2, 4, 7, and 10, and sacrificed on day 14. For the mice that were clinically unwell, they were euthanized as soon as possible.

5.7 RNA extraction and qPCR

RNA was extracted using the RNeasy kit (Qiagen), and total RNA was quantified with Nanodrop 2000. The RNA from the different samples in each experiment were made equal by diluting in RNase free water. Most qPCR experiments were conducted on 15ng of total RNA per sample. qPCR was done with the Luna Universal Probe One-Step RT-qPCR Kit (NEB). Primers and probes were synthesized by IDT (Table 5). All primer/probe sets were tested in-house and had efficiencies of 95-105%. Reactions were carried out in a CFX384 (Bio-rad). Each well was multiplexed for the gene of interest and the housekeeping gene. Cycle times and temperatures was as recommended by NEB with the Luna kit. Expression levels were calculated using the delta delta Ct method with B2M used as the housekeeping gene control.

Table 5 Primers and probes used for qPCR

Chimera-F	CAAGCGCGAGATCTTCGAC
Chimera-R	CTGTGTTCTGAGCGGGACTT
Chimera Probe	/56-FAM/TTTCACTTC/ZEN/CTCCCCGTAGCGG/3IABkFQ/
PRKACA-F	CAAGAAGGGCAGCGAGCA
PRKACA-R	CTGTGTTCTGAGCGGGACTT
PRKACA Probe	/56-FAM/AGAGCGTGA/ZEN/AAGAATTCTTAGCCAAAGCC/3IABkFQ/
DNAJB1-F	CAAGCGCGAGATCTTCGAC
DNAJB1-R	GAACTCAGCAAACATGGCAT
DNAJB1 Probe	/56-FAM/CCACTCCCC/ZEN/TTTAGGCCTTCCTC/3IABkFQ/
B2M-F	GGACTGGTCTTTCTATCTCTTGT
B2M-R	ACCTCCATGATGCTGCTTAC
B2M Probe	/5HEX/CCTGCCGTG/ZEN/TGAACCATGTGACT/3IABkFQ/

5.8 Protein isolation and immunoblotting

Total protein from organoids was extracted using RIPA buffer (Sigma) supplemented with cOmplete EDTA-free protease inhibitor, and PhosSTOP

phosphatase inhibitor (Roche). Protein concentrations were measured with the DC protein assay (Bio-Rad), and samples were diluted to an equal protein concentration. 4x NuPAGE LDS sample buffer and 10x NuPAGE sample reducing agent (Invitrogen) were added to the samples. Samples were heated at 100°C for 5 minutes, and then loaded on 4–12% Bis-Tris gels (NuPAGE) and run in MOPS buffer for 50 minutes at 200V. Transfer was performed using the iBlot 2 (Life Technologies). Membranes were blocked for 1 hour at room temperature with blocking buffer (5% milk in TBS-T) and then probed overnight at 4 °C with primary antibodies in blocking buffer. After washing in TBS-T, membranes were incubated for 1 hour at room temperature with horseradish peroxidase-conjugated appropriate secondary antibodies in blocking buffer. The membranes were washed again, incubated with SuperSignal West Femto Maximum Sensitivity Substrate (Thermo Scientific), and exposed to Amersham Hyperfilm (GE Healthcare).

Antibodies: PKA C-α (D38C6) Rabbit mAb (Cell Signaling Technology) at 1:3000, and goat anti-rabbit IgG A0545 (Sigma) at 1:50,000.

5.9 siRNA treatment of cells

siRNAs were transfected with Lipofectamine RNAiMAX (Thermo) with the manufacturer's recommendations. RNA was harvested at 24 hours.

5.10 RNA sequencing of in vivo tumors treated with ASOs

Ten slices of 10µm were cut from each sample in OCT (Optimal Cutting Temperature compound) blocks in a microtome Cryostat Leica CM3050 at -30ºC. RNA was extracted from these slices using the RNA levels were measured using QIAshredder columns and the RNeasy Mini Kit (Qiagen). RNA concentration was measured in a Nanodrop 2000c (Thermofisher) using the 260/280 ratio. RNA Integrity Values (RIN) were measured in an Agilent BioAnalyzer and TapeStation. Paired-end 2x150nt RNA-seq libraries were prepared using TruSeq Stranded Total RNA Sample Prep Kit with Ribo-Zero Gold for rRNA and mt-rRNA depletion (Illumina). These libraries were sequenced on an Illumina Novaseq SP instrument at 60M reads per sample. Quality assessment and trimming were performed using FastQC v0.11.9, MultiQC v1.9 (Ewels et al., 2016) and BBDuk (included in BBMap v38.89). Reads were mapped to the human reference genome hg38 with the EMSEMBL GRCh38.92 gene annotations, using STAR v2.7.7a (Dobin et al., 2013). Analysis of differential gene expression was conducted in R v4.0.2 and Rstudio v1.3.959 using DESeq2, excluding genes corresponding to rRNAs, mt-rRNAs and to immune and stromal signatures (Yoshihara et al., 2013). Results were analyzed in detail through PCA plots, heat maps and scatter plots.

References

Adrián, F. J., Ding, Q., Sim, T., Velentza, A., Sloan, C., Liu, Y., … Gray, N. S. (2006). Allosteric inhibitors of Bcr-abl–dependent cell proliferation. *Nature Chemical Biology*, *2*(2), 95–102. https://doi.org/10.1038/nchembio760

Besse, A., Wu, P., Bruni, F., Donti, T., Graham, B. H., Craigen, W. J., … Bonnen, P. E. (2015). The GABA Transaminase, ABAT, Is Essential for Mitochondrial Nucleoside Metabolism. *Cell Metabolism*, *21*(3), 417–427. https://doi.org/10.1016/j.cmet.2015.02.008

Brown, D. A., Kang, S. H., Gryaznov, S. M., DeDionisio, L., Heidenreich, O., Sullivan, S., … Nerenberg, M. I. (1994). Effect of phosphorothioate modification of oligodeoxynucleotides on specific protein binding. *Journal of Biological Chemistry*, *269*(43), 26801–26805. https://doi.org/10.1016/s0021-9258(18)47090-1

Buchdunger, E., Zimmermann, J., Mett, H., Meyer, T., Müller, M., Druker, B. J., & Lydon, N. B. (1996). Inhibition of the Abl protein-tyrosine kinase in vitro and in vivo by a 2-phenylaminopyrimidine derivative. Cancer research, 56(1), 100–104.

Burdick, A. D., Sciabola, S., Mantena, S. R., Hollingshead, B. D., Stanton, R., Warneke, J. A., … Whiteley, L. O. (2014). Sequence motifs associated with hepatotoxicity of locked nucleic acid—modified antisense oligonucleotides. *Nucleic Acids Research*, *42*(8), 4882–4891. https://doi.org/10.1093/nar/gku142

Burel, S. A., Hart, C. E., Cauntay, P., Hsiao, J., Machemer, T., Katz, M., … Henry, S. P. (2015). Hepatotoxicity of high affinity gapmer antisense oligonucleotides is mediated by RNase H1 dependent promiscuous reduction of very long pre-mRNA transcripts. *Nucleic Acids Research*, *44*(5), 2093–2109. https://doi.org/10.1093/nar/gkv1210

Caldwell, R. L., & Caprioli, R. M. (2005). Tissue Profiling by Mass Spectrometry. *Molecular & Cellular Proteomics*, *4*(4), 394–401. https://doi.org/10.1074/mcp.r500006-mcp200

Craig, J. R., Peters, R. L., Edmondson, H. A., & Omata, M. (1980). Fibrolamellar carcinoma of the liver: A tumor of adolescents and young adults with distinctive clinico-pathologic features. *Cancer*, *46*(2), 372–379. https://doi.org/10.1002/1097-0142(19800715)46:2<372::aid-cncr2820460227>3.0.co;2-s

Crooke, S. T., Witztum, J. L., Bennett, C. F., & Baker, B. F. (2018). RNA-Targeted Therapeutics. Cell metabolism, 27(4), 714–739. https://doi.org/10.1016/j.cmet.2018.03.004

Dieckmann, A., Hagedorn, P. H., Burki, Y., Brügmann, C., Berrera, M., Ebeling, M., … Schuler, F. (2018). A Sensitive In Vitro Approach to Assess the Hybridization-Dependent Toxic Potential of High Affinity Gapmer Oligonucleotides. *Molecular Therapy - Nucleic Acids*, *10*, 45–54. https://doi.org/10.1016/j.omtn.2017.11.004

Dobin, A., Davis, C. A., Schlesinger, F., Drenkow, J., Zaleski, C., Jha, S., … Gingeras, T. R. (2012). STAR: ultrafast universal RNA-seq aligner. *Bioinformatics*, *29*(1), 15–21. https://doi.org/10.1093/bioinformatics/bts635

Druker, B. J., Guilhot, F., O'Brien, S. G., Gathmann, I., Kantarjian, H., Gattermann, N., … Larson, R. A. (2006). Five-Year Follow-up of Patients Receiving Imatinib for Chronic Myeloid Leukemia. *New England Journal of Medicine*, *355*(23), 2408–2417. https://doi.org/10.1056/nejmoa062867

Druker, B. J., Ohno, S., Buchdunger, E., Tamura, S., Zimmermann, J., & Lydon, N. B. (1996). Selective Killing of BCR-ABL Positive Cells with a Specific Inhibitor of the ABL Tyrosine Kinase. *Cancer Genes*, 255–267. https://doi.org/10.1007/978-1-4615-5895-8_16

Edmondson, H. A. (1956). Differential Diagnosis Of Tumors And Tumor-Like Lesions Of Liver In Infancy And Childhood. *Archives of Pediatrics & Adolescent Medicine*, *91*(2), 168. https://doi.org/10.1001/archpedi.1956.02060020170015

Eggert, T., McGlynn, K. A., Duffy, A., Manns, M. P., Greten, T. F., & Altekruse, S. F. (2013). Fibrolamellar hepatocellular carcinoma in the USA, 2000–2010: A detailed report on

frequency, treatment and outcome based on the Surveillance, Epidemiology, and End Results database. *United European Gastroenterology Journal*, *1*(5), 351–357. https://doi.org/10.1177/2050640613501507

El-Serag, H. B., & Davila, J. A. (2004). Is fibrolamellar carcinoma different from hepatocellular carcinoma? A US population-based study. *Hepatology*, *39*(3), 798–803. https://doi.org/10.1002/hep.20096

Engelholm, L. H., Riaz, A., Serra, D., Dagnæs-Hansen, F., Johansen, J. V., Santoni-Rugiu, E., … Frödin, M. (2017). CRISPR/Cas9 Engineering of Adult Mouse Liver Demonstrates That the Dnajb1–Prkaca Gene Fusion Is Sufficient to Induce Tumors Resembling Fibrolamellar Hepatocellular Carcinoma. *Gastroenterology*, *153*(6). https://doi.org/10.1053/j.gastro.2017.09.008

Ewels, P., Magnusson, M., Lundin, S., & Käller, M. (2016). MultiQC: summarize analysis results for multiple tools and samples in a single report. *Bioinformatics*, *32*(19), 3047–3048. https://doi.org/10.1093/bioinformatics/btw354

Fagerberg, L., Hallström, B. M., Oksvold, P., Kampf, C., Djureinovic, D., Odeberg, J., … Uhlén, M. (2014). Analysis of the Human Tissue-specific Expression by Genome-wide Integration of Transcriptomics and Antibody-based Proteomics. *Molecular & Cellular Proteomics*, *13*(2), 397–406. https://doi.org/10.1074/mcp.m113.035600

Folch, J., Lees, M., & Stanley, G. H. S. (1957). A Simple Method For The Isolation And Purification Of Total Lipides From Animal Tissues. *Journal of Biological Chemistry*, *226*(1), 497–509. https://doi.org/10.1016/s0021-9258(18)64849-5

Gershon, P. D. (2013). Cleaved and Missed Sites for Trypsin, Lys-C, and Lys-N Can Be Predicted with High Confidence on the Basis of Sequence Context. *Journal of Proteome Research*, *13*(2), 702–709. https://doi.org/10.1021/pr400802z

Hagedorn, P. H., Yakimov, V., Ottosen, S., Kammler, S., Nielsen, N. F., Høg, A. M., … Lindow, M. (2013). Hepatotoxic Potential of Therapeutic Oligonucleotides Can Be Predicted from Their Sequence and Modification Pattern. *Nucleic Acid Therapeutics*, *23*(5), 302–310. https://doi.org/10.1089/nat.2013.0436

Honeyman, J. N., Simon, E. P., Robine, N., Chiaroni-Clarke, R., Darcy, D. G., Lim, I. I., … Simon, S. M. (2014). Detection of a Recurrent DNAJB1-PRKACA Chimeric Transcript in Fibrolamellar Hepatocellular Carcinoma. *Science*, *343*(6174), 1010–1014. https://doi.org/10.1126/science.1249484

Hu, B., Zhong, L., Weng, Y., Peng, L., Huang, Y., Zhao, Y., & Liang, X.-J. (2020). Therapeutic siRNA: state of the art. *Signal Transduction and Targeted Therapy*, *5*(1). https://doi.org/10.1038/s41392-020-0207-x

Javanbakht, H., Mueller, H., Walther, J., Zhou, X., Lopez, A., Pattupara, T., … Ottosen, S. (2018). Liver-Targeted Anti-HBV Single-Stranded Oligonucleotides with Locked Nucleic Acid Potently Reduce HBV Gene Expression In Vivo. *Molecular Therapy - Nucleic Acids*, *11*, 441–454. https://doi.org/10.1016/j.omtn.2018.02.005

Jeong, W., Rapisarda, A., Park, S. R., Kinders, R. J., Chen, A., Melillo, G., … Kummar, S. (2013). Pilot trial of EZN-2968, an antisense oligonucleotide inhibitor of hypoxia-inducible factor-1 alpha (HIF-1α), in patients with refractory solid tumors. *Cancer Chemotherapy and Pharmacology*, *73*(2), 343–348. https://doi.org/10.1007/s00280-013-2362-z

Kastenhuber, E. R., Lalazar, G., Houlihan, S. L., Tschaharganeh, D. F., Baslan, T., Chen, C.-C., … Lowe, S. W. (2017, December 12). *DNAJB1–PRKACA fusion kinase interacts with β-catenin and the liver regenerative response to drive fibrolamellar hepatocellular carcinoma*. PNAS. https://www.pnas.org/content/114/50/13076.

Kim, D.-H., Behlke, M. A., Rose, S. D., Chang, M.-S., Choi, S., & Rossi, J. J. (2004). Synthetic dsRNA Dicer substrates enhance RNAi potency and efficacy. *Nature Biotechnology*, *23*(2), 222–226. https://doi.org/10.1038/nbt1051

Kim, E., & Viatour, P. (2020). Hepatocellular carcinoma: old friends and new tricks. *Experimental & Molecular Medicine*, *52*(12), 1898–1907. https://doi.org/10.1038/s12276-020-00527-1

Kim, J., Hu, C., Moufawad El Achkar, C., Black, L. E., Douville, J., Larson, A., Pendergast, M. K., Goldkind, S. F., Lee, E. A., Kuniholm, A., Soucy, A., Vaze, J., Belur, N. R., Fredriksen, K., Stojkovska, I., Tsytsykova, A., Armant, M., DiDonato, R. L., Choi, J., Cornelissen, L., … Yu, T. W. (2019). Patient-Customized Oligonucleotide Therapy for a Rare Genetic Disease. The New England journal of medicine, 381(17), 1644–1652. https://doi.org/10.1056/NEJMoa1813279

Kim, J., Hu, C., Moufawad El Achkar, C., Black, L. E., Douville, J., Larson, A., … Yu, T. W. (2019). Patient-Customized Oligonucleotide Therapy for a Rare Genetic Disease. *New England Journal of Medicine*, *381*(17), 1644–1652. https://doi.org/10.1056/nejmoa1813279

Lalazar, G., & Simon, S. (2018). Fibrolamellar Carcinoma: Recent Advances and Unresolved Questions on the Molecular Mechanisms. *Seminars in Liver Disease*, *38*(01), 051–059. https://doi.org/10.1055/s-0037-1621710

Larsen, M. R., Thingholm, T. E., Jensen, O. N., Roepstorff, P., & Jørgensen, T. J. D. (2005). Highly Selective Enrichment of Phosphorylated Peptides from Peptide Mixtures Using Titanium Dioxide Microcolumns. *Molecular & Cellular Proteomics*, *4*(7), 873–886. https://doi.org/10.1074/mcp.t500007-mcp200

Liang, X.-H., Sun, H., Nichols, J. G., & Crooke, S. T. (2017). RNase H1-Dependent Antisense Oligonucleotides Are Robustly Active in Directing RNA Cleavage in Both the Cytoplasm and the Nucleus. *Molecular Therapy*, *25*(9), 2075–2092. https://doi.org/10.1016/j.ymthe.2017.06.002

Liu, P., Xie, S.-H., Hu, S., Cheng, X., Gao, T., Zhang, C., & Song, Z. (2017). Age-specific sex difference in the incidence of hepatocellular carcinoma in the United States. *Oncotarget*, *8*(40), 68131–68137. https://doi.org/10.18632/oncotarget.19245

Mathieson, T., Franken, H., Kosinski, J., Kurzawa, N., Zinn, N., Sweetman, G., … Savitski, M. M. (2018). Systematic analysis of protein turnover in primary cells. *Nature Communications*, *9*(1). https://doi.org/10.1038/s41467-018-03106-1

Matsuda, M., Amemiya, H., Kawaida, H., Okamoto, H., Hosomura, N., Asakawa, M., … Fujii, H. (2013). Typical fibrolamellar hepatocellular carcinoma in a Japanese boy: report of a case. *Surgery Today*, *44*(7), 1359–1366. https://doi.org/10.1007/s00595-013-0653-y

Mertins, P., Tang, L. C., Krug, K., Clark, D. J., Gritsenko, M. A., Chen, L., … Carr, S. A. (2018). Reproducible workflow for multiplexed deep-scale proteome and phosphoproteome analysis of tumor tissues by liquid chromatography–mass spectrometry. *Nature Protocols*, *13*(7), 1632–1661. https://doi.org/10.1038/s41596-018-0006-9

Okuda, K. (2002). Hepatocellular carcinoma — History, current status and perspectives. *Digestive and Liver Disease*, *34*(9), 613–616. https://doi.org/10.1016/s1590-8658(02)80200-6

Olsen, S. R., & Uhler, M. D. (1989). Affinity Purification of the Cα and Cβ Isoforms of the Catalytic Subunit of cAMP-dependent Protein Kinase. *Journal of Biological Chemistry*, *264*(31), 18662–18666. https://doi.org/10.1016/s0021-9258(18)51518-0

Pardanani, A., Wieben, E. D., Spelsberg, T. C., & Tefferi, A. (2002). Primer on Medical Genomics Part IV: Expression Proteomics. *Mayo Clinic Proceedings*, *77*(11), 1185–1196. https://doi.org/10.4065/77.11.1185

Rose, S. D. (2005). Functional polarity is introduced by Dicer processing of short substrate RNAs. *Nucleic Acids Research*, *33*(13), 4140–4156. https://doi.org/10.1093/nar/gki732

Ross, S. J., Revenko, A. S., Hanson, L. L., Ellston, R., Staniszewska, A., Whalley, N., … Macleod, A. R. (2017). Targeting KRAS-dependent tumors with AZD4785, a high-affinity

therapeutic antisense oligonucleotide inhibitor of KRAS. *Science Translational Medicine*, *9*(394). https://doi.org/10.1126/scitranslmed.aal5253

Rowley, J. D. (1973). A New Consistent Chromosomal Abnormality in Chronic Myelogenous Leukaemia identified by Quinacrine Fluorescence and Giemsa Staining. *Nature*, *243*(5405), 290–293. https://doi.org/10.1038/243290a0

Shruthi, B. S., Vinodhkumar, P., & Selvamani, M. (2016). Proteomics: A new perspective for cancer. *Advanced Biomedical Research*, *5*(1), 67. https://doi.org/10.4103/2277-9175.180636

Simon, E. P., Freije, C. A., Farber, B. A., Lalazar, G., Darcy, D. G., Honeyman, J. N., Chiaroni-Clarke, R., Dill, B. D., Molina, H., Bhanot, U. K., La Quaglia, M. P., Rosenberg, B. R., & Simon, S. M. (2015). Transcriptomic characterization of fibrolamellar hepatocellular carcinoma. Proceedings of the National Academy of Sciences of the United States of America, 112(44), E5916–E5925. https://doi.org/10.1073/pnas.1424894112

Smith, M. T., Blatt, E. R., Jedlicka, P., Strain, J. D., & Fenton, L. Z. (2008). Fibrolamellar Hepatocellular Carcinoma. *RadioGraphics*, *28*(2), 609–613. https://doi.org/10.1148/rg.282075153

Stipa, F., Yoon, S. S., Liau, K. H., Fong, Y., Jarnagin, W. R., D'Angelica, M., … DeMatteo, R. P. (2006). Outcome of patients with fibrolamellar hepatocellular carcinoma. *Cancer*, *106*(6), 1331–1338. https://doi.org/10.1002/cncr.21703

Surjan R. C., Dos Santos E. S., Basseres T., Makdissi F. F., & Machado M.A. (2017). A Proposed Physiopathological Pathway to Hyperammonemic Encephalopathy in a Non-Cirrhotic Patient with Fibrolamellar Hepatocellular Carcinoma without Ornithine Transcarbamylase (OTC) Mutation. *Am J Case Rep*, 18, 234–241. https://doi.org/10.12659/ajcr.901682

Swayze, E. E., Siwkowski, A. M., Wancewicz, E. V., Migawa, M. T., Wyrzykiewicz, T. K., Hung, G., … Bennett, and C. (2006). Antisense oligonucleotides containing locked nucleic acid improve potency but cause significant hepatotoxicity in animals. *Nucleic Acids Research*, *35*(2), 687–700. https://doi.org/10.1093/nar/gkl1071

Turnham, R. E., Smith, F. D., Kenerson, H. L., Omar, M. H., Golkowski, M., Garcia, I., … Scott, J. D. (2019). An acquired scaffolding function of the DNAJ-PKAc fusion contributes to oncogenic signaling in fibrolamellar carcinoma. *ELife*, *8*. https://doi.org/10.7554/elife.44187

Walker-Gray, R., Stengel, F., & Gold, M. G. (2017). Mechanisms for restraining cAMP-dependent protein kinase revealed by subunit quantitation and cross-linking approaches. *Proceedings of the National Academy of Sciences*, *114*(39), 10414–10419. https://doi.org/10.1073/pnas.1701782114

Wu, J. C., Merlino, G., & Fausto, N. (1994). Establishment and characterization of differentiated, nontransformed hepatocyte cell lines derived from mice transgenic for transforming growth factor alpha. *Proceedings of the National Academy of Sciences*, *91*(2), 674–678. https://doi.org/10.1073/pnas.91.2.674

Wylie, A. A., Schoepfer, J., Jahnke, W., Cowan-Jacob, S. W., Loo, A., Furet, P., … Sellers, W. R. (2017). The allosteric inhibitor ABL001 enables dual targeting of BCR–ABL1. *Nature*, *543*(7647), 733–737. https://doi.org/10.1038/nature21702

Yang, J. D., Altekruse, S. F., Nguyen, M. H., Gores, G. J., & Roberts, L. R. (2016). Impact of country of birth on age at the time of diagnosis of hepatocellular carcinoma in the United States. *Cancer*, *123*(1), 81–89. https://doi.org/10.1002/cncr.30246

Yoshihara, K., Shahmoradgoli, M., Martínez, E., Vegesna, R., Kim, H., Torres-Garcia, W., … Verhaak, R. G. W. (2013). Inferring tumour purity and stromal and immune cell admixture from expression data. *Nature Communications*, *4*(1). https://doi.org/10.1038/ncomms3612

Zhang, J. Z., Lu, T.-W., Stolerman, L. M., Tenner, B., Yang, J. R., Zhang, J.-F., … Zhang, J. (2020). Phase Separation of a PKA Regulatory Subunit Controls cAMP Compartmentation and Oncogenic Signaling. *Cell*, *182*(6). https://doi.org/10.1016/j.cell.2020.07.043

Zhang, J., Adrián, F. J., Jahnke, W., Cowan-Jacob, S. W., Li, A. G., Iacob, R. E., … Gray, N. S. (2010). Targeting Bcr–Abl by combining allosteric with ATP-binding-site inhibitors. *Nature*, *463*(7280), 501–506. https://doi.org/10.1038/nature08675

Zucker, S. N., Fink, E. E., Bagati, A., Mannava, S., Bianchi-Smiraglia, A., Bogner, P. N., … Nikiforov, M. A. (2014). Nrf2 Amplifies Oxidative Stress via Induction of Klf9. *Molecular Cell*, *53*(6), 916–928. https://doi.org/10.1016/j.molcel.2014.01.033